Finite element methods for nonlinear, dispersive equations

A Dissertation Presented for the

Doctor of Philosophy

Degree

The University of Tennessee, Knoxville

Michael Morgan Wise

May 2020

Dedication

"*O Father we welcome your words,*

And we will take heart for the future,

Remembering the past."[1]

Mater mea, fiducia mea.

[1] T.S. Eliot, "Choruses from 'The Rock': VIII"

Acknowledgments

The first chapter of this dissertation, regarding the *a priori* analysis of the finite element methods with which this work is concerned, is a reprint (up to minor typographical and grammatical amendments) of the material as it appears in *Journal of Scientfic Computing* (see [12]). In this project, Ohannes Karakashian was the primary investigator, directing the project and developing the analysis. The co-authors Jerry Bona and Hongqiu Chen were invaluable, lending their incomparable expertise regarding nonlinear, dispersive partial differential equations toward preparation of the manuscript and suggesting many useful experiments. The author of this dissertation, Michael Morgan Wise, verified the theory, developed all software implementations of the various methods used herein, investigated and validated the theory via a wide range of numerical experiments (a mere summary of which were presented in the published work), and prepared visualizations of the results. Finally, together, the authors compiled, reviewed, and edited the manuscript. During the development of this publication, the work of Ohannes Karakashian and Michael Morgan Wise was partially supported by NSF Grant DMS-1620288.

The work discussed in the latter half of this dissertation, namely *a posteriori* analysis of finite element methods for nonlinear, dispersive equations, was completed under the principal investigation of the author of this dissertation, Michael Morgan Wise, with indispensable guidance from his doctoral advisor, Ohannes Karakashian. Discussions with Andrew Majda and Joseph Biello were extremely useful toward understanding the appropriate interpretations of their mathematical models for the interaction of barotropic and equatorial baroclinic Rossby waves and ensuring that the approximations developed herein are meaningful in the context of physical application.

A wide variety of computational resources were utilized throughout the development of this dissertation. Indeed, the author cannot thank Ben Walker, Jr. of the Department of Mathematics at the University of Tennessee enough for his patience, technological assistance, and the useful input. Furthermore, the author acknowledges the use of the many machines available in the Department of Mathematics at the University of Tennessee. The author, again, gratefully acknowledges Ohannes Karakashian for his limitless patience, kind guidance, and methodical concern which developed a young man with a fondness for computer science into a well-rounded computational scientist and applied mathematician. The methods developed herein were implemented in the C programming language, with additional prototyping, code generation, and accessory tasks being completed using C++, Python, and SageMath. The CXSparse package of Timothy Davis was utilized for much of the sparse linear algebra, while Intel MKL was a valuable, scalable tool for dense linear algebra. Data visualization was effected using various means, including, but not limited to Matlab, Python, and Gnuplot. The computational work of the last half of this dissertation was generously supported via a Google Cloud Platform Research Credit Grant from Google for Education. It is highly unlikely that many of the most computationally intensive experiments presented in the later parts of this work could have been accomplished in the necessary time without the state-of-the-art hardware resources afforded by this support.

Finally, these acknowledgements would be disgracefully lacking without the recognition of the many who have guided, enabled, or even challenged the author to embark upon this journey, see it to its end, and begin a new one beyond anything which the author could have before imagined.

Abstract

The present study is concerned with the numerical approximation of solutions of systems of Korteweg-de Vries type, coupled through their nonlinear terms. We construct, analyze, and numerically validate two types of schemes that differ in their treatment of the third derivatives that appear in the system. This difference is fundamental, earning one method the moniker "conservative" due to its preservation, up to round-off error, of a fundamental invariant of the system. The other, slightly more-standard method is called "dissipative" for lack of this property. For both schemes, we prove convergence of a semidiscrete approximation from an *a priori* perspective and highlight differences in the assumptions required to analyze each scheme. We also derive a posteriori error estimates for the semidiscrete and fully discrete approximations obtained.

Finally, we provide numerical experiments that serve to validate the *a priori* and *a posteriori* theory. We experimentally contrast the accuracy of the conservative and dissipative schemes when integrations are made over long time intervals. Also, experiments regarding the effectivity of various *a posteriori* indicators developed for fully-discrete schemes are presented. We experimentally identify particular components of our estimators that provide independent

indicators of the spatial and temporal errors. We conclude by providing additional heuristic estimators based on the *a posteriori* estimates.

Preface

In this dissertation, we construct, analyze, and numerically validate finite element methods for the initial-boundary value problem (IBVP) for a coupled system of Korteweg-de Vries type equations, namely,

$$\begin{aligned} u_t + u_{xxx} + P(u,v)_x &= 0 \\ v_t + v_{xxx} + Q(u,v)_x &= 0 \end{aligned} \tag{1}$$

with periodic boundary conditions on the interval $[0,1]$. Here, the dependent variables $u = u(x,t)$ and $v = v(x,t)$ are real-valued functions and subscripts denote partial differentiation. The nonlinearities are taken to be homogeneous quadratic polynomials in u and v, *viz.* $P(u,v) = Au^2 + Buv + Cv^2$ and $Q(u,v) = Du^2 + Euv + Fv^2$ for given real coefficients $A, B, \ldots, F$.

The system (1) and other related couplings of nonlinear, dispersive equations appear in the literature in models for a wide variety of physical phenomena. Indeed, several asymptotic models developed by Majda and Biello to study the Madden-Julian Oscillation are relatives of the system above. These models employ coupled systems of two (see [34] and [8]) and three equations of Korteweg-de Vries type (see [35]) to study the nonlinear interaction of equatorial baroclinic and barotropic Rossby waves. In fact, in [8], Biello derived and experimentally studied a system that is a special case of (2.1). Yet, a plethora of physical models exist that utilize different, yet closely related couplings of equations combining nonlinear and dispersive effects. An excellent example is the Gear-Grimshaw system used to study the propagation of internal waves. In [29], Hakkaev considered a system quite similar to (2.1) with dispersion of BBM type. Finally, specializations of the surface water wave models of Bona, Chen, and Saut (see [14] and [15]) also feature a coupled KdV structure like that of the system (1). From a mathematical perspective, the system (1) is a paradigm class for the theoretical study of systems combining nonlinearity and dispersion. Indeed, it has provided a testbed for recent work developing new theory for PDEs of this kind. See, for example, [16, 11, Bona et al.]. Indeed, due to their versatility toward scientific application and their subtle mathematical properties, the study of coupled systems of nonlinear, dispersive equations is at the forefront of current research in both pure and applied mathematics.

As a result, accurate and efficient numerical simulations of such systems as (1) is of considerable interest. Nevertheless, despite the large body of work available for both mathematical theory and numerical methods for single equations of Korteweg-de Vries type available in the two decades since the new Millennium (see Chapter 1 for a thorough discussion of the literature), few analogous results are known for (1) and similar coupled systems of nonlinear, dispersive equations. Indeed, for what few numerical schemes are present in the literature, to the best of our knowledge, none exist that provide rigorous error estimates. In this dissertation, we ameliorate this deficit by providing the first construction of approximations of solutions to such systems that includes rigorous analysis of these approximations. Indeed, not only do we provide rigorous analysis of the error of our semidiscrete schemes from an *a priori* perspective but also we develop *a posteriori* error estimates for both semidiscrete and fully discrete approximations.

Before we conclude by describing the general layout of this dissertation, we briefly contrast *a priori* and *a posteriori* error estimates of numerical approximations of partial differential equations. The underlying difference is that *a priori* (Latin: "from the former") error estimates bound the error between the approximation and the exact solution in terms of the exact solution, while *a posteriori* (Latin: "from the latter") error estimates bound the error in terms of the computed approximation. Consequently, *a priori* error estimates are useful for showing theoretical convergence and for providing a rate thereof depending on the discretization parameters, but the resulting bound is not computable, in general, due to this dependence on the exact solution. As a result, these estimates are not directly useful toward commenting on the magnitude of the error of a given approximation one has computed, only toward claiming the errors behave with a particular theoretical rate, a rate that is known before (or *a priori* of) any computation of an approximation. Nevertheless, since *a posteriori* error estimates provide a bound in terms of the computed solution (and also possibly discretization parameters), they are designed so that the bounding quantity may be explicity computed after (or *a posteriori* of) the computation of an approximation. Indeed, unlike the *a priori* bounds which provide qualitative understanding (i.e., a rate) of the behavior of the error, the *a posteriori* bounds provide quantitative, explicitly computable bounds on the error. Indeed, because *a posteriori* estimates provide a real-time metric for the error of an approximation, they provide a theoretical platform for the development of adaptive finite element schemes.

This dissertation comprises two chapters: Chapter 1 is a reprint of our published work [12] and constructs, analyzes, and numerically validates two classes of finite element methods for the periodic IBVP presented above. These classes are called conservative and dissipative due to either the preservation of certain invariants of the system (1) (up to round-off error) or a lack of this property. The principal result of Chapter 1 regards convergence for the semidiscrete approximations of both classes through the development of *a priori* error estimates. After these results, we present a variety of numerical experiments. With the first set of experiments, we validate the theoretical results through a study of spatial convergence rates. With the second set of experiments, we compare and contrast the accuracy of the conservative and dissipative schemes by performing integrations over long time intervals. Chapter 1 concludes with a discussion of future work. Chapter 2 regards the *a posteriori* analysis of the finite element methods introduced in Chapter 1, developing *a posteriori* error estimates for semidiscrete and fully discrete schemes. The first key result of Chapter 2 is an *a posteriori* bound of the error of the conservative semidiscrete scheme, developed utilizing the dispersive reconstruction operator introduced in the work [31] of Karakashian and Makridakis from which this chapter obtains its inspiration. The second key result of Chapter 2 is an *a posteriori* error estimate for a conservative fully discrete scheme, which relies on a similar argument to that used to obtain the *a posteriori* estimates for the semidiscrete case, with the salient difference being that this argument utilizes a space-time reconstruction developed by using the dispersive reconstruction operator in conjunction with the temporal reconstruction ideas of [31] and [3]. The error estimate results are extended to the spatially dissipative formulations of Chapter 1, after which we provide numerical experiments to validate and explore the *a posteriori* theory. Studies of spatial and temporal rates of decrease are then considered, followed by an investigation of the effectivity of various error indicators. Finally, the chapter and the dissertation conclude with a discussion of open avenues for future research.

Table of Contents

List of Tables

List of Figures

Chapter 1

A priori error estimates for finite element methods for nonlinear, dispersive equations

Acknowledgment: The first chapter of this dissertation, regarding the *a priori* analysis of the finite element methods with which this dissertation is concerned, is a reprint (up to minor typographical and grammatical amendments) of the material as it appears in *Journal of Scientfic Computing* (see [12]). For the full acknowledgment regarding this work, see Acknowledgments beginning on Page iv of this dissertation.

1.1 Introduction

Nonlinear, dispersive wave equations arise in a number of important application areas. Because of this, and because their mathematical properties are interesting and subtle, their theory and applications have seen enormous development since the 1960s when they first came to the fore (see Miura [36] for a sketch of the early history of the subject). The theory for a single nonlinear, dispersive wave equation is well-developed by now, though there are still interesting open issues. The theory for coupled systems of such equations is much less developed, though they, too, arise as models of a range of physical phenomena. Considered here is a paradigm class of such systems, namely coupled Korteweg-de Vries equations. The systems we have in mind take the form

$$\begin{cases} u_t + u_{xxx} + P(u,v)_x = 0 \\ v_t + v_{xxx} + Q(u,v)_x = 0 \end{cases} \tag{1.1}$$

which comprise two independent linear Korteweg-de Vries equations coupled through nonlinear terms. Here, the dependent variables $u = u(x,t)$ and $v = v(x,t)$ are real-valued functions and subscripts connote partial differentiation. The nonlinearities are taken to be homogeneous quadratic polynomials in u and v, viz.,

$$P(u,v) = Au^2 + Buv + Cv^2, \qquad Q(u,v) = Du^2 + Euv + Fv^2,$$

with given real coefficients $A, B, \ldots, F$. Such systems and their close relatives arise as models for waves in a number of situations. For example, the model for Madden-Julian atmospheric oscillations recently developed by Majda and Biello [34] fits exactly[1] into this class of systems. The surface water wave models put forward in [14] and [15] have specializations with the same sort of coupled KdV structure as in (1.1) (see also [17] and [18]). The Gear-Grimshaw system [28] arising in internal wave propagation likewise has features similar to the simpler models

[1] Post-publication note: We note that this is only *exactly* true provided that the system features a unit coefficient on each dispersive term. In the case of non-unit coefficients, the Majda-Biello system can also be rescaled to correspond to the system herein considered.

in (1.1). A particular system of the type displayed above, but with BBM-type dispersion, was studied by Hakkaev [29].

1.1.1 Local and global well-posedness

The pure initial-value problem for these systems was studied in [4] and [16]. It transpires that the system (1.1) is always locally well posed in the $L^2(\mathbb{R})$–based Sobolev spaces $H^s(\mathbb{R}) \times H^s(\mathbb{R})$ for any $s > -\frac{3}{4}$. This result follows the general lines of development available already for the single Korteweg-de Vries equation

$$u_t + u_{xxx} + uu_x = 0 \tag{1.2}$$

(see [16], [25]). It was also shown that for solutions of (1.1) corresponding to $s \geq 0$, the integral

$$\Omega(u,v) = \int_{\mathbb{R}} \left(au^2 + buv + cv^2\right) \mathrm{d}x \tag{1.3}$$

is independent of time. The constants $a, b,$ and c comprise any nontrivial solution of the system

$$\left\{ \begin{aligned} &2Ba + (E-2A)b - 4Dc = 0 \\ &4Ca + (2F-B)b - 2Ec = 0 \end{aligned} \right. \tag{1.4}$$

of two linear equations in three unknowns. In case $s \geq 1$, the integral

$$\Theta(u,v) = \int_{\mathbb{R}} \Big(au_x^2 + bu_xv_x + cv_x^2 - R(u,v)\Big) \mathrm{d}x, \tag{1.5}$$

with

$$R(u,v) = \frac{\alpha}{3}u^3 + \beta u^2 v + \gamma u v^2 + \frac{\delta}{3}v^3, \tag{1.6}$$

is also independent of time if (u, v) solves (1.1). Here, the real constants α, β, γ, and δ depend upon the original coefficients, $A, B, \ldots, F$. When the quadratic form $\Upsilon(x, y) = ax^2+bxy+cy^2$ is positive-definite, which is to say, $4ac-b^2 > 0$, these invariants immediately allow the local theory to be extended to global well-posedness if $s \geq 0$. Pursuing a further, energy-type argument as in [25] and an observation in [11], this can be improved and it is now known that (1.1) is globally well posed for arbitrarily sized data in $H^s(\mathbb{R}) \times H^s(\mathbb{R})$ for any $s > -\frac{3}{4}$ when $4ac - b^2 \geq 0$.

Theory for the periodic initial-value problem for the Korteweg-de Vries equation (1.2) is slightly different from the problem posed in Sobolev spaces on $\mathbb{R}$. Thanks to the work of Kappeler and Topalov [30], we know the periodic initial-value problem is globally well posed in $H^s(\mathbb{T})$ for $s \geq -1$. Here, $\mathbb{T} = \mathbb{R}/\mathbb{Z}$ is the one-dimensional torus. However, the proof in such large spaces was made using the inverse-scattering formulation of the problem. As far as we can tell, the systems (1.1) do not generally possess an inverse-scattering theory, so the Kappeler-Topalov result does not easily generalize to them. Theory using harmonic analysis techniques has been developed by Bourgain in a series of papers and later improved by Kenig, Ponce, and Vega. The crowning achievement so far for the periodic initial-value problem using harmonic analysis and energy estimates is found in the paper of Colliander, Keel, Staffilani, Takaoka, and Tao [25] where detailed references to the work of Bourgain and Kenig, Ponce, and Vega can be found. The current state of the art using these techniques is that the problem is globally well posed in $H^s(\mathbb{T})$ provided $s > -\frac{1}{2}$.

For the systems (1.1), the well-posedness in $H^s(\mathbb{T})$ has not yet been dealt with. A straightforward Bona-Smith argument [19] together with the *a priori* $H^1(\mathbb{T})$-bound provided by the invariants (1.3) and (1.5) when $4ac - b^2 > 0$ (so that the quadratic form Υ is positive definite) yields global well-posedness for $s \geq 1$. It seems likely this can be improved, but global well-posedness in $H^s(\mathbb{T}) \times H^s(\mathbb{T})$ for values of $s \geq 1$ suffices to provide the backdrop for the error estimates which are one of the main contributions of the present essay.

1.1.2 Solitary waves

It was shown in [11] that when $4ac - b^2 > 0$, the systems (1.1) always possess solitary-wave solutions of the special form

$$(u_s(x,t), v_s(x,t)) = (\mu_1, \mu_2)\phi_\omega(x - \omega t) = 3\omega(\mu_1, \mu_2)\,\mathrm{sech}^2\left(\frac{\sqrt{\omega}}{2}(x - \omega t)\right). \tag{1.7}$$

The parameters μ_1 and μ_2 are real constants that are independent of the speed ω of propagation. It transpires that it is only the ratio $\mu = \mu_2/\mu_1$ that is in question here (or in special cases where $\mu_1 = 0$, the ratio $\nu = \mu_1/\mu_2$). These ratios satisfy the cubic equation

$$C\mu^3 + (B - F)\mu^2 + (A - E)\mu - D = 0$$

subject to the side condition $A + B\mu + C\mu^2 \neq 0$. In case $\mu_1 = 0$, this becomes

$$D\nu^3 + (E - A)\nu^2 + (F - B)\nu - C = 0$$

subject to $D\nu^2 + E\nu + F \neq 0$. For details, see [11] or [Bona et al.].

As the speed ω is independent of μ or ν, these solutions comprise smooth curves in function space of traveling waves. Such solutions were termed *proportional* solitary waves since both u and v have the same shape function. While such solutions always exist when $4ac - b^2 > 0$, they need not be unique even among proportional solutions. They will be used to implement accuracy tests in the numerical experiments. Introductory remarks about the numerical schemes are presented next.

1.1.3 Background for the numerical schemes

Design and analysis of numerical schemes to approximate solutions of the systems (1.1) is the focus of the present essay. Naturally, our treatment of this approximation problem is guided by the very considerable literature devoted to approximating solutions of the single KdV equation (1.2). The work described here finds its inspiration in the body of work on discontinuous Galerkin (DG) methods for KdV-type equations and their relatives.

Despite the existence of a surfeit of numerical schemes for the KdV equation, rigorous error estimates for them were rare until the new millenium. Early work that featured rigorous theory may be found in the the papers [38] of Wahlbin, [39] of Winther and [5] of Baker et al.

The main obstacle to deriving error bounds is the difficulty of constructing a viable projection for the dispersive (third derivative) term that would play a role similar to that of the elliptic projection in the context of parabolic and hyperbolic problems. The work of Chi-Wang Shu and collaborators, and in particular the articles [23], [41], [40], opened a new path for constructing such projections in the setting of the DG method and its local version, the local discontinuous Galerkin (LDG) method. These projections allowed error estimates for both the local and non-local versions of the DG method for the full nonlinear problem.

Later, again building on the work of Cheng and Shu [23], a DG scheme was put forward in [13] that had the salutary property of preserving up to round-off error the first two invariants of the KdV equation. Such schemes are called conservative, whereas the earlier schemes mentioned above were dissipative. That is, the scheme itself introduces dissipation into the approximation. As is often the case with Hamiltonian systems, schemes that preserve invariants of the motion have improved long-time behavior of the errors. This theme was pursued further in [33] through the development of a DG scheme preserving the third invariant, which can act as a Hamiltonian for the KdV equation.

More recently, *a posteriori* error estimates were obtained in [31] and [32] for both DG and LDG versions of schemes for the Generalized KdV equation. The key step introduced in [31] was a *reconstruction* operator that was used to obtain the first such estimates for nonlinear time-dependent equations of KdV-type. This operator can be adapted to the treatment of derivatives of arbitrarily high order and applies equally well to conservative and dissipative numerical schemes.[2]

The present work is an extension of the ideas and techniques alluded to above for a single, nonlinear, dispersive wave equation to coupled systems of such equations. It constitutes a first attempt at the construction of approximations of solutions to such systems including rigorous

[2]Post-publication note from MMW: This idea of *dispersive reconstruction* is the same idea which gave rise to the second half of this dissertation. Using this technique, this dissertation provides the first such *a posteriori* estimates for finite element methods of systems of nonlinear, dispersive time-dependent equations. Indeed, this work improves on the work of [31] for the single generalized KdV equation by providing methods which are conservative in space and in time and by further isolating spatial *a posteriori* indicators which are independent of time and temporal *a posteriori* indicators which are independent of space.

analysis of these approximations. Both conservative and dissipative formulations for the system (1.1) will be considered, with an eye to understanding the advantages and disadvantages of each. The conservative formulation has the property that the invariant $\Omega(u(\cdot,t),v(\cdot,t))$ defined in (1.3), with $\mathbb{R}$ replaced by $[0,1]$ and solutions (u,v) that are periodic of period one in space is constant in time, up to round-off error. On the other hand, for the dissipative method, $\Omega(u(\cdot,t),v(\cdot,t))$ is a monotone decreasing function of time. Of course, up to roundoff error, both schemes are such that the so-called "mass" quantities $\int_0^1 u(x,t)\,\mathrm{d}x$ and $\int_0^1 v(x,t)\,\mathrm{d}x$ are time-independent.

Both approaches appear to be worth studying and have differing characteristics on the theoretical as well as the computational level. For one, while the conservative approach offers the promise of improved error behavior over long time intervals, the analysis becomes much more arduous. Indeed, the definition of the projection operator is not local anymore and its well-posedness can be established only after some conditions are imposed on the degree of the polynomials used and the parity of the number of cells. While such restrictions might strike the reader as odd, they have been seen already in a number of related works (e.g. [13], [33] and [32]).

The paper is organized as follows: Section 1.2 is devoted to notation and other preliminary material including the function spaces that are relevant to the analysis that follows. The finite element spaces are then introduced. These consist of *continuous* piecewise polynomial functions defined on the period domain $\mathbb{T}$. The requirement of continuity is a small departure from the standard DG method. It is put into place to minimize the technical difficulties arising in the treatment of the nonlinearities (see Proposition 3.3 in [13]). Weak forms are also introduced for the nonlinear and dispersive terms. The forms considered herein for the dispersive term come in two flavors, conservative and dissipative, denoted $\mathcal{D}$ and $\tilde{\mathcal{D}}$, respectively (see (1.16) and (1.19)). They are inspired by the corresponding forms used in [13] and [23], respectively.

The analysis of the numerical schemes is effected by appropriate projection operators. These are constructed and their well-posedness as well as approximation properties examined in detail. As already mentioned, conservation causes the projection operator to be nonlocal, a fact that has as a consequence the above mentioned restrictions on the degree q of the piecewise polynomials and the number of cells in the mesh. For the conservative formulation, it is shown that the approximation power of the projection is optimal, which is to say $O(h^{q+1})$, only if the mesh is uniform. Otherwise, it is $O(h^q)$. On the other hand, the dissipative projection is entirely local and its well-posedness and optimal approximation properties are readily established without any conditions on the degree q or the mesh.

In Section 1.3, the conservative semi-discrete formulation is introduced. The integral $\Omega(u_h, v_h)$ of the semi-discrete approximations (u_h, v_h) is conserved and the problem is seen to be globally well posed whenever solutions a, b, and c of (1.4) satisfy the positive-definiteness condition $4ac - b^2 > 0$. It is also shown that the pair (u_h, v_h) converges to (u, v) at the rate of $O(h^q)$ if the mesh is uniform, but $O(h^{q-1})$ otherwise. A similar analysis is carried out using the dissipative form for the dispersive term to obtain semi-discrete approximations $(\tilde{u}_h, \tilde{v}_h)$. The analysis of well-posedness and convergence follows lines akin to those of the conservative method, so the details are only sketched. In particular, the convergence rate for this approach is shown to be $O(h^q)$ without any restrictions on q or the mesh. In Section 1.3.4, fully discrete schemes based on Implicit Runge-Kutta (IRK) time stepping methods belonging to the Gauss-Legendre family (cf. [Dekker and Verwer]) are put forward. The choice of this particular class of methods is motivated by their excellent accuracy and stability properties. A special feature of the stability for these methods allows us to show that when used in tandem with the conservative form $\mathcal{D}$, they yield fully discrete approximations (u^n, v^n) for which $\Omega(u^n, v^n)$ is constant, which is to say, $\Omega(u^{n+1}, v^{n+1}) = \Omega(u^n, v^n)$ at each time level n, up to roundoff error.

In the last section, results of numerical experiments are reported. These include actual convergence rates, behavior of Ω as a function of time, and an appraisal of the relative performance of the conservative and dissipative methods over long time intervals.

1.2 The Numerical Approximation

Details of the numerical approximations are now set forth. This begins with a discussion of the spatial discretization which leads directly to a semi-discrete approximation of the continuous problem.

1.2.1 The meshes

Let $\mathcal{T}_h$ denote a partition of the real interval $[0,1]$ of the form $0 = x_0 < x_1 < \cdots < x_M = 1$. We will also say that $\mathcal{T}_h$ is a *mesh* on $[0,1]$. The points x_m are called *nodes* while the intervals $I_m = [x_m, x_{m+1}]$ will be referred to as *cells*. The subscript h will connote the maximum length of the cells I_m, $m = 0, 1, \ldots, M-1$. The notation $x_m^- = x_m^+ = x_m$ will be useful in taking account, respectively, of left- and right-hand limits of discontinuous functions. The caveat followed throughout is that $x_0^- = x_M^-$ and $x_M^+ = x_0^+$ corresponding to the underlying spatial periodicity of the solutions being approximated.

1.2.2 Function spaces

For a real interval $I = [a_1, a_2]$, the Sobolev spaces $W^{s,p} = W^{s,p}(I)$, equipped with their usual norms will appear frequently. When $p = 2$, we also use $H^s = H^s(I)$ to denote $W^{s,2}(I)$. An unadorned norm $\|\cdot\|$ will always indicate the $L^2(I)$–norm. Use will also be made of the so-called *broken* Sobolev spaces $W^{s,p}(\mathcal{T}_h)$ that are defined as the finite Cartesian products $\prod_{I\in\mathcal{T}_h} W^{s,p}(I)$. Note that when $sp > 1$, the elements of $W^{s,p}(\mathcal{T}_h)$ are uniformly continuous when restricted to a given cell but may be discontinuous across nodes. For the purpose of indicating these potential discontinuities, the following notation is used: For $v \in H^k(\mathcal{T}_h) = W^{k,2}(\mathcal{T}_h)$ with $k \geq 1$, let v_m^+ and v_m^- denote the right-hand and left-hand limits, respectively, of v at the node x_m. The *jump* $[v]_m$ of v at x_m is $v_m^+ - v_m^-$, whereas the *average* $\{v\}_m$ of v at x_m is $\frac{1}{2}(v_m^+ + v_m^-)$. These are standard notations in the context of DG–methods. In all cases, the definitions are meant to adhere to the convention that $v_0^- = v_M^-$ and $v_M^+ = v_0^+$ which is tantamount to identifying x_0 and x_M.

For integer $m \geq 0$, $C^m([0,1])$ is the space of functions that are, together with classical derivatives of order up to m, continuous on $[0,1]$. The periodic versions of these spaces, namely,

$$C^m_{per}([0,1]) = \left\{v \in C^m([0,1]) : v^{(j)}(0) = v^{(j)}(1),\ j = 0, 1, \ldots, m\right\},$$

will also arise. For $m \geq 1$, set $H^m_{per}(\mathcal{T}_h) = C^0_{per}([0,1]) \cap H^m(\mathcal{T}_h)$.

The following, basic embedding inequality (see [2]) will find frequent use. For a mesh $\mathcal{T}_h$, $v \in H^1(\mathcal{T}_h)$ and any cell $I \in \mathcal{T}_h$, there is a constant c which is independent of the cell I such that

$$\|v\|_{L^\infty(I)} \leq c\Big(h_I^{-1/2}\|v\|_{L^2(I)} + h_I^{1/2}\|v_x\|_{L^2(I)}\Big), \tag{1.8}$$

where h_I is the length of I. Indeed, the dependence of (1.8) on the value of h_I is easily ascertained by a simple scaling argument. Note that (1.8) may also be viewed as a trace inequality.

1.2.3 The Finite Element spaces

The spatial approximations will be sought in the space of continuous and periodic piecewise polynomial functions V_h^q subordinate to the mesh $\mathcal{T}_h$, viz.,

$$V_h^q = \left\{ v \in C^0_{per}([0,1]) : \, v\big|_{I_m} \in \mathcal{P}_q(I_m), \, m = 0, 1, \ldots, M-1 \right\}$$

where $\mathcal{P}_q$ is the space of polynomials of degree q. The spaces V_h^q are subspaces of $H^m_{per}(\mathcal{T}_h)$ for any $m \geq 1$ and have well known, local approximation and inverse properties which are spelled out here for convenience (cf. [21]). Let $q \geq 2$ be fixed and let i, j be such that $0 \leq j \leq i \leq q+1$. Then, for any cell I and any function v in $W^{j,p}(I)$, there exists a function $\chi \in \mathcal{P}_q(I)$ such that

$$|v - \chi|_{W^{j,p}(I)} \leq c h_I^{i-j} |v|_{W^{i,p}(I)}, \quad p = 2, \infty, \tag{1.9}$$

where $|v|_{W^{j,p}(I)}$ denotes the seminorm of order j on the Sobolev space $W^{j,p}(I)$ and the constant c is independent of h_I. The equally well-known inverse inequalities

$$|\chi|_{W^{j,p}(I)} \leq c h_I^{\frac{1}{p} - \frac{1}{2} - j} |\chi|_I, \quad 0 \leq j \leq q+1, \; p = 2, \infty \tag{1.10}$$

for all $\chi \in \mathcal{P}_q(I)$ (see, again, [21]) will also find frequent use.

1.2.4 The weak formulations

The weak formulation of the problem begins with consideration of the nonlinear terms in (1.1), each of which are of the form $(uv)_x$. Keeping in mind that we will be working with continuous periodic functions, it is natural to define the form $\mathcal{N}$ via integration by parts, viz.,

$$\mathcal{N}(u, v; \chi) = -\sum_{I \in \mathcal{T}_h} (uv, \chi_x)_I, \quad u, v, \chi \in H^1(\mathcal{T}_h), \tag{1.11}$$

where $(\cdot, \cdot)_I$ denotes the inner product in L^2 over the cell I. The form $\mathcal{N}$ is actually a trilinear form and is well defined since $H^1(\mathcal{T}_h)$ is a Banach Algebra. This trilinear form is also obviously symmetric in its first two arguments. By virtue of the Riesz Representation Theorem, this form defines the associated nonlinear operator $\mathcal{N} : H^1(\mathcal{T}_h) \times H^1(\mathcal{T}_h) \to V_h^q$ whose $L^2([0, 1])$-inner product with any $\chi \in V_h^q$ is

$$(\mathcal{N}(u, v), \chi) = -\sum_{I \in \mathcal{T}_h} (uv, \chi_x)_I. \tag{1.12}$$

Other pertinent properties of $\mathcal{N}$ are summarized in the following lemma.

Lemma 1.1.

(i) The nonlinear form $\mathcal{N}$ defined by (1.11) is consistent in the sense that

$$\mathcal{N}(u, v; \chi) = ((uv)_x, \chi), \quad u, v, \chi \in H^1_{per}(\mathcal{T}_h). \tag{1.13}$$

(ii) For $u, v \in H^1_{per}(\mathcal{T}_h)$,

$$\mathcal{N}(u, v; v) = \frac{1}{2} \sum_{I \in \mathcal{T}_h} (v^2, u_x)_I. \tag{1.14}$$

Proof. (i) Integration by parts yields

$$\mathcal{N}(u,v;\chi) = \sum_{I\in\mathcal{T}_h}((uv)_x,\chi)_I - \sum_{m=0}^{M-1}[uv\chi]_m = ((uv)_x,\chi),$$

since the jump terms vanish because of the assumed continuity and periodicity conditions.

(ii) Since u, v are continuous and periodic, integration by parts yields

$$\mathcal{N}(u,v;v) = -\frac{1}{2}\sum_{I\in\mathcal{T}_h}((v^2)_x,u)_I = \frac{1}{2}\sum_{I\in\mathcal{T}_h}(v^2,u_x)_I.$$

□

A simple but important consequence of periodicity is that the integral $\int_0^1 (u^2)_x u \,\mathrm{d}x$ vanishes for $u \in C^1_{per}([0,1])$. As a direct consequence of the above lemma, we see that the form $\mathcal{N}$ preserves this property on $H^1_{per}(\mathcal{T}_h)$ and in particular on V_h^q.

Corollary 1.2. *The form $\mathcal{N}$ is conservative in the sense that*

$$\mathcal{N}(u,u;u) = 0, \quad u \in H^1_{per}(\mathcal{T}_h). \tag{1.15}$$

Proof. Let $u \in H^1_{per}(\mathcal{T}_h)$. Formula (1.11) implies that $\mathcal{N}(u,u;u) = -\sum_{I\in\mathcal{T}_h}(u^2,u_x)_I$ whereas (1.14) shows that $\mathcal{N}(u,u;u) = \frac{1}{2}\sum_{I\in\mathcal{T}_h}(u^2,u_x)_I$. The result follows. □

Attention is now turned to constructing a bilinear form to represent the dispersive (third derivative) terms. It is similar in spirit to the form $\mathcal{D}$ introduced in [13] with the difference being that the prevailing spaces are globally continuous.[3] For $u, \chi \in H^2(\mathcal{T}_h)$, define $\mathcal{D}$ by

$$\mathcal{D}(u,\chi) = \sum_{I \in \mathcal{T}_h} (u_x, \chi_{xx})_I + \sum_{m=0}^{M-1} \{u_x\}_m [\chi_x]_m. \tag{1.16}$$

The next lemma delineates properties of $\mathcal{D}$ that justify the particular form chosen in (1.16).

Lemma 1.3.

(i) The bilinear form $\mathcal{D}$ defined by (1.16) is consistent in the sense that

$$\mathcal{D}(u,\chi) = (u_{xxx}, \chi), \quad u \in H^3(\mathcal{T}_h) \cap C^2_{per}([0,1]),\ \chi \in H^2_{per}(\mathcal{T}_h). \tag{1.17}$$

(ii) The form $\mathcal{D}$ is skew-adjoint so that

$$\mathcal{D}(v,v) = 0, \quad \forall v \in H^2(\mathcal{T}_h). \tag{1.18}$$

Proof.

(i) Integrating by parts twice yields

$$\mathcal{D}(u,\chi) = \sum_{I \in \mathcal{T}_h} (u_{xxx}, \chi)_I - \sum_{m=0}^{M-1} [u_x \chi_x]_m + \sum_{m=0}^{M-1} [u_{xx}\chi]_m + \sum_{m=0}^{M-1} \{u_x\}_m [\chi_x]_m.$$

[3] Post-publication note from MMW: While this remark remains as innocuous as it appears during the *a priori* analysis, it gives rise to a crucial issue of the *a posteriori* analysis. Indeed, the choices of definition presented here for both the dissipative and conservative dispersive forms are but specializations of their discontinuous counterparts in [13] when test and trial spaces which are taken to be subsets of the space $H^2_{per}(\mathcal{T}_h)$. The discontinuous test functions used in the definition of a local dispersive reconstruction will necessitate the use of the more general dispersive forms presented in [13], which are also consistent for discontinuous test functions, unlike the forms herein presented, which are only consistent for test functions in $H^2_{per}(\mathcal{T}_h)$) (see (1.17) and (1.20)).

Since u_{xx} and χ are continuous and periodic, it follows that the jumps $[u_{xx}\chi]_m$ vanish. The identity $[u_x\chi_x]_m = \{u_x\}_m[\chi_x]_m + [u_x]_m\{\chi_x\}_m$ holds for $u, \chi \in H^2(\mathcal{T}_h)$. Since the jumps $[u_x]_m$ also vanish, the result follows.

(ii) To establish (1.18), note that $v_x v_{xx} = \dfrac{1}{2}(v_x^2)_x$. Thus

$$\sum_{I\in\mathcal{T}_h}(v_x, v_{xx})_I = -\frac{1}{2}\sum_{m=0}^{M-1}[v_x^2]_m.$$

The result now follows from the observation that $[v_x^2]_m = 2\{v_x\}_m[v_x]_m$.

□

It will also be convenient to define the operator counterpart $\mathcal{D} : H^2(\mathcal{T}_h) \to V_h^q$ of the bilinear form $\mathcal{D}(\cdot,\cdot)$ via the requirement

$$(\mathcal{D}u, \chi) = \mathcal{D}(u, \chi), \quad \forall \chi \in V_h^q.$$

The *dissipative* version

$$\tilde{\mathcal{D}}(u, \chi) = \sum_{I\in\mathcal{T}_h}(u_x, \chi_{xx})_I + \sum_{m=0}^{M-1} u_x(x_m^+)[\chi_x]_m \tag{1.19}$$

of the bilinear form $\mathcal{D}$ may also be used to represent the third derivative terms. The following lemma summarizes the properties of $\tilde{\mathcal{D}}$ that are the counterparts of those of $\mathcal{D}$ shown in Lemmas 1.1 and 1.3. The proofs are similar and therefore omitted.

Lemma 1.4.

(i) The bilinear form $\tilde{\mathcal{D}}$ defined in (1.19) is consistent in the sense that

$$\tilde{\mathcal{D}}(u,\chi) = (u_{xxx},\chi), \quad u \in H^3(\mathcal{T}_h) \cap C^2_{per}([0,1]),\ \chi \in H^2_{per}(\mathcal{T}_h). \tag{1.20}$$

(ii) The form $\tilde{\mathcal{D}}$ is dissipative, which is to say,

$$\tilde{\mathcal{D}}(v,v) = \frac{1}{2}\sum_{m=0}^{M-1}[v_x]_m^2, \quad v \in H^2(\mathcal{T}_h). \tag{1.21}$$

1.2.5 The dispersive projections

A *conservative* projection operator $P : C^1_{per}([0,1]) \to V_h^q$ adapted to the bilinear form $\mathcal{D}$ is now constructed following the ideas in [13]. In contrast to [13], the range of this projection is comprised of (globally) continuous, periodic functions.

For u in $C^1_{per}([0,1])$, the projection of u is the function $w = Pu$ in V_h^q that satisfies the conditions

$$\begin{aligned} (w,\chi)_I &= (u,\chi)_I, && \forall \chi \in \mathcal{P}_{q-3}(I),\ I \in \mathcal{T}_h, \\ w(x_m^+) &= u(x_m^+), && m = 0,1,\ldots,M-1, \\ w(x_m^-) &= u(x_m^-), && m = 0,1,\ldots,M-1, \\ \{w_x\}_m &= \{u_x\}_m, && m = 0,1,\ldots,M-1. \end{aligned} \tag{1.22}$$

Note that for $q = 2$ the first condition is vacuous. Also, since u and the elements of V_h^q are continuous and periodic, the second and third conditions can be equivalently expressed as $w(x_m) = u(x_m),\ m = 0,1,\ldots,M$. However, there is no guarantee that such a projection will be well defined. Indeed, due to the nonlocal nature of the fourth condition in (1.22), existence will be shown only when certain conditions on q and M are satisfied.

When it exists, the operator P plays a central role in establishing error estimates for the conservative, semi-discrete method and is adapted, as the next lemma shows, to the bilinear form $\mathcal{D}$.

Lemma 1.5. *For u in $C^1_{per}([0,1])$, if its projection $w = Pu$ defined in (1.22) exists, then it satisfies*

$$\mathcal{D}(w,\chi) = \mathcal{D}(u,\chi), \quad \chi \in V_h^q. \tag{1.23}$$

Proof. First, note that $[u\chi_{xx}]_m = [u]_m \chi_{xx}(x_m^-) + u_m^+[\chi_{xx}]_m$. Since u is continuous and periodic, the jumps $[u]_m$ are all zero. Because $w_m^+ = u_m^+$ and both u and w are continuous, it transpires that

$$[u\chi_{xx}]_m = u_m^+[\chi_{xx}]_m = w_m^+[\chi_{xx}]_m = [w]_m\chi_{xx}(x_m^-) + w_m^+[\chi_{xx}]_m = [w\chi_{xx}]_m.$$

In consequence, upon integrating by parts the term $\sum\limits_{I\in\mathcal{T}_h}(u_x,\chi_{xx})_I$ in (1.16), it follows at once from the above identity and the definition of w that

$$\begin{aligned}\mathcal{D}(u,\chi) &= -\sum_{I\in\mathcal{T}_h}(u,\chi_{xxx})_I - \sum_{m=0}^{M-1}[u\chi_{xx}]_m + \sum_{m=0}^{M-1}\{u_x\}_m[\chi_x]_m \\ &= -\sum_{I\in\mathcal{T}_h}(w,\chi_{xxx})_I - \sum_{m=0}^{M-1}[w\chi_{xx}]_m + \sum_{m=0}^{M-1}\{w_x\}_m[\chi_x]_m.\end{aligned}$$

A further integration by parts then yields

$$\mathcal{D}(u,\chi) = \sum_{I\in\mathcal{T}_h}(w_x,\chi_{xx})_I + \sum_{m=0}^{M-1}\{w_x\}_m[\chi_x]_m = \mathcal{D}(w,\chi).$$

The proof is complete. $\square$

Combining this result with (1.17), one sees that for $u \in C^3_{per}([0,1])$

$$\mathcal{D}w = P_0 u_{xxx}, \tag{1.24}$$

where P_0 is the L^2-projection operator into V_h^q.

Next a related projection operator $\tilde{P} \ : \ C^1_{per}([0,1]) \ \to \ V_h^q$ is defined which is adapted to the bilinear form $\tilde{\mathcal{D}}(\cdot,\cdot)$. It will be used in the analysis of the dissipative semi-discrete formulation. Interestingly, it also plays a role in the analysis of the projection P.

For $u \in C^1_{per}([0,1])$, its projection $\tilde{w} = \tilde{P}u$ is defined by the conditions

$$\begin{aligned}
(\tilde{w},\chi)_I &= (u,\chi)_I, && \forall \chi \in \mathcal{P}_{q-3}(I),\ I \in \mathcal{T}_h,\\
\tilde{w}(x_m^+) &= u(x_m^+), && m = 0,1,\ldots,M-1,\\
\tilde{w}(x_m^-) &= u(x_m^-), && m = 0,1,\ldots,M-1,\\
\tilde{w}_x(x_m^+) &= u_x(x_m^+) && m = 0,1,\ldots,M-1,
\end{aligned} \tag{1.25}$$

In contrast to (1.22), the conditions in (1.25) are entirely local to each cell. Hence, the proofs of existence and uniqueness of this projection are straightforward. Furthermore, classical finite element approximation theory (see again [21, Ciarlet]) can be brought to bear to show that $\tilde{w}$ is an optimal approximation to suitably regular u.

Proposition 1.6. *The projection operator $\tilde{P}$ is well-defined for $q \geq 2$. Furthermore, for any element $u \in W^{q+1,p}(\mathcal{T}_h) \cap C^1_{per}([0,1])$, the optimal approximation properties*

$$\|u - \tilde{w}\|_{W^{j,p}(I)} \leq c h_I^{q+1-j} |u|_{W^{q+1,p}(I)}, \quad I \in \mathcal{T}_h, \quad j = 0, 1, \quad p = 2, \infty, \tag{1.26}$$

obtain, where h_I is the length of cell I and c is independent of u and I.

Proof. The definition of $\tilde{P}$ is local to each cell and involves linear equations. Hence, to prove existence and uniqueness, it suffices to show that $u = 0$ implies $\tilde{w} = 0$.

For $\ell \geq 0$, let $P_\ell(t)$, be the usual Legendre polynomials that are orthogonal on $[-1, 1]$, normalized so that $P_\ell(1) = 1$. Given a cell $I_m = [x_m, x_{m+1}],\ m = 0, 1, \ldots, M-1$, consider the affine map

$$x = x(\xi) = \frac{h_m}{2}\xi + \frac{x_m + x_{m+1}}{2}, \quad -1 \leq \xi \leq 1, \tag{1.27}$$

that maps $[-1, 1]$ onto I_m. The family of rescaled Legendre polynomials $P_{m,\ell}(x)$ is defined by $P_{m,\ell}(x) = P_\ell(\xi)$ where x and ξ are related by (1.27). The polynomials $P_{m,\ell}$ are orthogonal with respect to the L^2-inner product on I_m.

Let $\tilde{w}_m$ denote the restriction of $\tilde{w}$ to I_m. It can be be expressed in terms of the rescaled Legendre polynomials thusly;

$$\tilde{w}_m(x) = \sum_{\ell=0}^{q} \alpha_{m,\ell} P_{m,\ell}(x) = \sum_{\ell=0}^{q} \alpha_{m,\ell} P_\ell(\xi).$$

The first equation in (1.25) and the orthogonality of the Legendre polynomials imply that

$$\alpha_{m,\ell} = 0, \quad \ell = 0, 1, \ldots, q-3. \tag{1.28}$$

Since $P_\ell(\pm 1) = (\pm 1)^\ell$, the second and third equations in (1.25) translate to

$$
\begin{aligned}
0 &= \tilde{w}_m(x_m^+) = \sum_{\ell=q-2}^{q} \alpha_{m,\ell} P_\ell(-1) = (-1)^{q-2} \left(\alpha_{m,q-2} - \alpha_{m,q-1} + \alpha_{m,q}\right) \\
0 &= \tilde{w}_m(x_{m+1}^-) = \sum_{\ell=q-2}^{q} \alpha_{m,\ell} P_\ell(1) = \alpha_{m,q-2} + \alpha_{m,q-1} + \alpha_{m,q}.
\end{aligned}
$$

It follows from these two equations that

$$
\alpha_{m,q-1} = 0 \quad \text{and} \quad \alpha_{m,q-2} + \alpha_{m,q} = 0. \tag{1.29}
$$

The fourth equation in (1.25) and the well-known identities $P'_\ell(\pm 1) = \frac{1}{2}(\pm 1)^{\ell-1}\ell(\ell+1)$ for any $\ell \in \{0\} \cup \mathbb{N}$ lead to

$$
\begin{aligned}
0 = \tilde{w}_x(x_m^+) &= \sum_{\ell=q-2}^{q} \alpha_{m,\ell} P'_{m,\ell}(x_m^+) = \frac{2}{h_m} \sum_{\ell=q-2}^{q} \alpha_{m,\ell} P'_\ell(-1) \qquad (1.30) \\
&= \frac{1}{h_m}(-1)^{q-3}\big((q-2)(q-1)\alpha_{m,q-2} - (q-1)q\,\alpha_{m,q-1} + q(q+1)\alpha_{m,q}\big).
\end{aligned}
$$

Using the fact that $\alpha_{m,q-1} = 0$ and the second equation in (1.29) together with the fact that the values of $(q-2)(q-1)$ and $q(q+1)$ are never the same reveals that $\alpha_{m,q-2} = \alpha_{m,q} = 0$. Thus, $\tilde{w} = 0$ whenever $u = 0$, so the projection operator is indeed well-defined.

The arguments above show that $\tilde{P}u = u$ whenever u belongs to V_h^q. The approximation properties (1.26) are established by an application of the Bramble-Hilbert Lemma. This completes the proof. $\square$

Proposition 1.7. *For even values of q, the projection operator P is not well defined in general. On the other hand, it is well defined for odd values of $q \geq 3$ provided the number M of cells is also odd.*

Proof. The machinery set up in the proof of Proposition 1.6 is applied to the difference $w - \tilde{w}$ rather than w. Existence, uniqueness, and approximation properties of w will be deduced from those that can be established for this difference.

Letting e denote the restriction of $w - \tilde{w}$ to I_m, it follows from the first three equations of (1.22) and (1.25) that $(e, \chi)_{I_m} = 0,\ \chi \in \mathcal{P}_{q-3}(I)$ and $e(x_m^+) = e(x_m^-) = 0$. Expanding in terms of the rescaled Legendre polynomials as before gives

$$e = \sum_{\ell=0}^{q} \alpha_{m,\ell} P_{m,\ell}(x) = \sum_{\ell=0}^{q} \alpha_{m,\ell} P_\ell(\xi),$$

and just as before, the analogs of (1.28) and (1.29) hold. Consequently, there results

$$\alpha_{m,\ell} = 0,\ \ell = 0, 1, \ldots, q-3, \quad \alpha_{m,q-1} = 0, \quad \alpha_{m,q-2} = -\alpha_{m,q}. \tag{1.31}$$

On the other hand, from the fourth equations in (1.22) and (1.25), there obtains

$$\{e_x\}_m = \frac{1}{2}\big(u_x(x_m) - \tilde{w}_x(x_m^-)\big) =: \eta_m. \tag{1.32}$$

This, in turn, translates into

$$
\begin{aligned}
\eta_m &= \frac{1}{h_m}\sum_{\ell=0}^{q}\alpha_{m,\ell}P'_\ell(-1)+\frac{1}{h_{m-1}}\sum_{\ell=0}^{q}\alpha_{m-1,\ell}P'_\ell(1)\\
&= (-1)^{q-3}\big((q-2)(q-1)\alpha_{m,q-2}-(q-1)q\alpha_{m,q-1}+q(q+1)\alpha_{m,q}\big)/(2h_m)\\
&\quad +\big((q-2)(q-1)\alpha_{m-1,q-2}+(q-1)q\alpha_{m-1,q-1}+q(q+1)\alpha_{m-1,q}\big)/(2h_{m-1}),
\end{aligned}
$$

using the fact that $\alpha_{m-1,\ell} = \alpha_{m,\ell} = 0,\ \ell = 0,1,\dots,q-3$. This last result can be further simplified since $\alpha_{m,q-1}=0$ and $\alpha_{m,q-2}=-\alpha_{m,q}$. The upshot is that

$$
\eta_m = (-1)^{q-3}\beta_m+\beta_{m-1},\quad \beta_m := (2q-1)\alpha_{m,q}/h_m,\ m=0,1,\dots,M-1, \tag{1.33}
$$

with the understanding that the indices are modulo M. This is a system of M linear equations in the unknowns $\beta_0,\dots,\beta_{M-1}$ and the projection w is well defined if and only if the system is uniquely solvable.

If q is even, the coefficient matrix of this linear system is circulant with first row $[-1,0,\dots,0,1]$. The nullspace of this matrix is the span of the vector $(1,1,\dots,1)$; hence the system (1.33) does not have a solution unless $\sum_{m=0}^{M-1}\eta_m = 0$, a property that cannot be assumed to hold in general.

On the other hand, if q is odd, the matrix is again circulant but with first row $[1,0,\dots,0,1]$. If M is even, the nullspace of the coefficient matrix is the span of the vector $(1,-1,\dots,1,-1)$ and the matrix is again singular. However, it is invertible if M is odd and its inverse is also circulant with first row $\frac{1}{2}[1,1,-1,1,\dots,1,-1]$. To summarize, if q and M are odd, then the coefficients $\{\alpha_{m,q}\}_{m=0}^{M-1}$ are well defined and therefore so is $e = w - \tilde{w}$, which in turn implies that w is well defined since $\tilde{w}$ is already uniquely defined. This completes the proof.

□

Proposition 1.8. *Suppose the assumptions of Proposition 1.7 are satisfied so that the conservative projection operator P is well defined. Then for $u \in C^1_{per}([0,1]) \cap W^{q+1,\infty}(\mathcal{T}_h)$, $j = 0, 1$ and $p = 2, \infty$, the following quasi-optimal approximation properties hold:*

$$\|u - Pu\|_{W^{j,p}(I)} \leq ch_I^{1+\frac{1}{p}-j} \sum_{J \in \mathcal{T}_h} h_J^q \|u^{(q+1)}\|_{L^\infty(J)}. \tag{1.34}$$

Here, h_J is the length of the interval J as before. If in addition the mesh $\mathcal{T}_h$ is uniform and u also belongs to $W^{q+2,\infty}(\mathcal{T}_h)$, the optimal approximation estimates

$$\|u - Pu\|_{W^{j,p}(I)} \leq ch^{\frac{1}{p}+q+1-j} \|u\|_{W^{q+2,\infty}(J)}, \tag{1.35}$$

are valid. Here, h is the uniform length of the intervals comprising the mesh.

Proof. The approximation properties of w will follow from those of $\tilde{w}$ displayed in (1.26) by finding suitable bounds for $e = w - \tilde{w}$. As seen in the proof of Proposition 1.7, for q and M odd, the system exhibited in (1.33) is uniquely solvable and yields

$$\beta_m = \frac{1}{2}\Big(\eta_m + \sum_{k=1}^{\frac{M-1}{2}} \big(\eta_{m+2k-1} - \eta_{m+2k}\big)\Big) \quad m = 0, 1, \ldots, M-1, \tag{1.36}$$

where the indices in the sum are all read modulo M.

Recall that $\alpha_{m,\ell} = 0,\ \ell = 0, 1, \ldots, q-3$, $\alpha_{m,q-1} = 0$ and $\alpha_{m,q-2} = -\alpha_{m,q}$. From the orthogonality of the $P_{m,\ell}$ and the well-known fact that $\|P_{m,\ell}\|^2_{I_m} = h_m/(2\ell+1)$, it follows that

$$\|e\|^2_{I_m} = \sum_{\ell=0}^{q} \alpha^2_{m,\ell} \|P_{m,\ell}\|^2_{I_m} = \frac{4q-2}{(2q-3)(2q+1)} h_m \alpha^2_{m,q}. \tag{1.37}$$

It is clear from the inequalities in (1.26) that

$$|\eta_\ell| = |u_x(x_\ell) - \tilde{w}_x(x_\ell^-)| \le c h^q_{\ell-1} \|u^{(q+1)}\|_{L^\infty(I_{\ell-1})}, \quad \ell = 0, 1, \ldots, M-1.$$

(Keep in mind that the indices ℓ are all taken modulo M.) Hence, it follows from (1.36), ignoring for the time being the alternating signs, that

$$|\alpha_{m,q}| = \frac{h_m}{2q-1} |\beta_m| \le c h_m \sum_{J \in \mathcal{T}_h} h^q_J \|u^{(q+1)}\|_{L^\infty(J)}. \tag{1.38}$$

Combining this with (1.37) gives

$$\|e\|_I \le c h_I^{3/2} \sum_{J \in \mathcal{T}_h} h^q_J \|u^{(q+1)}\|_{L^\infty(J)}. \tag{1.39}$$

Since $u - w = u - \tilde{w} - e$, (1.26) and (1.39) lead to (1.34) with $p = 2, j = 0$. Moreover, using (1.39) and the inequalities (1.8) and (1.10) applied to e together with (1.26) gives (1.34) for the remaining cases $p = \infty,\ j = 0, 1$ and $p = 2, j = 1$.

The estimate (1.34) can be improved by exploiting the alternating signs in (1.36). Indeed, the techniques appearing in the proof of Proposition 3.2 of [13], show that

$$\eta_\ell = h_{\ell-1}^q \sum_{j=0}^{q-1} \rho_j u^{(q+1)}(\zeta_{\ell-1,j}), \quad \zeta_{\ell-1,j} \in I_{\ell-1}, \tag{1.40}$$

where $\rho_j, j = 0, 1, \ldots, q-1$ depend only on q. If $h_\ell = h$, then (1.40) and the Mean-Value Theorem can be used to extract an extra power of h, viz.,

$$\begin{aligned} |\eta_\ell - \eta_{\ell+1}| &= h^q \sum_{j=0}^{q-1} |\rho_j| \left| u^{(q+1)}(\zeta_{\ell-1,j}) - u^{(q+1)}(\zeta_{\ell,j}) \right| \\ &\leq c h^{q+1} \|u^{(q+2)}\|_{L^\infty(I_{\ell-1} \cup I_\ell)}. \end{aligned} \tag{1.41}$$

The proof of (1.35) follows as before. □

Remark. *Commentary is in order concerning the conditions imposed in Propositions 2 and 3.*

(i) It should be emphasized that the condition that both q and M are odd pertain only to the existence and approximation properties of the conservative projection operator. The conservative semi-discrete approximation (1.44) is well defined, independently of this assumption.

(ii) Obviously, there is no problem with creating meshes $\mathcal{T}_h$ with an odd number M of cells. Moreover, this property is easily preserved in a process of repeated refinement or coarsening at later times in the temporal integration. Numerical experiments indicate that the convergence rates are the same, whether or not the mesh possesses an odd number of cells and so we have tentatively concluded that this restriction is simply an artifact of our proof, which relies upon the projection.

(iii) With $h = \max h_I$, using the fact that $\sum_{J\in\mathcal{T}_h} h_J = 1$, it follows from (1.34) that

$$\|u - w\| \leq ch^q \|u\|_{W^{q+1,\infty}(0,1)}, \tag{1.42}$$

which is quasi-optimal. Similarly, if the mesh is uniform, the estimate (1.35) leads to the optimal bound

$$\|u - w\| \leq ch^{q+1} \|u\|_{W^{q+2,\infty}(0,1)}. \tag{1.43}$$

Note that the characterization of optimality refers to the exponent of h and not the regularity required of u. Henceforth, we shall write $\|u - w\| \leq ch^\mu$ with $\mu = q + 1$ or q (depending on whether the mesh is uniform or not), omitting the dependence of c on u.

1.3 The semi-discrete approximations: Existence, uniqueness and error estimates

1.3.1 The conservative semi-discrete formulation

The stage is set for defining the semi-discrete approximation to solutions of the system (1.1). For a given partition $\mathcal{T}_h$, let u_h, v_h in $V_h^q \times [0, T]$ be the solutions of the coupled system

$$\begin{bmatrix} u_{ht} \\ v_{ht} \end{bmatrix} + \begin{bmatrix} A & B & C \\ D & E & F \end{bmatrix} \begin{bmatrix} \mathcal{N}(u_h, u_h) \\ \mathcal{N}(u_h, v_h) \\ \mathcal{N}(v_h, v_h) \end{bmatrix} + \begin{bmatrix} \mathcal{D}u_h \\ \mathcal{D}v_h \end{bmatrix} = \begin{bmatrix} 0 \\ 0 \end{bmatrix}, \tag{1.44}$$

of first-order in time operator equations with initial data $u_h^0, v_h^0 \in V_h^q$. The initial data will of course be a suitable approximation of initial data u_0, v_0 for (1.1) (see Theorem 1.11).

Expanding u_h and v_h in terms of a basis for the finite-dimensional space V_h^q, it is readily seen that (1.44) is equivalent to an initial-value problem for a system of ordinary differential equations of the form $(U_t, V_t) = \mathcal{F}(U, V)$ where $\mathcal{F}$ is quadratic and, consequently, locally Lipschitz continuous. It is then immediate that this system has existence and uniqueness of a solution corresponding to given initial data u_h^0, v_h^0, at least locally in time.

The following lemma is central to our development.

Lemma 1.9. *Let (a, b, c) be a non-trivial solution of the system (1.4). If $u, v \in V_h^q$, the following identity holds*

$$\mathcal{I}(u, v) := \int_0^1 [2au + bv \;\; bu + 2cv] \begin{bmatrix} A & B & C \\ D & E & F \end{bmatrix} \begin{bmatrix} \mathcal{N}(u, u) \\ \mathcal{N}(u, v) \\ \mathcal{N}(v, v) \end{bmatrix} = 0. \tag{1.45}$$

Proof. In detail, $\mathcal{I}(u, v)$ is written as

$$\begin{aligned} \mathcal{I}(u, v) = \quad & 2aA\mathcal{N}(u, u; u) + bA\mathcal{N}(u, u; v) + 2aB\mathcal{N}(u, v; u) + bB\mathcal{N}(u, v; v) \\ & + 2aC\mathcal{N}(v, v; u) + bC\mathcal{N}(v, v; v) + bD\mathcal{N}(u, u; u) + 2cD\mathcal{N}(u, u; v) \\ & + bE\mathcal{N}(u, v; u) + 2cE\mathcal{N}(u, v; v) + bF\mathcal{N}(v, v; u) + 2cF\mathcal{N}(v, v; v). \end{aligned}$$

The four terms of the form $\mathcal{N}(w,w;w)$ all vanish on account of (1.15). For the remaining terms, the elementary relations

$$\mathcal{N}(u,u;v) = -2\mathcal{N}(u,v;u) \quad \text{and} \quad \mathcal{N}(v,v;u) = -2\mathcal{N}(u,v;v)$$

lead to the formula

$$\mathcal{I}(u,v) = \mathcal{N}(u,v;u)\Big[2Ba + (E-2A)b - 4Dc\Big] + \mathcal{N}(u,v;v)\Big[-4Ca + (B-2F)b + 2Ec\Big].$$

The fact that (a,b,c) is a solution to (1.4) thus implies that $\mathcal{I}(u,v) = 0$ and concludes the proof.

□

Theorem 1.10. *Suppose (a,b,c) is a solution of the system (1.4). Let (u_h, v_h) be a solution pair of (1.44). Then the quantity $\Omega(u_h, v_h)$ is independent of time. Furthermore, if $b^2 < 4ac$, the solution is global in time and uniformly bounded.*

Proof. Multiply the first equation in (1.44) by $2au_h + bv_h$, the second equation by $bu_h + 2cv_h$ and integrate the sum of these over the the period domain $[0,1]$. The result is

$$\begin{aligned}\frac{\mathrm{d}}{\mathrm{d}t}\Omega(u_h,v_h) + \mathcal{I}(u_h,v_h) \quad &+ \quad 2a\mathcal{D}(u_h,u_h) + b\big(\mathcal{D}(u_h,v_h) + \mathcal{D}(v_h,u_h)\big) \\ &+ \quad 2c\mathcal{D}(v_h,v_h) = 0. \end{aligned} \tag{1.46}$$

Lemma 1.9 reveals that $\mathcal{I}(u_h, v_h) = 0$. The skew-symmetry of $\mathcal{D}$ implies that $\mathcal{D}(u_h, u_h)$, $\mathcal{D}(v_h, v_h)$ and $\mathcal{D}(u_h, v_h) + \mathcal{D}(v_h, u_h)$ vanish. Therefore,

$$\frac{\mathrm{d}}{\mathrm{d}t}\Omega(u_h, v_h) = 0, \tag{1.47}$$

whence $\Omega(u_h, v_h)$ is independent of time.

If $b^2 < 4ac$ then there is a positive constant σ such that $\sigma \int_0^1 (u_h^2 + v_h^2) dx \leq \Omega(u_h, v_h)$ so that both $\|u_h\|$ and $\|v_h\|$ remain bounded as long as the solution exists. In view of the equivalence of norms on the finite-dimensional space V_h^q, $\|u_h\|_\infty$ and $\|v_h\|_\infty$ and consequently the components of U and V are also uniformly bounded as long as the solution exists. This conclusion allows the local existence theory made via Picard iteration to be continued indefinitely, leading to a global solution which is necessarily uniformly bounded in time. □

1.3.2 Error estimates for the conservative semi-discrete approximation

A preliminary observation is helpful. Let u and v be smooth and periodic solutions of the system (1.1). In view of the consistency of the form $\mathcal{N}$ shown in (1.13) (equivalently that of the operator $\mathcal{N}$), it follows that $\mathcal{N}(u, u) = P_0((u^2)_x)$, $\mathcal{N}(u, v) = P_0((uv)_x)$ and $\mathcal{N}(v, v) = P_0((v^2)_x)$ where P_0 is the L^2-projection onto V_h^q as before. Since $\mathcal{D}$ is similarly consistent (see (1.17)), $\mathcal{D}u = P_0 u_{xxx}$, $\mathcal{D}v = P_0 v_{xxx}$. By applying P_0 to the system (1.1), there obtains

$$\begin{bmatrix} P_0 u_t \\ P_0 v_t \end{bmatrix} + \begin{bmatrix} A & B & C \\ D & E & F \end{bmatrix} \begin{bmatrix} \mathcal{N}(u,u) \\ \mathcal{N}(u,v) \\ \mathcal{N}(v,v) \end{bmatrix} + \begin{bmatrix} \mathcal{D}u \\ \mathcal{D}v \end{bmatrix} = \begin{bmatrix} 0 \\ 0 \end{bmatrix}. \tag{1.48}$$

The strategy is to make a comparison of u_h, v_h with the projections $w^{(u)} := Pu$, $w^{(v)} := Pv$ of u and v, respectively, as defined via (1.22). Consider the new quantities

$$\begin{aligned}
\zeta^{(u)} &= u_h - w^{(u)}, \\
\zeta^{(v)} &= v_h - w^{(v)}, \\
\eta^{(u)} &= u - w^{(u)}, \text{ and} \\
\eta^{(v)} &= v - w^{(v)}.
\end{aligned}$$

Replace $\mathcal{D}u$ by $\mathcal{D}w^{(u)}$ and $\mathcal{D}v$ by $\mathcal{D}w^{(v)}$ in (1.48) using Lemma 1.5 and then subtract the result from (1.44). There emerges the error equation

$$\begin{aligned}
&\begin{bmatrix} \zeta_t^{(u)} \\ \zeta_t^{(v)} \end{bmatrix} + \begin{bmatrix} A & B & C \\ D & E & F \end{bmatrix} \begin{bmatrix} \mathcal{N}(u_h, u_h) - \mathcal{N}(w^{(u)}, w^{(u)}) \\ \mathcal{N}(u_h, v_h) - \mathcal{N}(w^{(u)}, w^{(v)}) \\ \mathcal{N}(v_h, v_h) - \mathcal{N}(w^{(v)}, w^{(v)}) \end{bmatrix} + \begin{bmatrix} \mathcal{D}\zeta^{(u)} \\ \mathcal{D}\zeta^{(v)} \end{bmatrix} \\
&= \begin{bmatrix} P_0\eta_t^{(u)} \\ P_0\eta_t^{(v)} \end{bmatrix} + \begin{bmatrix} A & B & C \\ D & E & F \end{bmatrix} \begin{bmatrix} \mathcal{N}(u, u) - \mathcal{N}(w^{(u)}, w^{(u)}) \\ \mathcal{N}(u, v) - \mathcal{N}(w^{(u)}, w^{(v)}) \\ \mathcal{N}(v, v) - \mathcal{N}(w^{(v)}, w^{(v)}) \end{bmatrix},
\end{aligned}$$

where $(w_t^{(u)}, w_t^{(v)})$ has been subtracted from both sides. This system is written as $Q_t + Q_1 + Q_2 = Q_3 + Q_4$ for convenience.

As in the proof of Lemma 1.9, multiply the latter system from the left by the vector $\tilde{Q}(t) = [2a\zeta^{(u)} + b\zeta^{(v)} \;\; b\zeta^{(u)} + 2c\zeta^{(v)}]$ and integrate over $[0,1]$ to derive

$$\int_0^1 \tilde{Q}Q_t \,\mathrm{d}x = \frac{\mathrm{d}}{\mathrm{d}t}\Omega(\zeta^{(u)}, \zeta^{(v)}). \tag{1.49}$$

A previous calculation shows that

$$\int_0^1 \tilde{Q}Q_2 \,\mathrm{d}x = 2a\mathcal{D}(\zeta^{(u)}, \zeta^{(u)}) + b\big(\mathcal{D}(\zeta^{(u)}, \zeta^{(v)}) + \mathcal{D}(\zeta^{(v)}, \zeta^{(u)})\big) + 2c\mathcal{D}(\zeta^{(v)}, \zeta^{(v)}) = 0. \tag{1.50}$$

Applying the identities

$$\begin{aligned}
\mathcal{N}(u_h, u_h) - \mathcal{N}(w^{(u)}, w^{(u)}) &= \mathcal{N}(\zeta^{(u)}, \zeta^{(u)}) + 2\mathcal{N}(w^{(u)}, \zeta^{(u)}) \\
\mathcal{N}(u_h, v_h) - \mathcal{N}(w^{(u)}, w^{(v)}) &= \mathcal{N}(\zeta^{(u)}, \zeta^{(v)}) + \mathcal{N}(w^{(v)}, \zeta^{(u)}) + \mathcal{N}(w^{(u)}, \zeta^{(v)}) \qquad (1.51) \\
\mathcal{N}(v_h, v_h) - \mathcal{N}(w^{(v)}, w^{(v)}) &= \mathcal{N}(\zeta^{(v)}, \zeta^{(v)}) + 2\mathcal{N}(w^{(v)}, \zeta^{(v)}),
\end{aligned}$$

allows the conclusion

$$\begin{aligned}
\int_0^1 \tilde{Q}Q_1 \,\mathrm{d}x &= \mathcal{I}(\zeta^{(u)}, \zeta^{(v)}) \qquad (1.52) \\
&\quad + \mathcal{N}(w^{(u)}, \zeta^{(u)}; \zeta^{(u)})(4Aa + 2Db) + \mathcal{N}(w^{(v)}, \zeta^{(u)}; \zeta^{(u)})(2Ba + Eb) \\
&\quad + \mathcal{N}(w^{(u)}, \zeta^{(v)}; \zeta^{(v)})(Bb + 2Ec) + \mathcal{N}(w^{(v)}, \zeta^{(v)}; \zeta^{(v)})(2Cb + 4Fc) \\
&\quad + \mathcal{N}(w^{(u)}, \zeta^{(v)}; \zeta^{(u)})(2Ba + Eb) + \mathcal{N}(w^{(u)}, \zeta^{(u)}; \zeta^{(v)})(2Ab + 4Dc) \\
&\quad + \mathcal{N}(w^{(v)}, \zeta^{(v)}; \zeta^{(u)})(4Ca + 2Fb) + \mathcal{N}(w^{(v)}, \zeta^{(u)}; \zeta^{(v)})(Bb + 2Ec).
\end{aligned}$$

On account of Lemma 1.9, $\mathcal{I}(\zeta^{(u)},\zeta^{(v)}) = 0$. Let $Q_{1,1}$ denote the first four of the last eight terms in (1.52). Formula (1.14) permits this to be rewritten as

$$\begin{aligned} Q_{1,1} &= \big(2Aa + Db\big) \sum_{I\in\mathcal{T}_h} \big((\zeta^{(u)})^2, w_x^{(u)}\big)_I + \big(Ba + Eb/2\big) \sum_{I\in\mathcal{T}_h} \big((\zeta^{(u)})^2, w_x^{(v)}\big)_I \\ &\quad + \big(Bb/2 + Ec\big) \sum_{I\in\mathcal{T}_h} \big((\zeta^{(v)})^2, w_x^{(u)}\big)_I + \big(Cb + 2Fc\big) \sum_{I\in\mathcal{T}_h} \big((\zeta^{(v)})^2, w_x^{(v)}\big)_I. \end{aligned}$$

Now it results from (1.34) with $p = \infty,\ j = 1$ that if $h = \max h_I$, then

$$\begin{aligned} \|w_x^{(u)}\|_{L^\infty(I)} \quad + \quad \|w_x^{(v)}\|_{L^\infty(I)} &\le c \sum_{J\in\mathcal{T}_h} h_J^q \Big(\|u^{(q+1)}\|_{L^\infty(J)} + \|v^{(q+1)}\|_{L^\infty(J)} \Big) \\ &\le c h^{q-1} \Big(\|u^{(q+1)}\|_{L^\infty([0,1])} + \|v^{(q+1)}\|_{L^\infty([0,1])} \Big) \sum_{J\in\mathcal{T}_h} h_J. \end{aligned}$$

Since $\sum_{J\in\mathcal{T}_h} h_J = 1$, it follows that

$$\|w_x^{(u)}\|_{L^\infty(I)} + \|w_x^{(v)}\|_{L^\infty(I)} \le c. \tag{1.53}$$

This in turn leads to the bound

$$\big|Q_{1,1}\big| \le c\big(\|\zeta^{(u)}\|^2 + \|\zeta^{(v)}\|^2\big). \tag{1.54}$$

In handling the next two terms, which are denoted by $Q_{1,2}$, it is crucial that

$2Ba + Eb = 2Ab + 4Dc$, a fact that flows from the first equation in (1.4). Because of this relation,

$$
\begin{aligned}
Q_{1,2} &= -(2Ba + Eb) \sum_{I \in \mathcal{T}_h} \Big(\big(w^{(u)} \zeta^{(v)}, \zeta_x^{(u)} \big)_I + \big(w^{(u)} \zeta^{(u)}, \zeta_x^{(v)} \big)_I \Big) \\
&= (2Ba + Eb) \sum_{I \in \mathcal{T}_h} \big(w_x^{(u)}, \zeta^{(u)} \zeta^{(v)} \big)_I .
\end{aligned}
$$

In view of (1.53), it is concluded that

$$
\big| Q_{1,2} \big| \le c \| \zeta^{(u)} \| \| \zeta^{(v)} \| \le \frac{c}{2} \Big(\| \zeta^{(u)} \|^2 + \| \zeta^{(v)} \|^2 \Big). \tag{1.55}
$$

It is also the case that $4Ca + 2Fb = Bb + 2Ec$, so that if $Q_{1,3}$ denotes the final two terms in (1.52), then

$$
\begin{aligned}
Q_{1,3} &= -(4Ca + 2Fb) \sum_{I \in \mathcal{T}_h} \Big(\big(w^{(v)} \zeta^{(v)}, \zeta_x^{(u)} \big)_I + \big(w^{(v)} \zeta^{(u)}, \zeta_x^{(v)} \big)_I \Big) \\
&= (4Ca + 2Fb) \sum_{I \in \mathcal{T}_h} \big(w_x^{(v)}, \zeta^{(u)} \zeta^{(v)} \big)_I .
\end{aligned}
$$

Consequently, the inequality

$$
\big| Q_{1,3} \big| \le c \| \zeta^{(u)} \| \| \zeta^{(v)} \| \le \frac{c}{2} \big(\| \zeta^{(u)} \|^2 + \| \zeta^{(v)} \|^2 \big) \tag{1.56}
$$

may be extracted. Combining (1.54), (1.55) and (1.56) yields

$$
\int_0^1 \tilde{Q} Q_1 \, \mathrm{d}x \le c \big(\| \zeta^{(u)} \|^2 + \| \zeta^{(v)} \|^2 \big). \tag{1.57}
$$

Next, consider the term $\int_0^1 \tilde{Q}Q_3 \, \mathrm{d}x$. Since the time derivative commutes with P, it transpires that

$$\left| \int_0^1 \tilde{Q}Q_3 \, \mathrm{d}x \right| \leq ch^\mu \Big(\|u_t\|_{W^{\mu+1,\infty}([0,1])} + \|v_t\|_{W^{\mu+1,\infty}([0,1])} \Big) \Big(\|\zeta^{(u)}\| + \|\zeta^{(v)}\| \Big) \tag{1.58}$$

(see Proposition 1.8 and part (iii) of Remark 1 following its proof). It remains to estimate the term $\int_0^1 \tilde{Q}Q_4 \, \mathrm{d}x$. Using integration by parts, it can be arranged as

$$\int_0^1 \tilde{Q}Q_4 dx = \sum_{\alpha,\beta,\gamma} \sum_{I \in \mathcal{T}_h} \left(c^1_{\alpha,\beta,\gamma} (\eta^{(\alpha)} \eta^{(\beta)}_x, \zeta^{(\gamma)})_I + c^2_{\alpha,\beta,\gamma} (w^{(\alpha)} \eta^{(\beta)}_x, \zeta^{(\gamma)})_I + c^3_{\alpha,\beta,\gamma} (w^{(\alpha)}_x \eta^{(\beta)}, \zeta^{(\gamma)})_I \right)$$

where each of the indices α, β, γ can be u or v and $c^i_{\alpha,\beta,\gamma}$ are constants depending on $A, B, \ldots, F$ as well as a, b, and c. Unfortunately the cancellations that occurred in the estimation of $\int_0^1 \tilde{Q}Q_1 dx$ do not appear here and, as will be seen, the terms in the second sum will cause a loss of one power of h.

Using (1.34) and (1.35) with $p = \infty,\ j = 0, 1$, it follows that

$$\|\eta^{(\beta)}\|_{L^\infty(I)} \leq ch^\mu \text{ and } \|\eta^{(\beta)}_x\|_{L^\infty(I)} \leq ch^{\mu-1}. \tag{1.59}$$

Since $\|w^{(\alpha)}\|_{L^\infty(I)}$ and $\|w^{(\alpha)}_x\|_{L^\infty(I)}$ are bounded, it is deduced that

$$\int_0^1 \tilde{Q}Q_4 \, \mathrm{d}x \leq ch^{\mu-1} \left(\|\zeta^{(u)}\| + \|\zeta^{(v)}\| \right) \tag{1.60}$$

The pieces above are now assembled to establish the convergence of the conservative semi-discrete approximations.

Theorem 1.11. *Suppose the solutions u, v of the system (1.1) are sufficiently smooth and periodic. Assume also that the relation $b^2 < 4ac$ holds. Then for initial data u_h^0, v_h^0 that are $O(h^q)$ approximations of $u(\cdot, 0)$, $v(\cdot, 0)$, respectively, the error bound*

$$\|u(t) - u_h(t)\| + \|v(t) - v_h(t)\| \leq ce^{ct}h^{q-1} \tag{1.61}$$

holds for the conservative semi-discrete approximations. If the mesh is uniform, then the bound on the right side is replaced by $ce^{ct}h^q$.

Proof. Gathering (1.49), (1.50) and (1.57)-(1.60) gives the inequality

$$\frac{\mathrm{d}}{\mathrm{d}t}\Omega(\zeta^{(u)}(t), \zeta^{(v)}(t)) \leq ch^{2\mu-2} + c\big(\|\zeta^{(u)}\|^2 + \|\zeta^{(v)}\|^2\big). \tag{1.62}$$

As seen before, $b^2 < 4ac$ implies that

$$\sigma\big(\|\zeta^{(u)}\|^2 + \|\zeta^{(v)}\|^2\big) \leq \Omega(\zeta^{(u)}, \zeta^{(v)}). \tag{1.63}$$

Hence an application of Gronwall's inequality to (1.62) yields

$$\Omega(\zeta^{(u)}(t), \zeta^{(v)}(t)) \leq ce^{ct}h^{2\mu-2}\Omega(\zeta^{(u)}(0), \zeta^{(v)}(0)). \tag{1.64}$$

Another application of (1.63) and the triangle inequality gives the bound (1.61). Finally, recall that $\mu = q + 1$ when the mesh is uniform. This gives the $O(h^q)$ error bound and concludes the proof. $\square$

Remark. *It is worth emphasizing the role played by the fact that the constants a, b and c satisfy* (1.4)*. This is precisely what allowed the quantities $Q_{1,2}$ and $Q_{1,3}$ to be written in a form that ultimately resulted in the estimates* (1.55) *and* (1.56) *being expressed solely in terms of the L^2-norms of $\zeta^{(u)}$ and $\zeta^{(v)}$.*

1.3.3 The dissipative formulation

The dissipative formulation is obtained by using the operator $\tilde{\mathcal{D}}$ instead of $\mathcal{D}$ in (1.44). The analysis of this method follows closely to that of the conservative one and so we content ourselves with highlighting the minor differences.

As far as the existence and uniqueness of the approximations $\tilde{u}_h, \tilde{v}_h$ are concerned, (1.46) still holds and $\mathcal{I}(\tilde{u}_h, \tilde{v}_h)$ vanishes also since the nonlinear forms are identical for both methods. Furthermore, using the identity

$$[\tilde{u}_{hx}\tilde{v}_{hx}]_m = \tilde{u}_{hx}(x_m^+)[\tilde{v}_{hx}]_m + \tilde{v}_{hx}(x_m^-)[\tilde{u}_{hx}]_m,$$

it is seen that $\tilde{\mathcal{D}}(\tilde{u}_h, \tilde{v}_h) + \tilde{\mathcal{D}}(\tilde{v}_h, \tilde{u}_h) = \sum_{m=0}^{M-1} [\tilde{u}_{hx}]_m[\tilde{v}_{hx}]_m$. Combining this with (1.21) leads to

$$\frac{\mathrm{d}}{\mathrm{d}t}\Omega(\tilde{u}_h, \tilde{v}_h) + \sum_{m=0}^{M-1} \left(a[\tilde{u}_{hx}]_m^2 + b[\tilde{u}_{hx}]_m[\tilde{v}_{hx}]_m + c[\tilde{v}_{hx}]_m^2\right) = 0.$$

The condition $b^2 < 4ac$ implies that the sum appearing above is nonnegative. In fact it is bounded from below by $\sigma \sum_{m=0}^{M-1} \left([\tilde{u}_{hx}]_m^2 + [\tilde{v}_{hx}]_m^2\right)$. It is therefore the case that $\frac{\mathrm{d}}{\mathrm{d}t}\Omega(\tilde{u}_h, \tilde{v}_h) \leq 0$ which means that $\Omega(\tilde{u}_h, \tilde{v}_h)$ is bounded for all time by its value at $t = 0$. This indeed motivates calling this method dissipative. The global existence and uniqueness of $\tilde{u}_h, \tilde{v}_h$ follow as before.

The error estimates for the dissipative method can be established using the same approach followed for the conservative method. The major difference is that $\tilde{u}_h$ and $\tilde{v}_h$ are now compared to $\tilde{w}^{(u)}$ and $\tilde{w}^{(v)}$, respectively. The optimal, local estimates (1.26) are used, together with the bounds on $\tilde{w}^{(u)}$, $\tilde{w}_x^{(u)}$, $\tilde{w}^{(v)}$, $\tilde{w}_x^{(v)}$ in the L^∞-norm. Note that the latter hold without any quasi-uniformity restrictions on the mesh. One power of h is still lost due to the nonlinear terms.

Theorem 1.12. *Suppose the solution (u, v) of the system (1.1) is sufficiently smooth and that the relation $b^2 < 4ac$ holds. Then for initial data $\tilde{u}_h^0$, $\tilde{v}_h^0$ that are $O(h^q)$ approximations to $u(\cdot, 0)$, $v(\cdot, 0)$, respectively, the error bound*

$$\|u(t) - \tilde{u}_h(t)\| + \|v(t) - \tilde{v}_h(t)\| \leq ce^{ct}h^q. \tag{1.65}$$

is valid for the dissipative, semi-discrete approximations.

1.3.4 The fully discrete approximations

In this subsection, consideration is given to adding time-stepping to the semi-discrete scheme studied above. It will turn out that a good choice of the time stepping, namely the implicit Runge-Kutta (IRK) methods belonging to the Gauss-Legendre family results in a fully discrete scheme that continues to preserve the functional Ω, up to roundoff error of course.

Let $0 = t^0 < t^1 < \cdots < t^N = T$ be a partition of the temporal interval $[0, T]$ with $t^n = n\kappa$, $n = 0, \ldots, N$ where κ is the stepsize. The IRK methods are specified by an $s \times s$ matrix $A = (a_{ij})$, an s-vector $\tau = \{\tau_1, \ldots, \tau_s\}$ of temporal interpolation nodes and an s-vector $\mathbf{w} = \{w_1, \ldots, w_s\}$ of weights. These are often represented in tableau form, $\dfrac{A|\tau}{\mathbf{w}|}$. For the initial-value problem of an ordinary differential equation $y' = f(t, y)$, the discrete time stepping is given by the mapping $y^n \to y^{n+1}$ with $y^{n+1} = y^n + \kappa \sum_{i=1}^{s} w_i f(t^n + \kappa\tau_i, y^{n,i})$ where the s *intermediate values* $\{y^{n,i}\}_{i=1}^{s}$ are solutions of the system

$$y^{n,i} = y^n + \kappa \sum_{j=1}^{s} a_{ij} f(t^n + \kappa\tau_j, y^{n,j}), \quad i = 1, 2, \ldots, s.$$

Certain classes of IRK methods possess a particularly strong type of stability, namely that of *algebraic stability*, viz.,

$$w_i \geq 0,\ i = 1, 2, \ldots, s, \tag{1.66}$$

the $s \times s$ matrix $m_{ij} := a_{ij}w_i + a_{ji}w_j - w_i w_j$ is positive semi-definite.

Two classes of IRK schemes with this property are the Radau-IIA and Gauss-Legendre methods. For the latter, the matrix M in (1.66) vanishes identically. It is precisely this feature that imparts them with the conservation properties that are sought here. The next table shows the first three members of the Gauss-Legendre family, corresponding to $s = 1$, 2, and 3.

Table 1.1: Gauss-Legendre Implicit Runge-Kutta methods: $s = 1, 2$, and 3

$$\begin{array}{c|c} \frac{1}{2} & \frac{1}{2} \\ \hline 1 & \end{array}$$

$$\begin{array}{cc|c} \frac{1}{4} & \frac{1}{4} - \frac{1}{2\sqrt{3}} & \frac{1}{2} - \frac{1}{2\sqrt{3}} \\ \frac{1}{4} + \frac{1}{2\sqrt{3}} & \frac{1}{4} & \frac{1}{2} + \frac{1}{2\sqrt{3}} \\ \hline \frac{1}{2} & \frac{1}{2} & \end{array}$$

$$\begin{array}{ccc|c} \frac{5}{36} & \frac{80 - 24\sqrt{15}}{360} & \frac{50 - 12\sqrt{15}}{360} & \frac{1}{2} - \frac{\sqrt{15}}{10} \\ \frac{50 + 15\sqrt{15}}{360} & \frac{2}{9} & \frac{50 - 15\sqrt{15}}{360} & \frac{1}{2} \\ \frac{50 + 12\sqrt{15}}{360} & \frac{80 + 24\sqrt{15}}{360} & \frac{5}{36} & \frac{1}{2} + \frac{\sqrt{15}}{10} \\ \hline \frac{5}{18} & \frac{8}{18} & \frac{5}{18} & \end{array}$$

For smooth problems the order of accuracy is $2s$. The first two methods are used in the numerical experiments reported in Section 4. They are referred to as RK1 and RK2, respectively.

The fully discrete method that arises from using an IRK method to approximate solutions of the semi-discrete formulation (1.44) of our systems is as follows:

$$u^{n+1} = u^n - \kappa \sum_{i=1}^{s} w_i f_u^i, \quad u^{n,i} = u^n - \kappa \sum_{j=1}^{s} a_{ij} f_u^j, \quad i = 1, 2, \ldots, s, \tag{1.67}$$

$$v^{n+1} = v^n - \kappa \sum_{i=1}^{s} w_i f_v^i, \quad v^{n,i} = v^n - \kappa \sum_{j=1}^{s} a_{ij} f_v^j, \quad i = 1, 2, \ldots, s \tag{1.68}$$

where the quantities f_u^j, f_v^j given by

$$\begin{bmatrix} f_u^i \\ f_v^i \end{bmatrix} = \begin{bmatrix} A & B & C \\ D & E & F \end{bmatrix} \begin{bmatrix} \mathcal{N}(u^{n,i}, u^{n,i}) \\ \mathcal{N}(u^{n,i}, v^{n,i}) \\ \mathcal{N}(v^{n,i}, v^{n,i}) \end{bmatrix} + \begin{bmatrix} \mathcal{D}u^{n,i} \\ \mathcal{D}v^{n,i} \end{bmatrix} \tag{1.69}$$

are introduced to simplify the notation.

Theorem 1.13. *The fully discrete scheme using the conservative spatial formulation together with the Gauss-Legendre IRK methods has the property that*

$$\Omega(u^{n+1}, v^{n+1}) = \Omega(u^n, v^n), \; n \geq 0. \tag{1.70}$$

That is, the continuous invariant Ω, when evaluated on discrete approximations is time-step independent.

Proof. From (1.67), it is seen that

$$\begin{aligned}(u^{n+1})^2 &= (u^n)^2 - 2\kappa\sum_{j=1}^{s} w_j u^n f_u^j + \kappa^2 \sum_{i,j=1}^{s} w_i w_j f_u^i f_u^j \\ &= (u^n)^2 - 2\kappa\sum_{j=1}^{s} w_j \Big(u^{n,j} + \kappa\sum_{i=1}^{s} a_{ji} f_u^i\Big) f_u^j + \kappa^2 \sum_{i,j=1}^{s} w_i w_j f_u^i f_u^j \\ &= (u^n)^2 - 2\kappa\sum_{j=1}^{s} w_j u^{n,j} f_u^j - \kappa^2 \sum_{i,j=1}^{s} m_{ij} f_u^i f_u^j \\ &= (u^n)^2 - 2\kappa\sum_{j=1}^{s} w_j u^{n,j} f_u^j,\end{aligned} \tag{1.71}$$

where the last identity reflects the vanishing of the array M. By entirely similar calculations, there appears

$$\begin{aligned}(v^{n+1})^2 &= (v^n)^2 - 2\kappa\sum_{j=1}^{s} w_j v^{n,j} f_v^j \\ u^{n+1}v^{n+1} &= u^n v^n - \kappa\sum_{j=1}^{s} w_j u^{n,j} f_v^j - \kappa\sum_{j=1}^{s} w_j v^{n,j} f_u^j.\end{aligned} \tag{1.72}$$

Multiply (1.71) by a, the first equation in (1.72) by c and the second equation in (1.72) by b, sum the results and integrate over $[0,1]$. These calculations, which are almost identical to those seen in the proofs of Lemma 1.9 and Theorem 1.10 show that

$$\begin{aligned}\Omega(u^{n+1}, v^{n+1}) &= \Omega(u^n, v^n) - \kappa\sum_{j=1}^{s} w_j \Big(2a(f_u^j, u^{n,j}) + b(f_u^j, v^{n,j}) + b(f_v^j, u^{n,j}) + 2c(f_v^j, v^{n,j})\Big) \\ &= \Omega(u^n, v^n) - \kappa\sum_{j=1}^{s} w_j \Big(\mathcal{I}(u^{n,j}, v^{n,j}) + 2a\mathcal{D}(u^{n,j}, u^{n,j}) + b\big(\mathcal{D}(u^{n,j}, v^{n,j}) \\ &\qquad + \mathcal{D}(v^{n,j}, u^{n,j})\big) + 2c\mathcal{D}(v^{n,j}, v^{n,j})\Big).\end{aligned} \tag{1.73}$$

In particular, it emerged from those previous proofs that

$$\mathcal{I}(u^{n,j},v^{n,j})=\mathcal{D}(u^{n,j},u^{n,j})=\mathcal{D}(u^{n,j},v^{n,j})+\mathcal{D}(v^{n,j},u^{n,j})=\mathcal{D}(v^{n,j},v^{n,j})=0. \tag{1.74}$$

These identities, when used in (1.73) establish the temporal conservation property (1.70) of the fully discrete schemes. □

Remark. *In the dissipative spatial formulation that uses the form $\tilde{\mathcal{D}}$ instead of $\mathcal{D}$, we still have $\mathcal{I}(u^{n,j},v^{n,j})=0$. However, the remaining terms in (1.74) do not vanish. Instead, it can be shown that the quantity*

$$2a\tilde{\mathcal{D}}(u^{n,j},u^{n,j})+b\big(\tilde{\mathcal{D}}(u^{n,j},v^{n,j})+\tilde{\mathcal{D}}(v^{n,j},u^{n,j})\big)+2c\tilde{\mathcal{D}}(v^{n,j},v^{n,j})$$

appearing in (1.73) is equal to $\sum_{m=0}^{M-1}\Big(a[u_x^{n,j}]_m^2+b[u_x^{n,j}]_m[v_x^{n,j}]_m+c[v_x^{n,j}]_m^2\Big)$. Since we are operating under the assumption that $4ac-b^2>0$, the latter sum is greater than $\sigma\sum_{m=0}^{M-1}\big([u_x^{n,j}]_m^2+[v_x^{n,j}]_m^2\big)$, for some positive σ, and is therefore nonnegative. In view of this, the nonnegativity of κ and the weights w_j, the inequality $\Omega(u^{n+1},v^{n+1})\le\Omega(u^n,v^n)$ obtains for the dissipative formulation.

Remark. *For other algebraically stable IRK methods, the fully discrete approximations will no longer enjoy the conservation property (1.70) that obtains for those generated by the Gauss-Legendre methods. On the other hand, it is clear from the proof above that the stability result $\Omega(u^{n+1},v^{n+1})\le\Omega(u^n,v^n)$ will replace (1.70).*

1.4 Numerical Experiments

1.4.1 The test cases

To adapt the experiments to the interval $[0, 1]$, the third derivative terms in (1.1) are multiplied by a small parameter ϵ to be specified shortly. The parameters $A, B, \ldots, F$ are taken to be

$$A = \frac{1}{8}, \quad B = \frac{1}{8}, \quad C = \frac{1}{32}, \quad D = \frac{1}{8}, \quad E = 1, \quad F = -\frac{9}{32}. \tag{1.75}$$

These choices result in $a = \frac{118}{17}$, $b = -\frac{28}{17}$, and $c = 1$, which in turn yields the positive discriminant $4ac - b^2 = \frac{7240}{289}$.

To check the accuracy and convergence rates, two types of solutions of (1.1) were used. These are both proportional traveling waves of the form $(u, v) = (u, 2u)$. The first is adapted from the well known *cnoidal-wave* solution of the KdV equation,

$$u(x, t) = \lambda\, \mathrm{cn}^2\big(4K(m)(x - \omega t - x_0) : m\big) \tag{1.76}$$

where $cn(z) = cn(z : m)$ is the Jacobi elliptic function with modulus $m \in (0, 1)$ (see [1]) and the parameters have the values $m = 0.9$, $\lambda = 192m\epsilon K(m)^2$, $\omega = 64\epsilon(2m-1)K(m)^2$, $\epsilon = \frac{1}{576}$ whilst $x_0 = \frac{1}{2}$ centers the initial value in the middle of the interval. Here, the function $K = K(m)$ is the complete elliptic integral of the first kind and the parameters are so organized that u and v have spatial period 1.

The second class of solutions is an approximation of the proportional solitary-wave solutions that were discussed in Section 1.1.2. The parameters $A, B, \ldots, F$ are the same as for the cnoidal-wave type solutions, and it is still the case that $(u, v) = (u, 2u)$, but now

$$u(x,t) = \Lambda \operatorname{sech}^2\big(K(x - \omega t - x_0)\big), \tag{1.77}$$

with $\Lambda = 1$, $\omega = \Lambda/3$, $\epsilon = \frac{1}{5760}$, $K = \frac{1}{2}\sqrt{\frac{\Lambda}{3\epsilon}}$ and $x_0 = \frac{1}{2}$ to again center the initial wave profile. With $v = 2u$, this is an exact solution of the system which is manifestly not periodic in space. Owing to its symmetry about its crest and its exponential decay away from the crest, the initial data can be rendered periodic by simply restricting the above solution at $t = 0$ to the computational domain $[0, 1]$ and imposing periodic boundary conditions across $x = 0$ and $x = 1$. The resulting periodicized initial data yields a periodic solution of the system. It is known from previous theory that the resulting solution is approximated to within order ϵ by the restriction of $(u, 2u)$ to the period domain $[0, 1]$ over a time interval of order $\frac{1}{\epsilon}$ (c.f. [9] and [22]). The small value of ϵ used in the experiments with proportional solitary waves thus yields a solution, the accuracy of whose numerical approximation can be determined by comparison with the exact solution $(u, 2u)$ with u as in (1.77). Much of the numerical work on the KdV equation has made use of this small trick to check for accuracy and convergence, especially when issues surrounding solitary waves are under consideration.

1.4.2 Spatial Convergence Rates

A set of experiments was designed to measure the spatial convergence rates of our schemes. In particular, we wanted to assess the extent of agreement of what is observed empirically with the theoretical predictions made earlier. Of course, there is always interest in the asymptotic constants whose existence is suggested by the error estimates. (There is a considerable practical difference between a scheme that throws up an error of 10^2h^2, say, and one whose error looks like $10^{-2}h^2$.) But, especial interest is also focused on discovering whether the parity of q has a significant impact on the convergence rates for the conservative formulation (see the discussion in Section 3).

Tables 1.2, 1.3, 1.4, and 1.5 correspond to $q = 2$, 3, 4 and 5. They show, respectively, the results obtained with uniform meshes of M cells for both conservative and dissipative methods and for the cnoidal and solitary-wave solutions just described. The time step κ was taken as 10^{-5} in Tables 1.2, 1.3, and 1.4, whilst in Table 1.5, the results pertaining to several different time steps are displayed. The L^2-norms of the errors are shown only for u. Since v is proportional to u, it is not surprising that the errors for v appear to be proportional to those for u.

Before engaging in a discussion of the results displayed in Tables 1.2, 1.3, 1.4, and 1.5, it is worth remarking that the determination of convergence rates is somewhat delicate, especially for the larger values of q. This is due to the very small errors achieved even for relatively small numbers M of spatial intervals. The errors are sufficiently small that the effects of roundoff, which are very difficult to estimate precisely, cannot be ignored and may affect the rates.

For $q = 2$, Table 1.2 shows clearly convergence rates of 2 and 3 for the conservative and dissipative methods, respectively, for both the cnoidal and solitary wave solutions. For $q = 4$, the rates shown in Table 1.4, while less definitive, seem to indicate a similar reduction of order for the conservative method. For the odd values $q = 3$ and $q = 5$, the rates appear to be $q + 1$ for both methods. One noticeable exception is in Table 1.5(b) where we see the rates of 3.62 and 8.41 for the conservative method. However, using the errors at $M = 25$ and $M = 100$ we obtain the robust rate of 6.02.

Table 1.2: $q = 2, T = 1, \kappa = 10^{-5}$, RK1

(a) Cnoidal solution

	Conservative		Dissipative	
M	L^2 Error	Rate	L^2 Error	Rate
10	3.27×10^{-1}	—	4.02×10^{-1}	—
20	9.90×10^{-2}	1.73	1.12×10^{-2}	1.84
40	2.58×10^{-2}	1.94	1.71×10^{-2}	2.71
80	6.52×10^{-3}	1.99	2.20×10^{-3}	2.96
160	1.64×10^{-3}	1.99	2.74×10^{-4}	3.00
320	4.09×10^{-4}	2.00	3.41×10^{-5}	3.01

(b) Solitary-wave Solution

	Conservative		Dissipative	
M	L^2 Error	Rate	L^2 Error	Rate
10	1.41×10^{-1}	—	2.32×10^{-1}	—
20	5.96×10^{-2}	1.24	1.07×10^{-1}	1.12
40	1.90×10^{-2}	1.65	3.86×10^{-2}	1.47
80	5.19×10^{-3}	1.88	6.24×10^{-3}	2.63
160	1.32×10^{-3}	1.97	8.14×10^{-4}	2.94
320	3.32×10^{-4}	2.00	1.02×10^{-4}	3.00

Table 1.3: $q = 3, T = 1, \kappa = 10^{-5}$, RK2

(c) Cnoidal solution

	Conservative		Dissipative	
M	L^2 Error	Rate	L^2 Error	Rate
40	2.81×10^{-5}	—	1.05×10^{-4}	—
80	1.23×10^{-6}	4.51	3.70×10^{-6}	4.83
160	7.28×10^{-8}	4.08	1.56×10^{-7}	4.57
320	4.50×10^{-9}	4.02	8.75×10^{-9}	4.15

(d) Solitary-wave solution

	Conservative		Dissipative	
M	L^2 Error	Rate	L^2 Error	Rate
40	2.55×10^{-3}	—	1.27×10^{-3}	—
80	1.01×10^{-5}	7.98	4.48×10^{-5}	4.82
160	4.65×10^{-7}	4.43	1.52×10^{-6}	4.88
320	2.42×10^{-8}	4.27	5.82×10^{-8}	4.71

Table 1.4: $q = 4$, $T = 1$, $\kappa = 10^{-5}$, RK2

(a) Cnoidal solution

	Conservative		Dissipative	
M	L^2 Error	Rate	L^2 Error	Rate
10	5.21×10^{-3}	—	4.92×10^{-3}	—
20	5.43×10^{-5}	6.58	6.66×10^{-5}	6.21
40	3.46×10^{-6}	3.97	1.29×10^{-6}	5.69
80	1.59×10^{-7}	4.44	3.83×10^{-8}	5.07
120	2.99×10^{-8}	4.12	5.04×10^{-9}	5.00

(b) Solitary-wave solution

	Conservative		Dissipative	
M	L^2 Error	Rate	L^2 Error	Rate
10	3.76×10^{-2}	—	4.82×10^{-2}	—
20	2.51×10^{-3}	3.90	2.23×10^{-3}	4.43
40	1.78×10^{-5}	7.13	2.90×10^{-5}	6.26
80	1.09×10^{-6}	4.03	4.81×10^{-7}	5.91
120	1.72×10^{-7}	4.55	5.78×10^{-8}	5.06

Table 1.5: $q = 5$, $T = 1$, $\kappa = 1/160, 1/1280, 1/10240$, RK1

(a) Cnoidal solution

	Conservative		Dissipative	
M	L^2 Error	Rate	L^2 Error	Rate
25	2.32×10^{-3}	—	2.32×10^{-3}	—
50	3.64×10^{-5}	5.99	3.64×10^{-5}	5.99
100	5.68×10^{-7}	6.00	5.71×10^{-7}	6.00

(b) Solitary-wave solution

	Conservative		Dissipative	
M	L^2 Error	Rate	L^2 Error	Rate
25	8.63×10^{-4}	—	8.56×10^{-4}	—
50	7.01×10^{-5}	3.62	1.32×10^{-5}	6.02
100	2.05×10^{-7}	8.41	2.06×10^{-7}	6.01

As far as the conservative method is concerned, the data strongly indicates order reduction by one for even q. On the other hand the parity of the number of cells appeared to be immaterial. Concerning the order reduction of one due to the nonlinear terms seen in Theorems 1.11 and 1.12 affecting both methods, it can be reasonably concluded that this is an artifact of the proof. If indeed it does not owe to a fundamental phenomenon, an interesting open problem is highlighted.

1.4.3 Long time simulations

Overall, the errors for the two methods are comparable, at least on time scales of order 1. The conservative method has a slight edge for the odd values $q = 3, 5$ of the order of the piecewise polynomials that comprise the spatial basis, the opposite being true for the even orders $q = 2, 4$. Next is undertaken a comparative study of the long-time behaviour of the two methods. The working expectation here is that the conservation of the invariant Ω should have beneficial consequences when it comes to long-time calculations.

Figures 1.1, 1.2, 1.3, and 1.4 that are exhibited provide a descriptive view of the approximations of solitary-wave solutions up to time $T = 1000$ for the two methods. They correspond to $q = 2$, $M = 80$, $q = 2$, $M = 160$, $q = 3$, $M = 80$, $q = 3$, $M = 160$, respectively.

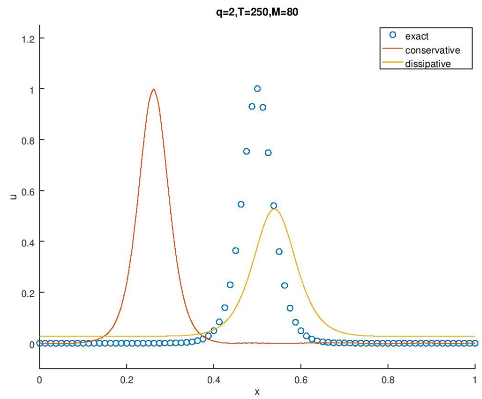

(a) $t = 250$

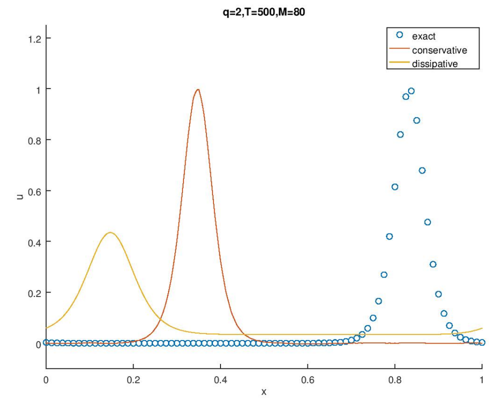

(b) $t = 500$

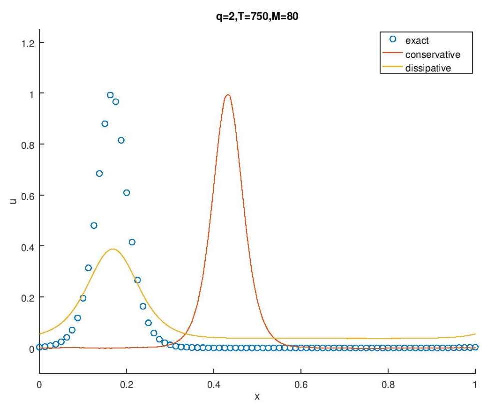

(c) $t = 750$

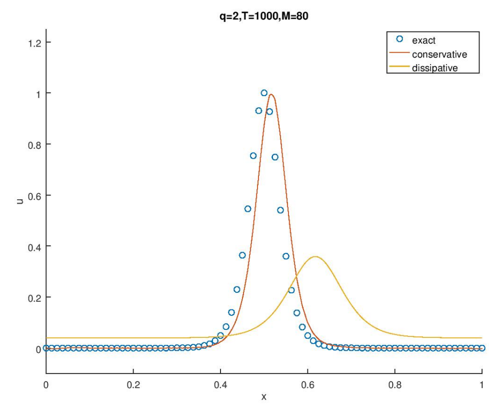

(d) $t = 1000$

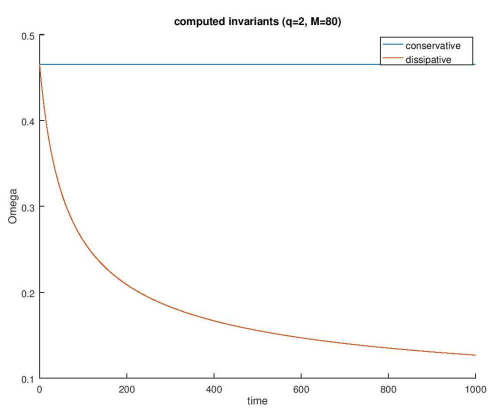

(e) computed values of Ω

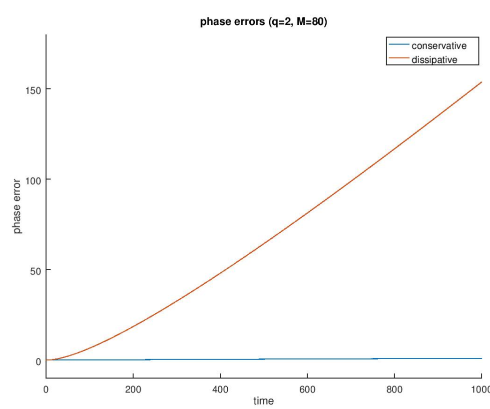

(f) phase error

Figure 1.1: $q = 2, M = 80$

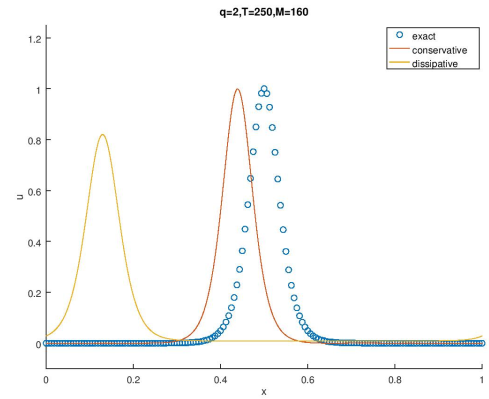

(a) $t = 250$

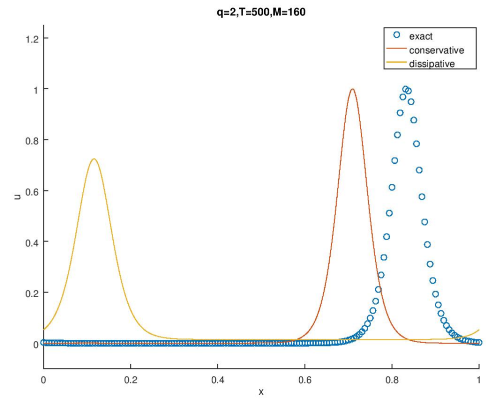

(b) $t = 500$

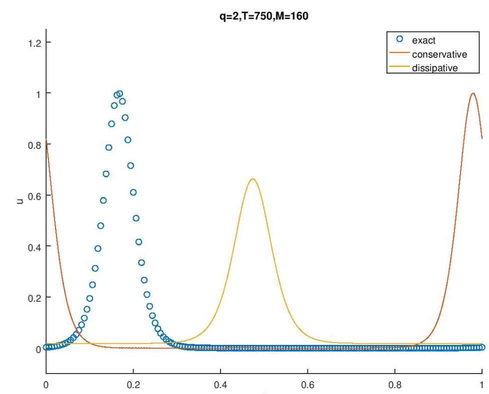

(c) $t = 750$

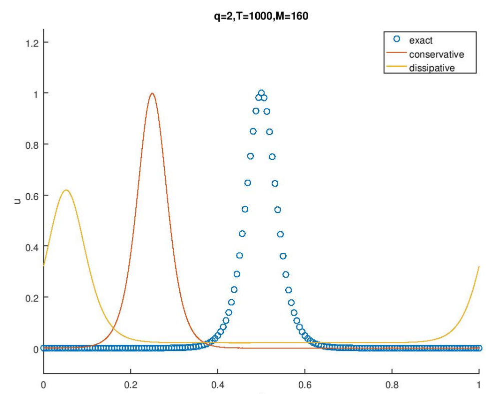

(d) $t = 1000$

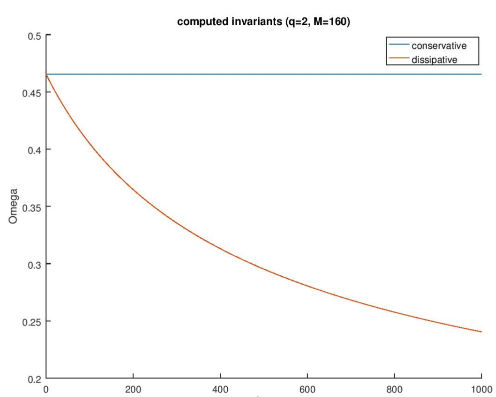

(e) computed values of Ω

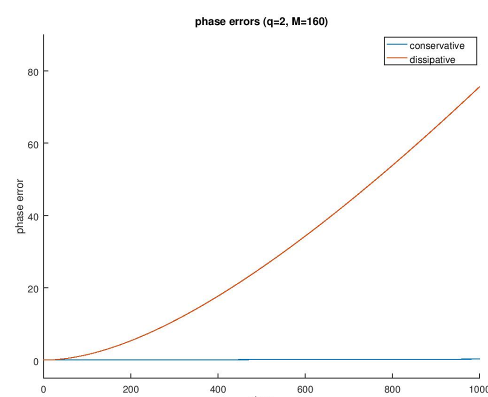

(f) phase error

Figure 1.2: $q = 2$, $M = 160$

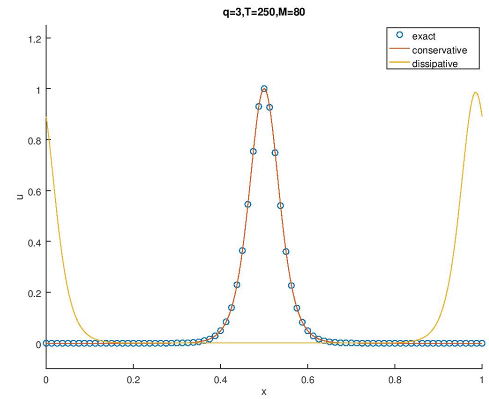

(a) $t = 250$

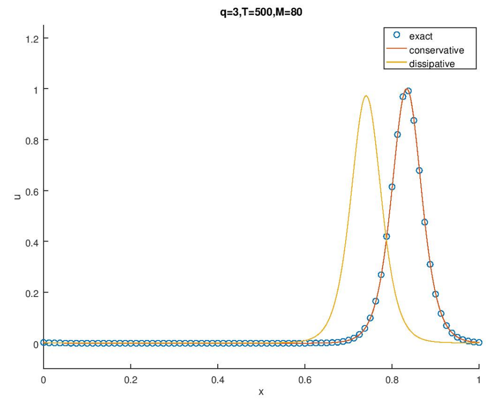

(b) $t = 500$

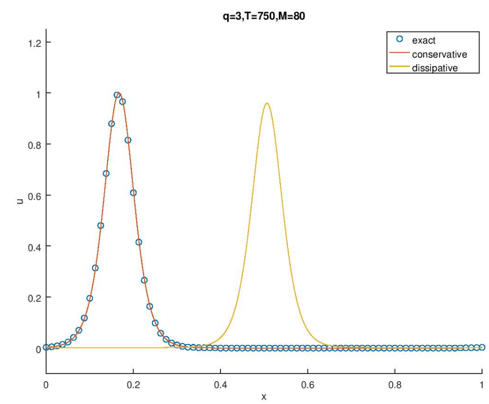

(c) $t = 750$

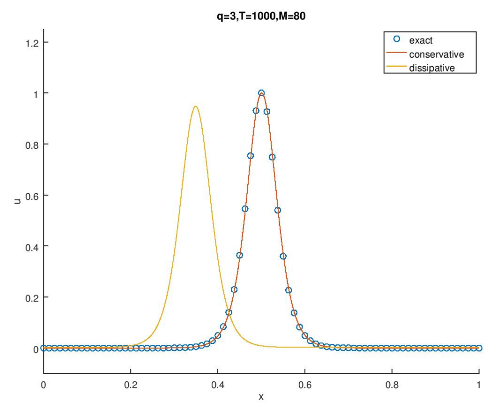

(d) $t = 1000$

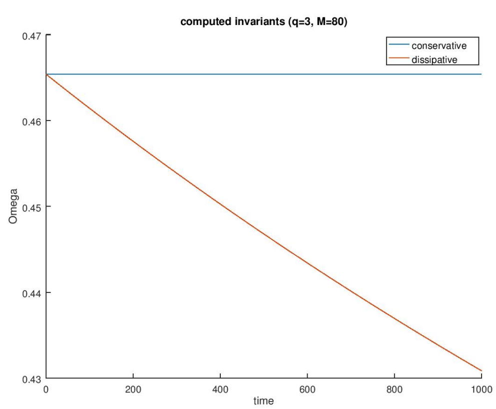

(e) computed values of Ω

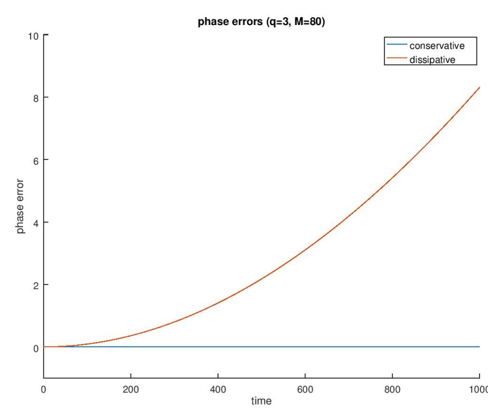

(f) phase error

Figure 1.3: $q = 3, M = 80$

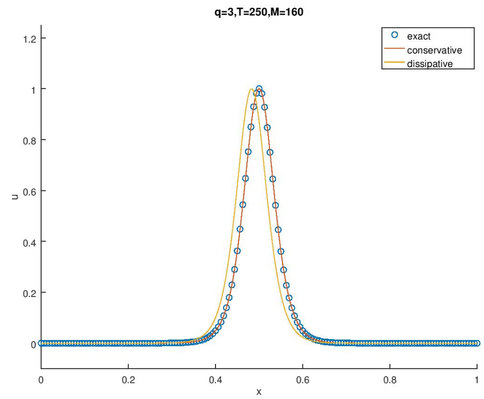

(a) $t = 250$

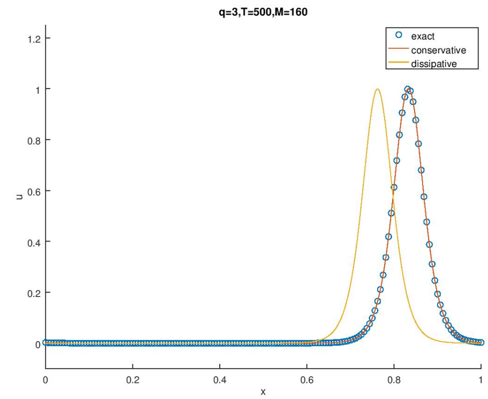

(b) $t = 500$

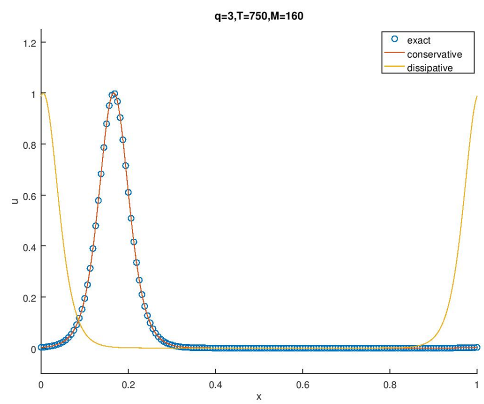

(c) $t = 750$

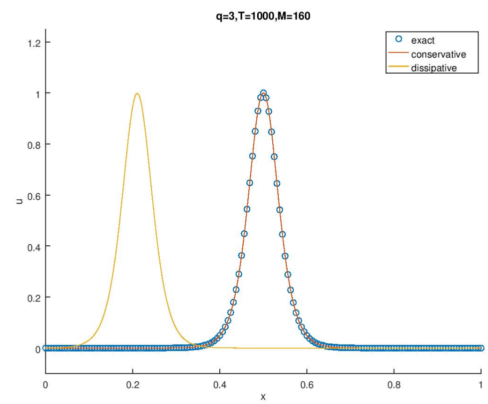

(d) $t = 1000$

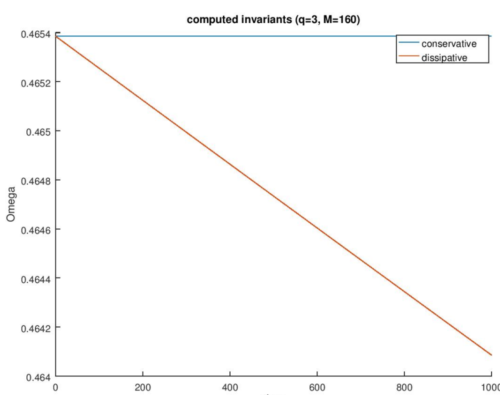

(e) computed values of Ω

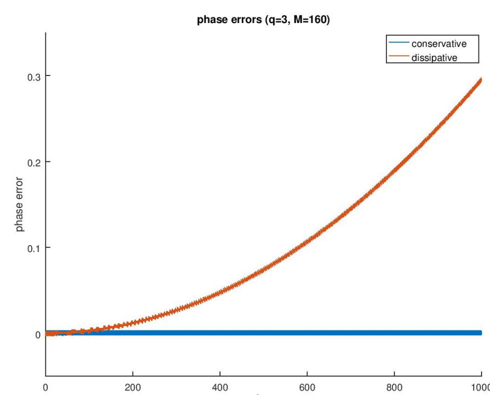

(f) phase error

Figure 1.4: $q = 3$, $M = 160$

The graphs of the quantity Ω exhibited in part (e) of each figure show agreement with the theory. That is to say, Ω is sensibly invariant when the integration is performed using the conservative method, whereas it is monotonically decreasing when the dissipative method is employed. This decrease appears to be a linear function of time as can be seen clearly in the more accurate simulations corresponding to $q = 3$.

Before embarking on an interpretation of the remaining graphs, some commentary is helpful. In the context of the numerical approximation of solitary-wave solutions of nonlinear, dispersive equations of KdV type, a plethora of experiments have shown that a lag develops between the locations of the crest of the solution and its approximations. This lag, or phase error, grows in time to a point where it becomes the majority contributor to the overall error. It can be mitigated by increased accuracy and the use of conservative numerical methods, but it cannot be completely eliminated. In fact, the solitary-wave solution being approximated is known to be orbitally stable (see [11]). This means that if the system is initiated with initial data (u_0, v_0) that is close to a solitary-wave solution $(r(x-\omega t), s(x-\omega t))$ at $t = 0$, then the solution (u, v) emanating from (u_0, v_0) will always be close to that solitary wave in *shape*. More precisely, because $4ac - b^2 > 0$ in conjunction with another condition spelled out in [11], the quantity

$$\inf_{\theta\in\mathbb{R}} \int_{\mathbb{R}} \Big(u(x,t) - r(x-\theta)\Big)^2 + \Big(v(x,t) - s(x-\theta)\Big)^2 \, \mathrm{d}x \tag{1.78}$$

is uniformly small for all time. The minimization (1.78) defines a function $\theta = \theta(t)$ and the phase error is then taken to be

$$e(t) \;=\; |\theta(t) - \omega t|. \tag{1.79}$$

What is important to realize is that while a perturbation stays close in shape, the corresponding solution (u, v) appears to resolve into a solitary wave which in general has a slightly different speed of propagation. In consequence, the phase error necessarily grows linearly with time. The growth cannot be too fast since it is known that

$$|\theta'(t) - \omega|$$

always remains small (see e.g. [20], [37]).

One can think of the numerical scheme as a perturbation of the continuous initial-value problem. Viewed in this light, and taking into account the above discussion of the continuous problem, one expects a phase error to be associated with the numerical approximation of the solution. The main purpose of the longer-time experiments is to offer a numerical study of the phase error, by which we mean the gap between the location of the crest of the solitary wave solution at time t and its numerical approximation at the same time. Thus in (1.78), (u, v) will be the numerical approximation of the solution and (r, s) will be the relevant proportional solitary wave. For $q = 2$, $M = 80$, both conservative and dissipative methods show significant phase errors with the former proving superior to the latter. Another striking aspect is the marked loss of amplitude the approximation suffers when using the dissipative method, whereas the conservative approximations appear to be remarkably accurate in shape. Furthermore, the dissipative approximation seems to have spread to the point where the solution no longer gets back to zero away from its crest. In Figure 1.2, doubling the number of cells has resulted in a quantitative improvement for both methods with the conservative method continuing to hold an edge. The phase errors persist for both methods, however.

Figures 1.3 and 1.4 correspond to $q = 3,\ M = 80$ and $q = 3,\ M = 160$, respectively. Since q is odd, the conservative method has the same convergence rate as the dissipative method for these runs. The phase error appears to be eliminated when using the conservative scheme, whereas it still persists albeit to a less severe degree for the dissipative method. For $M = 80$, a small decrease in amplitude for the latter method is still present. Finally, we note that there is indication of superlinear growth of the phase error in all the runs involving the dissipative method.

Summary and future work We have constructed conservative and dissipative finite element methods for a system of Korteweg-de Vries type equations coupled through their nonlinearities. The associated semi-discrete approximations have been investigated in detail and shown to be globally well posed when certain relationships hold between the coefficients of the nonlinear terms. These are the same conditions that had been used previously in proving the well-posedness of the continuous system (1.1).

The semi-discrete approximations were shown to converge to the associated solutions of the full system of PDEs and spatial convergence rates provided. For the dissipative scheme, this follows standard lines. However, interesting additional conditions on the parity of the degree of the piecewise polynomial basis for the finite element space and on the number of cells were needed for the analysis of the conservative method. While a little puzzling, such conditions have appeared in other works associated with the analysis of conservative methods.

A number of tests have been conducted to provide a limited but illuminating assessment of the actual impact of these conditions and also to provide a comparative view of the performance of the conservative and dissipative methods. Based on this evidence, it is safe to conclude that the conservative method with $q = 3$ offers an efficient and effective tool for simulations over very long time intervals.

In a companion project further investigation of the systems of the form (1.1) is in progress. This includes questions of blow-up for the systems not satisfying the condition $4ac - b^2 \geq 0$ that figured so prominently in the present work and instability and interaction results for the proportional solitary waves.

Chapter 2

A posteriori error estimates for finite element methods for nonlinear, dispersive equations

2.1 Introduction

In this chapter, we continue to consider finite element methods for the initial-boundary value problem (IBVP) for a coupled system of Korteweg-de Vries type equations

$$\begin{aligned} u_t + u_{xxx} + P(u,v)_x = 0 \\ v_t + v_{xxx} + Q(u,v)_x = 0 \end{aligned} \tag{2.1}$$

with periodic boundary conditions on the interval $[0, 1]$, yet from an *a posteriori* perspective. We remind the reader that, here, the dependent variables $u = u(x, t)$ and $v = v(x, t)$ are real-valued functions, subscripts denote partial differentiation, and the nonlinearities are taken to be homogeneous quadratic polynomials in u and v, *viz.* $P(u,v) = Au^2 + Buv + Cv^2$ and $Q(u,v) = Du^2 + Euv + Fv^2$ for given real coefficients $A, B, \ldots, F$.

2.1.1 Local and global well-posedness

We review a few results from Chapter 1 [12] crucial to the theory developed in this chapter, devoting particular attention to a crucial invariant of (2.1) and a positive-definiteness condition that is useful to the theory for not only the PDE system but also the corresponding numerical schemes. For a detailed discussion regarding local and global well-posedness of IBVPs for the system (2.1) as well as a review of related theory for the single KdV equation, we refer the reader to our previous work [12, Section 1.1], reprinted in Chapter 1 of this dissertation.

As we discussed in Chapter 1, it is well-known that for solutions of the system (2.1) that are in $H^s(\mathbb{R}) \times H^s(\mathbb{R})$ for $s \geq 0$, the integral

$$\Omega(u,v) = \int_{\mathbb{R}} \left(au^2 + buv + cv^2\right) \mathrm{d}x \tag{2.2}$$

is independent of time. We remind the reader that the constants $a, b,$ and c comprise any nontrivial solution of the system

$$\begin{aligned} 2Ba + (E - 2A)b - 4Dc &= 0 \\ 4Ca + (2F - B)b - 2Ec &= 0 \end{aligned} \tag{2.3}$$

of two linear equations in three unknowns. If $s \geq 1$, the integral

$$\Theta(u,v) = \int_{\mathbb{R}} \Big(au_x^2 + bu_xv_x + cv_x^2 - R(u,v) \Big) \, \mathrm{d}x, \tag{2.4}$$

with

$$R(u,v) = \frac{\alpha}{3}u^3 + \beta u^2 v + \gamma u v^2 + \frac{\delta}{3}v^3, \tag{2.5}$$

is also time-independent for u, v that solve the system (2.1). Here, the real constants α, β, γ, and δ depend upon the original coefficients, $A, B, \dots, F$. For their explicit form, see [11, Equation (2.6)]. We remind the reader that when the quadratic form $\Upsilon(x,y) = ax^2 + bxy + cy^2$ is positive-definite, which is to say, $b^2 - 4ac < 0$ (a condition that will also appear in the numerical analysis below), it is these invariants that allow the local theory to be extended to global well-posedness if $s \geq 0$. Via a further, energy-type argument as in [25] and an observation from [11], this result can be improved so that (2.1) is globally well posed for arbitrarily sized data in $H^s(\mathbb{R}) \times H^s(\mathbb{R})$ for any $s > -\frac{3}{4}$ if $b^2 - 4ac \leq 0$.

However, for the systems (2.1), the well-posedness in $H^s(\mathbb{T})$ is not as well-studied. Yet, an argument like that of Bona-Smith [19] taken with the *a priori* $H^1(\mathbb{T})$-bound provided by the invariants (2.2) and (2.4) when $b^2 - 4ac < 0$ indeed yields global well-posedness for $s \geq 1$. While this result seems ripe for improvement, global well-posedness in $H^s(\mathbb{T}) \times H^s(\mathbb{T})$ for $s \geq 1$ again suffices for the error estimates of this chapter. Indeed, mimicing the PDE theory, it is crucial for the *a posteriori* analysis below to assume that the constants a, b, and c satisfy the positive-definiteness condition $b^2 - 4ac < 0$.

2.1.2 Background for the *a posteriori* analysis

Due to their wide-ranging use in application and theory, efficient, accurate numerical approximation of nonlinear, dispersive systems is of great interest and the general focus of this dissertation. As mentioned above, this chapter is the sequel to [12] (Chapter 1), where we introduced conservative and dissipative finite element schemes for the IBVP above and provided *a priori* error estimates for the semidiscrete approximations. In this chapter, we develop error estimates for the semidiscrete and fully discrete schemes from an *a posteriori* perspective. Indeed, our principal result bounds the L^2 error between the solution of the IBVP and the fully discrete approximation thereof by a computable quantity. Finally, for the fully discrete schemes, we decompose the computable upper bound into several reliable estimators of the L^2 error. Of these estimators, one estimator is observed to be an indicator for only the temporal error, while another is observed to be an indicator for only the spatial errors. To the best of our knowledge, each of our results are the first of their kind for the system (2.1) and for any corresponding numerical methods extant.

This work finds inspiration in the work of Karakashian and Makridakis [31], which developed *a posteriori* error estimates for semidiscrete and (temporally dissipative) fully discrete discontinuous Galerkin (dG) schemes for the single generalized Korteweg-de Vries (gKdV) equation. The *dispersive reconstruction operator* that was fundamental to their analysis is equally useful here. Given a discrete function w_h, this operator constructs a function w, called the *dispersive reconstruction*, which is twice continuously differentiable and satisfies the equations in the system (2.1) in the strong sense up to a computable forcing term. We can then subtract the resulting equations from the original system (2.1) to obtain an error equation that holds in the strong sense and features a computable right hand side. At this point, arguments similar to those used in the *a priori* analysis can be employed to obtain the desired result for the semidiscrete approximations. Combining the dispersive reconstruction and existing techniques for temporal reconstruction (see [31, 3]), we construct a fully discrete reconstruction and apply a similar argument to obtain *a posteriori* bounds for the fully discrete schemes. It is also of interest to note that, since the coefficients of the system (2.1) can be chosen such that the system comprises two decoupled KdV equations, our work improves upon that of Karakashian and Makridakis in that our fully discrete schemes are temporally conservative. In addition, our work has the additional feature of providing estimators which exhibit dependence on time and space independently. Finally, since we construct a fully discrete reconstruction which is continuous in time, the analysis for our work is much less tedious than that of [31] which features a fully discrete reconstruction which is discontinuous in time.

This chapter is organized as follows: In Section 2, we provide essential preliminaries and a summary of key results from [12] upon which this work is based. In Section 3, we quote the definition of the (spatial) dispersive reconstruction operator $\mathcal{R}$ and summarize the results from [31] which will be useful in the analysis. In Section 4, we develop *a posteriori* error estimates for the semidiscrete formulation introduced in Section 3 of [12]. In Section 5, we develop *a posteriori* error estimates for the fully discrete schemes from [12] which rely on the single-stage implicit Runge-Kutta method of Gauss-Legendre type (Midpoint Rule; henceforth, RK1) for their temporal discretization. In Section 6, we provide numerical experiments which illustrate the behavior of the various indicators. In particular, we provide evidence that the upper bounds supplied by the *a posteriori* error estimates appear to converge to zero, as a function of temporal discretization parameter, at the same quadratic rate of the underlying temporal discretization method, RK1. We also provide evidence that the upper bounds supplied by the *a posteriori* error estimates appear to converge to zero for polynomial degree $q > 2$, albeit suboptimally. The suboptimality is to be expected due to the nonlinearities and the dispersive operators which arise in the estimators. We also study the effectiveness of the estimators for a wide variety of temporal and spatial discretization parameters, investigating how this spatial suboptimality can impact practical use of these estimators. Finally, we provide heuristic factors to correct this suboptimality, yielding heuristic estimators with $\mathcal{O}(1)$ effectivity indices for all polynomial degrees $q \geq 2$.

2.2 Preliminaries

For ease of the reader, we review preliminaries and notation from Chapter 1 and the literature that is important to the analysis presented below. We utilize the same notational conventions as Chapter 1 with regard to meshes and function spaces.

2.2.1 The finite element spaces

As before, the spatial approximations will be sought in the space of continuous and periodic piecewise polynomial functions V_h^q subordinate to the mesh $\mathcal{T}_h$, viz.,

$$V_h^q = \left\{ v \in C^0_{per}([0,1]) : \, v\big|_{I_m} \in \mathcal{P}_q(I_m), \, m = 0, 1, \ldots, M-1 \right\}$$

where $\mathcal{P}_q$ is the space of polynomials of degree q. However, we will also make use of an analogous discontinuous space. By $V_h^{q,\mathrm{dG}}$, we denote the space of discontinuous piecewise polynomials subordinate to the mesh $\mathcal{T}_h$, i.e.,

$$V_h^{q,\mathrm{dG}} = \{v : v|_I \in \mathcal{P}_q(I), I \in \mathcal{T}_h\}.$$

2.2.2 The weak formulation

In this section, we review the weak formulations that form the basis for the semidiscrete and fully discrete methods developed in [12]. In this, we contrast the dispersive forms developed therein with those of the dG methods discussed in [13] and [31]. We begin by recalling the weak formulations developed for the nonlinear terms in (2.1), each of which are of the form $(uv)_x$. Keeping in mind that we will primarily work with continuous periodic functions, recall that, in [12], we defined the form $\mathcal{N}$ via integration by parts, viz.,

$$\mathcal{N}(u, v; \chi) = -\sum_{I\in\mathcal{T}_h} (uv, \chi_x)_I, \quad u, v, \chi \in H^1(\mathcal{T}_h), \tag{2.6}$$

where $(\cdot,\cdot)_I$ denotes the inner product in L^2 over the cell I. By virtue of the Riesz Representation Theorem, we defined the associated nonlinear operator $\mathcal{N} : H^1(\mathcal{T}_h) \times H^1(\mathcal{T}_h) \to V_h^q$ (some abuse of notation is committed here) whose $L^2([0, 1])$-inner product with any $\chi \in V_h^q$ is

$$(\mathcal{N}(u, v), \chi) = -\sum_{I\in\mathcal{T}_h} (uv, \chi_x)_I. \tag{2.7}$$

For ease of reference, we review the pertinent properties of $\mathcal{N}$ and quote the following lemma [12, Lemma 1].

Lemma 2.1.

(i) The nonlinear form $\mathcal{N}$ defined by (2.6) *is consistent in the sense that*

$$\mathcal{N}(u, v; \chi) = ((uv)_x, \chi)\,, \quad u, v, \chi \in H^1_{per}(\mathcal{T}_h). \tag{2.8}$$

(ii) For $u, v \in H^1_{per}(\mathcal{T}_h)$,

$$\mathcal{N}(u, v; v) = \frac{1}{2} \sum_{I \in \mathcal{T}_h} (v^2, u_x)_I. \tag{2.9}$$

We remind the reader of the following particularly useful consequence of periodicity: that the integral $\int_0^1 (u^2)_x u \,\mathrm{d}x$ vanishes for $u \in C^1_{per}([0,1])$. We quote a direct consequence [12, Corollary 1] of the above lemma, in which we see that the form $\mathcal{N}$ preserves this property on $H^1_{per}(\mathcal{T}_h)$ and in particular on V_h^q.

Corollary 2.2. *The form $\mathcal{N}$ is conservative in the sense that*

$$\mathcal{N}(u, u; u) = 0, \quad u \in H^1_{per}(\mathcal{T}_h). \tag{2.10}$$

We now review the bilinear forms we introduced in Chapter 1 for the dispersive (third derivative) terms. These are is similar in spirit to the form $\mathcal{D}$ introduced in [13] and utilized in [31] (discussed at the end of this section) with the difference being that the prevailing spaces are globally continuous. For $u, \chi \in H^2(\mathcal{T}_h)$, define $\mathcal{D}$ by

$$\mathcal{D}(u, \chi) = \sum_{I \in \mathcal{T}_h} (u_x, \chi_{xx})_I + \sum_{m=0}^{M-1} \{u_x\}_m [\chi_x]_m. \tag{2.11}$$

The next lemma [12, Lemma 2] reviews the properties of $\mathcal{D}$ that justified the choice of the particular form chosen in (2.11).

Lemma 2.3.

(i) The bilinear form $\mathcal{D}$ defined by (2.11) is consistent in the sense that

$$\mathcal{D}(u,\chi) = (u_{xxx},\chi), \quad u \in H^3(\mathcal{T}_h) \cap C^2_{per}([0,1]),\ \chi \in H^2_{per}(\mathcal{T}_h). \tag{2.12}$$

(ii) The form $\mathcal{D}$ is skew-adjoint so that

$$\mathcal{D}(v,v) = 0, \quad \forall v \in H^2(\mathcal{T}_h). \tag{2.13}$$

As in Chapter 1, we will make use of the operator counterpart $\mathcal{D} : H^2(\mathcal{T}_h) \to V_h^q$ (another abuse of notation is committed here) of the bilinear form $\mathcal{D}(\cdot,\cdot)$ via the requirement

$$(\mathcal{D}u,\chi) = \mathcal{D}(u,\chi), \quad \forall \chi \in V_h^q.$$

The *dissipative* version

$$\tilde{\mathcal{D}}(u,\chi) = \sum_{I \in \mathcal{T}_h} (u_x,\chi_{xx})_I + \sum_{m=0}^{M-1} u_x(x_m^+)[\chi_x]_m \tag{2.14}$$

of the bilinear form $\mathcal{D}$ may also be used to represent the third derivative terms. The following lemma [12, Lemma 3] summarizes the useful properties of $\tilde{\mathcal{D}}$ that are the counterparts of those of $\mathcal{D}$ shown in Lemmas 2.1 and 2.3.

Lemma 2.4.

(i) The bilinear form $\tilde{\mathcal{D}}$ defined in (2.14) is consistent in the sense that

$$\tilde{\mathcal{D}}(u,\chi) = (u_{xxx},\chi), \quad u \in H^3(\mathcal{T}_h) \cap C^2_{per}([0,1]),\ \chi \in H^2_{per}(\mathcal{T}_h). \tag{2.15}$$

(ii) The form $\tilde{\mathcal{D}}$ is dissipative, which is to say,

$$\tilde{\mathcal{D}}(v,v) = \frac{1}{2}\sum_{m=0}^{M-1}[v_x]_m^2, \quad v \in H^2(\mathcal{T}_h). \tag{2.16}$$

In contrast, we now introduce the dispersive operators developed for the dG method of [13, 31], as they will be used in the definition of the dispersive reconstruction in the next section. The operators $\mathcal{D}^{\mathrm{dG}} : H^3(\mathcal{T}_h) \to V_h^{q,\mathrm{dG}}$ and $\tilde{\mathcal{D}}^{\mathrm{dG}} : H^3(\mathcal{T}_h) \to V_h^{q,\mathrm{dG}}$ are defined in [13, 31] in a similar way to the operators $\mathcal{D}$ and $\tilde{\mathcal{D}}$ so that for any $\chi \in V_h^{q,\mathrm{dG}}$,

$$(\mathcal{D}^{\mathrm{dG}}u,\chi) = -\sum_{I\in\mathcal{T}_h}(u,\chi_{xxx})_I - \sum_{j=0}^{M-1}u_{xx}(x_j^+)[\chi]_j + \sum_{j=0}^{M-1}\{u_x\}_j[\chi_x]_j - \sum_{j=0}^{M-1}u(x_j^-)[\chi_{xx}]_j \tag{2.17}$$

and

$$(\tilde{\mathcal{D}}^{\mathrm{dG}}u,\chi) = -\sum_{I\in\mathcal{T}_h}(u,\chi_{xxx})_I - \sum_{j=0}^{M-1}u_{xx}(x_j^+)[\chi]_j + \sum_{j=0}^{M-1}u_x(x_j^+)[\chi_x]_j - \sum_{j=0}^{M-1}u(x_j^-)[\chi_{xx}]_j. \tag{2.18}$$

Note that since $V_h^q \subset V_h^{q,\mathrm{dG}}$, the operators $\mathcal{D}$ (similarly, $\tilde{\mathcal{D}}$) and $\mathcal{D}^{\mathrm{dG}}$ (similarly, $\tilde{\mathcal{D}}^{\mathrm{dG}}$) coincide on V_h^q. Indeed, integration by parts reveals that

$$\sum_{I\in\mathcal{T}_h}(u,\chi_{xxx})_I = -\sum_{\mathcal{T}_h}(u_x,\chi_{xx})_I - \sum_{j=0}^{M-1}[u\chi_{xx}]_m.$$

Using the identity $[u\chi_{xx}]_j = u(x_j^-)[\chi_{xx}]_j + [u]_j\chi_{xx}(x_j^+)$ and comparing (2.17) and (2.11) shows that $\mathcal{D}$ and $\mathcal{D}^{\mathrm{dG}}$ coincide when u and χ both belong to V_h^q. In addition, while the consistency and skew-adjointness properties listed in Lemma 2.3 for $\mathcal{D}$ hold for $\mathcal{D}^{\mathrm{dG}}$, they also hold given the more relaxed condition that $\chi \in H^3(\mathcal{T}_h)$ (see [31, 13, Lemma 2.2]). Similarly, consistency and dissipation results analogous to those shown for $\tilde{\mathcal{D}}$ in Lemma 2.4 also hold for $\tilde{\mathcal{D}}^{\mathrm{dG}}$ with the relaxed condition that $\chi \in H^3(\mathcal{T}_h)$.

We quote the following bound [31, Lemma 2.3] which is useful in understanding the error estimators which feature the operator $\mathcal{D}$.

Lemma 2.5. *Let $u \in H^3(\mathcal{T}_h)$. For each cell $I = [x_m, x_{m+1}]$, $j = 0, \ldots, M-1$, the following local bound holds:*

$$\|\mathcal{D}^{\mathrm{dG}}u\|_I^2 \leq c\left(\|u_{xxx}\|_I^2 + h_m^{-5}[u]_m^2 + h_m^{-3}[u_x]_m^2 + h_m^{-1}[u_{xx}]_{m+1}^2\right). \tag{2.19}$$

2.3 The dispersive reconstruction operator

The main tool used to develop the *a posteriori* error estimates is a (spatial) dispersive reconstruction operator $\mathcal{R}$ corresponding to the third order differential operators in (2.1) as well as to the discrete variant $\mathcal{D}$ defined above. We highlight the considerations which motivated the definition of the dispersive reconstruction operator in [31, Section 3]:

(i) For $u \in H^3(\mathcal{T}_h)$, the dispersive reconstruction $\mathcal{R}u$ should be (efficiently) computable. Indeed, it is highly desirable that this reconstruction be able to be computed locally on each cell.

(ii) $\mathcal{R}u$ should be globally smooth so that $(\mathcal{R}u)_{xxx}$ in the strong sense. Indeed, this will allow the reconstruction of the approximations u_h, v_h to satisfy the original system in the strong sense, up to a computable forcing term.

(iii) Finally, it is useful for a reconstruction operator to be a right inverse of the corresponding dispersive projection (see [12, (2.15)] and [31, (20)]). For more details, we refer the interested reader to [31].

We now quote the definition of the dispersive reconstruction of Karakashian and Makridakis [31, Theorem 3.1].

Theorem 2.6. *For each $u \in H^3(\mathcal{T}_h)$, there corresponds a unique $\sigma := \mathcal{R}u \in C^2([0,1]) \cap V_h^{q+3,\mathrm{dG}}$ such that for each cell $I = [x_m, x_{m+1}]$, $m = 0, \dots, M-1$ in $\mathcal{T}_h$ there holds*

$$
\begin{aligned}
(\sigma_{xxx}, \chi)_I &= (\mathcal{D}^{\mathrm{dG}} u, \chi), \quad \textit{for all } \chi \in V_h^{q,\mathrm{dG}}(I), \\
\sigma(x_m^+) &= u(x_m^-) \\
\sigma_x(x_m^+) &= \{u_x\}_m, \\
\sigma_{xx}(x_m^+) &= u_{xx}(x_m^+).
\end{aligned}
\tag{2.20}
$$

Karakashian and Makridakis showed that the reconstruction σ can indeed be computed locally and efficiently. In addition, they showed several useful approximation properties for this reconstruction. These properties, which will prove useful in our discussion of the estimators to be developed below, are quoted here [31, Theorem 3.2 and Remark 3.2]. The fact that V_h^q is a subspace of V_h^{dG} and the fact that $\mathcal{D}$ and $\mathcal{D}^{\mathrm{dG}}$ coincide on V_h^q are the reasons motivating our use of the same reconstruction operator of Karakashian and Makridakis.

Theorem 2.7 (approximation properties of $\mathcal{R}$)**.**

(i) Suppose that $u \in C^2([0,1]) \cap H^{q+4}(\mathcal{T}_h)$*. For each* $I \in \mathcal{T}_h$*,*

$$|u - \mathcal{R}u|_{j,I} \leq c h_I^{q+4-j} |u|_{q+4,I}, \quad j = 0, 1, \ldots q+4. \tag{2.21}$$

(ii) Suppose $u \in H^{q+4}(\mathcal{T}_h)$*. For* $j = 0, 1, \ldots, 3$ *and* $I = [x_m, x_{m+1}] \in \mathcal{T}_h$*,*

$$\begin{aligned} |u - \mathcal{R}u|_{j,I} \leq c \Big(& h_I^{q+4-j} |u|_{q+4,I} + h_m^{\frac{1}{2}-j} |[u]_m| + h_m^{\frac{3}{2}-j} \left(|[u_x]_m| + |[u_x]_{m+1}| \right) \\ & + h_m^{\frac{5}{2}-j} |[u_{xx}]_{m+1}| \Big) \end{aligned} \tag{2.22}$$

Indeed, if $w_h \in V_h^{q,\mathrm{dG}}$ *is an* $\mathcal{O}(h^\mu)$ *approximation to a smooth function* w *in the sense that*

$$\|w - w_h\|_I + h_I \|(w - w_h)_x\| \leq c h_I^\mu, \quad \forall I \in \mathcal{T}_h,$$

the $H^j(I)$ *seminorm of the reconstruction error is bounded as follows:*

$$|w_h - \mathcal{R}w_h|_{j,I} \leq c h^{\mu - j}. \tag{2.23}$$

2.4 *A posteriori* error estimates for the semidiscrete approximations

We now construct *a posteriori* error estimates for the semidiscrete approximations. For brevity, we conduct the argument for the conservative semidiscrete scheme of [12]. Nearly identical arguments effect *a posteriori* error estimates for the dissipative scheme of [12]. We relegate the discussion of this matter to Section 2.6.

In our previous work [12, (3.1)], we defined the (conservative) semidiscrete approximation to the solution (u, v) of the IBVP for (2.1) as the solutions u_h, v_h in $V_h^q \times [0, T]$ of the coupled system

$$\begin{bmatrix} u_{ht} \\ v_{ht} \end{bmatrix} + \begin{bmatrix} A & B & C \\ D & E & F \end{bmatrix} \begin{bmatrix} \mathcal{N}(u_h, u_h) \\ \mathcal{N}(u_h, v_h) \\ \mathcal{N}(v_h, v_h) \end{bmatrix} + \begin{bmatrix} \mathcal{D}u_h \\ \mathcal{D}v_h \end{bmatrix} = \begin{bmatrix} 0 \\ 0 \end{bmatrix}, \tag{2.24}$$

of first-order in time operator equations with initial data $u_h^0, v_h^0 \in V_h^q$. Here, the initial data is a suitable (i.e., at least $\mathcal{O}(h^q)$) approximation of the initial data u_0, v_0 for the IBVP (see [12, (Theorem 3.2)]). Indeed, the L^2 projection into V_h^q or the Lagrange interpolant more than satisfy this condition.

For comparison, we recall that in [12] the following *a priori* bound for the semidiscrete scheme (2.24) was established:

$$\|(u-u_h)(t)\| + \|(v-v_h)(t)\| \leq ch^{\mu}, \quad 0 \leq t \leq T$$

where (for the conservative scheme) $\mu = q-1$ in general and $\mu = q$ if the underlying mesh $\mathcal{T}_h$ is uniform. We note that, for the dissipative scheme, the result holds for $\mu = q$ with no additional mesh conditions necessary.

The following lemma (which is but a smooth analog of Lemma 5 of [12]) is useful to the *a posteriori* analysis to come:

Lemma 2.8. *Let* (a,b,c) *be a nontrivial solution of the system* (2.3)*. If* $u, v \in C^1_{per}([0,1])$*, the following identity holds*

$$\mathcal{I}(u,v) := \int_0^1 [2au + bv \;\; bu + 2cv] \begin{bmatrix} A & B & C \\ D & E & F \end{bmatrix} \begin{bmatrix} (u^2)_x \\ (uv)_x \\ (v^2)_x \end{bmatrix} = 0. \tag{2.25}$$

Proof. Since the nonlinear *form* $\mathcal{N}(\cdot\,,\;\cdot;\;\cdot)$ is consistent for arguments in $H^1_{per}(\mathcal{T}_h)$ and u, v are in $C^1_{per}([0,1]) \subset H^1_{per}(\mathcal{T}_h)$, the result follows from the proof of Lemma 5 of [12]. □

The next result provides *a posteriori* error control of $u - u_h$ and $v - v_h$ in terms of reconstruction errors $u_h - \mathcal{R}u_h$ and $v_h - \mathcal{R}v_h$ and the initial errors $(u - \mathcal{R}u_h)(0)$ and $(v - \mathcal{R}v_h)(0)$. It is crucial to note that $\mathcal{R}u_h$ and $\mathcal{R}v_h$ can be explicitly constructed from u_h, so that each term in the right-hand side of the estimate of (2.9) is computable. This, of course, assumes that u_h, v_h have been computed via some means, e.g., the Method of Lines.

Theorem 2.9. *Suppose that u, v are sufficiently smooth solutions to (2.1) and that for (a, b, c) a nontrivial solution of (2.3) the inequality $b^2 - 4ac < 0$ holds. Let $u_h, v_h : [0, T] \to V_h^q \times V_h^q$ be the solutions of the scheme (2.24) and let $\mathcal{R}u_h, \mathcal{R}v_h$ denote the respective dispersive reconstructions of u_h, v_h as defined in (2.6). For any $t \geq 0$,*

$$\|(u - u_h)(t)\| + \|(v - v_h)(t)\| \leq \Phi_{recon}(t) + ce^{Ct}\left(\Phi_{initial}(0) + \int_0^t \left(\Phi_{time}(s) + \Phi_{nonlin}(s)\right) \mathrm{d}s\right), \tag{2.26}$$

where the constant C in e^{Ct} depends on the $|\mathcal{R}u_h|_{W^{1,\infty}([0,1])}$ and $|\mathcal{R}v_h|_{W^{1,\infty}([0,1])}$. Here, $\Phi_{initial}$, Φ_{recon}, Φ_{time}, and Φ_{nonlin} denote the following quantities:

$$\Phi_{recon}(t) := \|(u_h - \mathcal{R}u_h)(t)\| + \|(v_h - \mathcal{R}v_h)(t)\|, \tag{2.27}$$

$$\Phi_{initial}(0) := \|(u - \mathcal{R}u_h)(0)\| + \|(v - \mathcal{R}v_h)(0)\|, \tag{2.28}$$

$$\Phi_{time}(t) := \|(u_h - \mathcal{R}u_h)_t(t)\| + \|(v_h - \mathcal{R}v_h)_t(t)\|, \text{ and} \tag{2.29}$$

$$\begin{aligned} \Phi_{nonlin}(t) := &\left\|A\left(\mathcal{N}(u_h, u_h) - \left((\mathcal{R}u_h)^2\right)_x\right)\right\| + \left\|D\left(\mathcal{N}(u_h, u_h) - \left((\mathcal{R}u_h)^2\right)_x\right)\right\| \\ &+ \left\|B\left(\mathcal{N}(u_h, v_h) - (\mathcal{R}u_h\mathcal{R}v_h)_x\right)\right\| + \left\|E\left(\mathcal{N}(u_h, v_h) - (\mathcal{R}u_h\mathcal{R}v_h)_x\right)\right\| \\ &+ \left\|C\left(\mathcal{N}(v_h, v_h) - \left((\mathcal{R}v_h)^2\right)_x\right)\right\| + \left\|F\left(\mathcal{N}(v_h, v_h) - \left((\mathcal{R}v_h)^2\right)_x\right)\right\|. \end{aligned} \tag{2.30}$$

Proof. Recall that $\mathcal{R}u_h, \mathcal{R}v_h$ belong to $C^2([0,1]) \cap V_h^{q+3}$ and that $(\mathcal{R}u_h)_{xxx} = \mathcal{D}u_h$ and $(\mathcal{R}v_h)_{xxx} = \mathcal{D}v_h$ in the strong sense. Therefore, from the semidiscrete system in (2.24), we have

$$\begin{bmatrix} u_{ht} \\ v_{ht} \end{bmatrix} + \begin{bmatrix} A & B & C \\ D & E & F \end{bmatrix} \begin{bmatrix} \mathcal{N}(u_h, u_h) \\ \mathcal{N}(u_h, v_h) \\ \mathcal{N}(v_h, v_h) \end{bmatrix} + \begin{bmatrix} (\mathcal{R}u_h)_{xxx} \\ (\mathcal{R}v_h)_{xxx} \end{bmatrix} = \begin{bmatrix} 0 \\ 0 \end{bmatrix}, \tag{2.31}$$

Letting $e^{(u)} = u - \mathcal{R}u_h$, $e^{(v)} = v - \mathcal{R}v_h$, $r^{(u)} = u_h - \mathcal{R}u_h$, and $r^{(v)} = v_h - \mathcal{R}v_h$, where u, v form a solution to the IBVP for (2.1), we get

$$\begin{bmatrix} e_t^{(u)} \\ e_t^{(v)} \end{bmatrix} + \mathcal{A} \begin{bmatrix} (u^2)_x - \left((\mathcal{R}u_h)^2\right)_x \\ (uv)_x - (\mathcal{R}u_h \mathcal{R}v_h)_x \\ (v^2)_x - \left((\mathcal{R}v_h)^2\right)_x \end{bmatrix} + \begin{bmatrix} (e^{(u)})_{xxx} \\ (e^{(v)})_{xxx} \end{bmatrix} = \begin{bmatrix} r_t^{(u)} \\ r_t^{(v)} \end{bmatrix} + \mathcal{A} \begin{bmatrix} \mathcal{N}(u_h, u_h) - \left((\mathcal{R}u_h)^2\right)_x \\ \mathcal{N}(u_h, v_h) - (\mathcal{R}u_h \mathcal{R}v_h)_x \\ \mathcal{N}(v_h, v_h) - \left((\mathcal{R}v_h)^2\right)_x \end{bmatrix} \tag{2.32}$$

where $\mathcal{A}$ denotes the matrix $\begin{bmatrix} A & B & C \\ D & E & F \end{bmatrix}$. This system is written as $Q_t + Q_1 + Q_2 = Q_3 + Q_4$ for convenience.

Multiply this system from the left by the vector $\tilde{Q}(t) = [2ae^{(u)} + be^{(v)} \quad be^{(u)} + 2ce^{(v)}]$ and integrate over $[0,1]$ to obtain

$$\int_0^1 \tilde{Q}Q_t \,\mathrm{d}x + \int_0^1 \tilde{Q}Q_1 \,\mathrm{d}x + \int_0^1 \tilde{Q}Q_2 \,\mathrm{d}x = \int_0^1 \tilde{Q}Q_3 \,\mathrm{d}x + \int_0^1 \tilde{Q}Q_4 \,\mathrm{d}x. \tag{2.33}$$

Computing the first term, we see that

$$\int_0^1 \tilde{Q}Q_t \,\mathrm{d}x = \frac{\mathrm{d}}{\mathrm{d}t}\Omega(e^{(u)}, e^{(v)}). \tag{2.34}$$

Noting that

$$
\begin{aligned}
u^2 - (\mathcal{R}u_h)^2 &= (e^{(u)})^2 + 2\mathcal{R}u_h e^{(u)}, \\
uv - \mathcal{R}u_h\mathcal{R}v_h &= e^{(u)}e^{(v)} + \mathcal{R}v_h e^{(u)} + \mathcal{R}u_h e^{(v)}, \text{ and} \\
v^2 - (\mathcal{R}v_h)^2 &= (e^{(v)})^2 + 2\mathcal{R}v_h e^{(v)}
\end{aligned}
\tag{2.35}
$$

allows the conclusion

$$
\begin{aligned}
\int_0^1 \tilde{Q}Q_1 \,\mathrm{d}x = \mathcal{I}(e^{(u)}, e^{(v)}) & \\
&+ (4Aa + 2Db)\left((\mathcal{R}u_h e^{(u)})_x, e^{(u)}\right) + (2Ba + Eb)\left((\mathcal{R}v_h e^{(u)})_x, e^{(u)}\right) \\
&+ (Bb + 2Ec)\left((\mathcal{R}u_h e^{(v)})_x, e^{(v)}\right) + (2Cb + 4Fc)\left((\mathcal{R}v_h e^{(v)})_x, e^{(v)}\right) \\
&+ (2Ba + Eb)\left((\mathcal{R}u_h e^{(v)})_x, e^{(u)}\right) + (2Ab + 4Dc)\left((\mathcal{R}u_h e^{(u)})_x, e^{(v)}\right) \\
&+ (4Ca + 2Fb)\left((\mathcal{R}v_h e^{(u)})_x, e^{(u)}\right) + (Bb + 2Ec)\left((\mathcal{R}v_h e^{(u)})_x, e^{(v)}\right).
\end{aligned}
\tag{2.36}
$$

Invoking Lemma 2.8, $\mathcal{I}(e^{(u)}, e^{(v)}) = 0$. Let $Q_{1,1}$ denote the first four of the last eight terms in (2.36). Twice integrating by parts on each term (or by application of (2.9), as each function here is smooth and periodic and the form $\mathcal{N}(\cdot\,,\ \cdot\,;\ \cdot)$ is consistent), we obtain

$$
\begin{aligned}
Q_{1,1} = (2Aa + Db)&\left(\left(e^{(u)}\right)^2, (\mathcal{R}u_h)_x\right) + (Ba + Eb/2)\left(\left(e^{(u)}\right)^2, (\mathcal{R}v_h)_x\right) \\
&+ (Bb/2 + Ec)\left(\left(e^{(v)}\right)^2, (\mathcal{R}u_h)_x\right) + (Cb + 2Fc)\left(\left(e^{(v)}\right)^2, (\mathcal{R}v_h)_x\right).
\end{aligned}
$$

As a result, since, if $b^2 - 4ac < 0$, there is a positive constant σ such that for any $\phi, \psi \in L^2(\mathcal{T}_h)$ we have $\sigma \displaystyle\int_0^1 \left(\phi^2 + \psi^2\right) \, \mathrm{d}x \leq \Omega(\phi, \psi)$. From this, we obtain

$$|Q_{1,1}| \leq c_{\mathcal{R}u_h, \mathcal{R}v_h, \mathcal{A}} \left(\|e^{(u)}\|^2 + \|e^{(v)}\|\right) \leq \frac{c_{\mathcal{R}u_h, \mathcal{R}v_h, \mathcal{A}}}{\sigma} \Omega(e^{(u)}, e^{(v)}). \tag{2.37}$$

Here, the constant $c_{\mathcal{R}u_h, \mathcal{R}v_h, \mathcal{A}}$ depends on the constants in the expression for $Q_{1,1}$ and $|\mathcal{R}u_h|_{W^{1,\infty}([0,1])}$ and $|\mathcal{R}v_h|_{W^{1,\infty}([0,1])}$ We denote the next two terms of (2.36) by $Q_{1,2}$. From the definition of (a, b, c) given in (2.3), we know that $2Ba + Eb = 2Ab + 4Dc$. As a result, integrating by parts on each term twice reveals that

$$\begin{aligned} Q_{1,2} &= -(2Ba + Eb) \left(\left(\mathcal{R}u_h e^{(v)}, \left(e^{(u)}\right)_x\right) + \left(\mathcal{R}u_h e^{(u)}, \left(e^{(v)}\right)_x\right) \right) \\ &= (2Ba + Eb) \left((\mathcal{R}u_h)_x, e^{(u)} e^{(v)} \right). \end{aligned}$$

As a result, we obtain

$$\begin{aligned} |Q_{1,2}| &\leq C_{\mathcal{R}u_h, \mathcal{A}} \|e^{(u)} e^{(v)}\|^2 \\ &\leq C_{\mathcal{R}u_h, \mathcal{A}} \|e^{(u)}\| \|e^{(v)}\| \\ &\leq \frac{C_{\mathcal{R}u_h, \mathcal{A}}}{2} \left(\|e^{(u)}\|^2 + \|e^{(v)}\|^2\right) \\ &\leq \frac{C_{\mathcal{R}u_h, \mathcal{A}}}{2\sigma} \Omega(e^{(u)}, e^{(v)}), \end{aligned} \tag{2.38}$$

where $C_{\mathcal{R}u_h, \mathcal{A}}$ depends on $|\mathcal{R}u_h|_{W^{1,\infty}([0,1])}$ and the constant $2Ba + Eb$. We denote the final two terms of (2.36) by $Q_{1,3}$. The fact $4Ca + 2Fb = Bb + 2Ec$ allows a nearly identical argument to that conducted for $Q_{1,2}$, yielding the bound

$$|Q_{1,3}| \leq \frac{C_{\mathcal{R}v_h,\mathcal{A}}}{2\sigma}\Omega(e^{(u)}, e^{(v)}). \tag{2.39}$$

Combining the bounds (2.37), (2.38), and (2.39), it is clear that

$$|Q_1| \leq C_{\mathcal{R}u_h,\mathcal{R}v_h,\mathcal{A},\sigma}\Omega(e^{(u)}, e^{(v)}), \tag{2.40}$$

where here $C_{\mathcal{R}u_h,\mathcal{R}v_h,\mathcal{A},\sigma}$ is dependent on $\mathcal{R}u_h, \mathcal{R}v_h, \mathcal{A}$, and σ through the constants in (2.37), (2.38), and (2.39). For sufficiently smooth ϕ, ψ periodic on $[0, 1]$, note that $(\phi_{xxx}, \psi) = -(\psi_{xxx}, \phi)$. Consequently,

$$\int_0^1 \tilde{Q}Q_2 \,\mathrm{d}x = 2a\left(e^{(u)}_{xxx}, e^{(u)}\right) + b\left(\left(e^{(u)}_{xxx}, e^{(v)}\right) + \left(e^{(v)}_{xxx}, e^{(u)}\right)\right) + 2c\left(e^{(v)}_{xxx}, e^{(v)}\right) = 0. \tag{2.41}$$

It remains to compute the terms on the right side of (2.33). Note that

$$\int_0^1 \tilde{Q}Q_3 \,\mathrm{d}x = 2a(r^{(u)}_t, e^{(u)}) + b\left((r^{(u)}_t, e^{(v)}) + (r^{(v)}_t, e^{(u)})\right) + 2c(r^{(v)}_t, e^{(v)}).$$

As a result,

$$\left|\int_0^1 \tilde{Q}Q_3 \,\mathrm{d}x\right| \leq C_{\mathcal{A},\sigma}\left(\|r^{(u)}_t\|^2 + \|r^{(u)}_t\|^2 + \Omega(e^{(u)}, e^{(v)})\right), \tag{2.42}$$

where the constant $C_{\mathcal{A},\sigma}$ depends on $\mathcal{A}$ and σ from the positive definiteness condition. It remains to bound $\int_0^1 \tilde{Q}Q_4$. Let $\zeta_0 = \mathcal{N}(u_h, u_h) - \left((\mathcal{R}u_h)^2\right)_x$, $\zeta_1 = \mathcal{N}(u_h, v_h) - (\mathcal{R}u_h\mathcal{R}v_h)_x$, and

$\zeta_2 = \mathcal{N}(v_h, v_h) - \left((\mathcal{R}v_h)^2\right)_x$. Note that

$$\begin{aligned}
\int_0^1 \tilde{Q}Q_4 \,\mathrm{d}x &= \int_0^1 [2ae^{(u)} + be^{(v)} \quad be^{(u)} + 2ce^{(v)}] \begin{bmatrix} A\zeta_0 + B\zeta_1 + C\zeta_2 \\ D\zeta_0 + E\zeta_1 + F\zeta_2 \end{bmatrix} \mathrm{d}x \\
&= 2a(A\zeta_0 + B\zeta_1 + C\zeta_2, e^{(u)}) + b(A\zeta_0 + B\zeta_1 + C\zeta_2, e^{(v)}) \\
&\quad + b(D\zeta_0 + E\zeta_1 + F\zeta_2, e^{(u)}) + 2c(D\zeta_0 + E\zeta_1 + F\zeta_2, e^{(v)})
\end{aligned}$$

so that

$$\begin{aligned}
\int_0^1 \tilde{Q}Q_4 \,\mathrm{d}x \leq C_{\mathcal{A}} &\left(\|A\zeta_0 + B\zeta_1 + C\zeta_2\|^2 + \|D\zeta_0 + E\zeta_1 + F\zeta_2\|^2\right. \\
&\left.\|e^{(u)}\|^2 + \|e^{(v)}\|^2\right) \\
&\leq C_{\mathcal{A}} \left(\|A\zeta_0 + B\zeta_1 + C\zeta_2\|^2 + \|D\zeta_0 + E\zeta_1 + F\zeta_2\|^2 + \Omega(e^{(u)}, e^{(v)})\right) \\
&\leq C_{\mathcal{A},\sigma} \left(\|A\zeta_0\|^2 + \|B\zeta_1\|^2 + \|C\zeta_2\|^2 + \|D\zeta_0\|^2 + \|E\zeta_1\|^2 + \|F\zeta_2\|^2\right. \\
&\quad \left.+\Omega(e^{(u)}, e^{(v)})\right).
\end{aligned} \tag{2.43}$$

Combining (2.34), (2.40), (2.41), (2.42), and (2.43) yields

$$\begin{aligned}
\frac{\mathrm{d}}{\mathrm{d}t}\Omega(e^{(u)}, e^{(v)}) \leq C_{\mathcal{R}u_h,\mathcal{R}v_h,\mathcal{A},\sigma} &\Big(\Omega(e^{(u)}, e^{(v)}) + \|r_t^{(u)}\|^2 + \|r_t^{(v)}\|^2 \\
&+ \left\|A\left(\mathcal{N}(u_h, u_h) - \left((\mathcal{R}u_h)^2\right)_x\right)\right\|^2 + \left\|D\left(\mathcal{N}(u_h, u_h) - \left((\mathcal{R}u_h)^2\right)_x\right)\right\|^2 \\
&+ \|B\left(\mathcal{N}(u_h, v_h) - (\mathcal{R}u_h\mathcal{R}v_h)_x\right)\|^2 + \|E\left(\mathcal{N}(u_h, v_h) - (\mathcal{R}u_h\mathcal{R}v_h)_x\right)\|^2 \\
&+ \left\|C\left(\mathcal{N}(u_h, u_h) - \left((\mathcal{R}u_h)^2\right)_x\right)\right\|^2 + \left\|F\left(\mathcal{N}(v_h, v_h) - \left((\mathcal{R}v_h)^2\right)_x\right)\right\|^2\Big),
\end{aligned} \tag{2.44}$$

for a constant $C_{\mathcal{R}u_h,\mathcal{R}v_h,\mathcal{A},\sigma}$ that depends on $\mathcal{R}u_h$, $\mathcal{R}v_h$, $\mathcal{A}$, and σ through the constants in (2.34), (2.40), (2.41), (2.42), and (2.43).

Applying a differential form of Gronwall's inequality (see, e.g., [27, Appendix B, Inequality j.]) results in

$$
\begin{aligned}
\Omega(e^{(u)}, e^{(v)}) \leq e^{Ct} \big(\Omega(e^{(u)}(0), e^{(v)}(0)) \\
&+ \int_0^t \Big(\|r_t^{(u)}(s)\|^2 + \|r_t^{(v)}(s)\|^2 \\
&\quad + \left\| A \left(\mathcal{N}(u_h, u_h) - \left((\mathcal{R}u_h)^2\right)_x\right)(s) \right\|^2 \\
&\quad + \left\| D \left(\mathcal{N}(u_h, u_h) - \left((\mathcal{R}u_h)^2\right)_x\right)(s) \right\|^2 \\
&\quad + \left\| B \left(\mathcal{N}(u_h, v_h) - (\mathcal{R}u_h\mathcal{R}v_h)_x\right)(s) \right\|^2 \\
&\quad + \left\| E \left(\mathcal{N}(u_h, v_h) - (\mathcal{R}u_h\mathcal{R}v_h)_x\right)(s) \right\|^2 \\
&\quad + \left\| C \left(\mathcal{N}(v_h, v_h) - \left((\mathcal{R}v_h)^2\right)_x\right)(s) \right\|^2 \\
&\quad + \left\| F \left(\mathcal{N}(v_h, v_h) - \left((\mathcal{R}v_h)^2\right)_x\right)(s) \right\|^2 \Big) \,\mathrm{d}s.
\end{aligned}
\tag{2.45}
$$

From $b^2 < 4ac$,

$$\sigma \left(\|e^{(u)}\|^2 + \|e^{(v)}\|^2\right) \leq \Omega(e^{(u)}, e^{(v)}).$$

Application of this fact, some elementary algebraic inequalities, and the triangle inequality yields the result. $\square$

Remark. *Recall that in Theorem 2.9, the constant C in the exponential term which comes from Gronwall's inequality depends on $|\mathcal{R}u_h|_{W^{1,\infty}([0,1])}$ and $|\mathcal{R}v_h|_{W^{1,\infty}([0,1])}$. This dependence on the reconstructions can be replaced by analogous dependence on u and v via a nearly identical* *argument utilizing the observations*

$$
\begin{aligned}
u^2 - (\mathcal{R}u_h)^2 &= -(e^{(u)})^2 + 2ue^{(u)} \\
uv - \mathcal{R}u_h\mathcal{R}v_h &= -e^{(u)}e^{(v)} + ve^{(u)} + ve^{(v)}, \textit{ and} \\
v^2 - (\mathcal{R}v_h)^2 &= -(e^{(v)})^2 + 2ue^{(v)}
\end{aligned}
\tag{2.46}
$$

in lieu of (2.35)*. However, the resulting bound in terms of* u *and* v *is not computable in general. We remark that Theorem* 2.9 *utilizes a constant dependent upon the reconstructions so that the upper bound on the errors* $u - u_h$ *and* $v - v_h$ *is entirely computable, provided, of course, that* u_h *and* v_h *have been computed by some means.*

2.5 *A posteriori* error estimates for the fully discrete schemes

To develop *a posteriori* error estimates for the fully discrete scheme, we adopt a similar approach to that followed by Karakashian and Makridakis in [31] for the single gKdV equation in that we form a pair of two time-stepping schemes. The first, or *main*, scheme is used to generate the fully discrete approximations and the second is used at each timestep to develop an estimation. Indeed, the essential issue is to use these two schemes to construct a vector valued function with components that are spatially smooth, temporally continuous, and satisfy the system (2.1) in the strong sense but with a computable forcing term.

The analysis presented here has several advantages over the work of [31], even when applied to methods for the single gKdV equation.

1. The analysis is simpler mainly due to the fact that the space-time reconstructions of u_h and v_h are continuous in time (i.e., across the temporal nodes). Consequently, the number of

resulting error indicators (also referred to below as estimators) is now three. In [31], an additional fourth indicator was necessary because of the discontinuous nature of the space-time reconstruction employed therein.

2. In [31], the Backward Euler scheme was used to produce the fully discrete approximations, whereas the midpoint rule played an auxiliary role in order to produce the *a posteriori* error estimation. Here, the main scheme is the midpoint rule, which, in addition to being more accurate (second order in time, as opposed to the first order in time accuracy of the Backward Euler scheme), is conservative in time in the sense that $\|u_h^{n+1}\| = \|u_h^n\|$ and $\|v_h^{n+1}\| = \|v_h^n\|$ for all n.

2.5.1 The fully discrete schemes

Let $0 = t^0 < t^1 < \cdots < t^N = T$ be a partition of the temporal interval $[0, T]$ and $\kappa^n = t^{n+1} - t^n$ for $n = 0, 1, \ldots, N-1$. Herein, we generate the fully discrete approximations u_M^n, v_M^n to $u(\cdot, t^n), v(\cdot, t^n)$ by the one-stage implicit Runge-Kutta method of Gauss-Legendre type (RK1). Indeed, the approximations u_M^n, v_M^n are given by

$$\begin{bmatrix} \dfrac{u_M^{n+1} - u_M^n}{\kappa^n} \\ \\ \dfrac{v_M^{n+1} - v_M^n}{\kappa^n} \end{bmatrix} + \begin{bmatrix} A & B & C \\ D & E & F \end{bmatrix} \begin{bmatrix} \mathcal{N}(u_M^{n,1}, u_M^{n,1}) \\ \mathcal{N}(u_M^{n,1}, v_M^{n,1}) \\ \mathcal{N}(v_M^{n,1}, v_M^{n,1}) \end{bmatrix} + \begin{bmatrix} \mathcal{D}(u_M^{n,1}) \\ \mathcal{D}(v_M^{n,1}) \end{bmatrix} = \begin{bmatrix} 0 \\ 0 \end{bmatrix}, \tag{2.47}$$

where the values $u_M^{n,1}$ and $v_M^{n,1}$ are given by $u_M^{n,1} = (u_M^n + u_M^{n+1})/2$ and $v_M^{n,1} = (v_M^n + v_M^{n+1})/2$. The initial conditions u_M^0 and v_M^0 are defined via $u_M^0 := u_h(0)$ and $v_M^0 := v_h(0)$.

At each timestep t^n, we employ a step of the Implicit Euler method to supply an estimation for the error generated by the RK1 method. These values u_E^{n+1} and v_E^{n+1}, obtained from a single iteration of Implicit Euler at timestep t^n, are given via

$$\begin{bmatrix} \dfrac{u_E^{n+1} - u_M^n}{\kappa^n} \\ \\ \dfrac{v_E^{n+1} - v_M^n}{\kappa^n} \end{bmatrix} + \begin{bmatrix} A & B & C \\ \\ D & E & F \end{bmatrix} \begin{bmatrix} \mathcal{N}(u_E^{n+1}, u_E^{n+1}) \\ \\ \mathcal{N}(u_E^{n+1}, v_E^{n+1}) \\ \\ \mathcal{N}(v_E^{n+1}, v_E^{n+1}) \end{bmatrix} + \begin{bmatrix} \mathcal{D}(u_E^{n+1}) \\ \\ \mathcal{D}(v_E^{n+1}) \end{bmatrix} = \begin{bmatrix} 0 \\ \\ 0 \end{bmatrix}. \tag{2.48}$$

We stress that, at each timestep t^n, the initial values for the Implicit Euler scheme are the approximations u_M^n, v_M^n at t^n as generated by the RK1 method.

The well-definedness of these schemes can be shown via a variant of Brouwer's Fixed Point Theorem in a manner similar to [6]. Further, uniqueness and convergence can also be shown under appropriate CFL conditions.

To derive *a posteriori* estimates, we apply an argument similar to that of Karakashian and Makridakis [31], which has roots in the work of Akrivis, Makridakis, and Nochetto for parabolic problems (see, for example, [3]). Indeed, for simplicity, we generate fully discrete approximations using RK1, only the first member ($s = 1$) of the s-stage Implicit Runge-Kutta methods of Gauss-Legendre type. The estimates constructed herein can be generalized for larger $s \in \mathbb{N}$ through arguments similar to those of [3]. In addition, here we impose the simplifying assumption that the finite element spaces are fixed in time. This assumption can certainly be removed and the more general case can be considered via a careful argument along the lines of [7].

2.5.2 The fully discrete reconstruction

The fully discrete reconstructions are defined as the functions $\hat{u}, \hat{v} : [0,T] \to C^2([0,1]) \cap V_h^{q+3}$ which on each interval $I_n = [t^n, t^{n+1}]$ are defined by

$$\hat{u}(t) = \mathcal{R}\left(u_M^n + \int_{t^n}^{t} F_0(s)\,\mathrm{d}s\right) \tag{2.49}$$

and

$$\hat{v}(t) = \mathcal{R}\left(v_M^n + \int_{t^n}^{t} F_1(s)\,\mathrm{d}s\right) \tag{2.50}$$

where

$$F(t) := \begin{bmatrix} F_0(t) \\ \\ F_1(t) \end{bmatrix} = \left(\begin{bmatrix} \dfrac{u_M^{n+1} - u_M^n}{\kappa_n} \\ \dfrac{v_M^{n+1} - v_M^n}{\kappa_n} \end{bmatrix}\right) \ell_{\frac{1}{2}}(t) + \left(\begin{bmatrix} \dfrac{u_E^{n+1} - u_M^n}{\kappa_n} \\ \dfrac{v_E^{n+1} - v_M^n}{\kappa_n} \end{bmatrix}\right) \ell_1(t). \tag{2.51}$$

Here, $\ell_{\frac{1}{2}}(t) = \dfrac{2}{\kappa_n}(t^{n+1} - t)$ and $\ell_1(t) = \dfrac{2}{\kappa_n}(t - t^{n,1})$ are the basis functions of the space of functions affine in t which correspond to the nodes $t^{n,1} := (t^n + t^{n+1})/2$ and t^{n+1}, respectively. As a result, $\hat{u}, \hat{v}$ are each computable and piecewise polynomial in space and time.

A key property of the fully discrete reconstruction

The next lemma elucidates the relationship of the fully discrete reconstructions $\hat{u}, \hat{v}$ to the piecewise affine interpolants of u_M^n, v_M^n on each interval I_n. We commit a small abuse of notation below: the application of $\mathcal{R}$ to a vector is used to denote the application of $\mathcal{R}$ to each argument thereof.

Lemma 2.10. *Let $U(t), V(t)$ denote the piecewise affine in time interpolant of the fully discrete approximations u_M^n, v_M^n. On each interval $I_n = [t^n, t^{n+1}]$, for any $t \in I_n$,*

$$\begin{bmatrix} \hat{u}(t) \\ \hat{v}(t) \end{bmatrix} = \mathcal{R}\left(\begin{bmatrix} U(t) \\ V(t) \end{bmatrix} + \frac{1}{4}\begin{bmatrix} u_M^{n+1} - u_E^{n+1} \\ v_M^{n+1} - v_E^{n+1} \end{bmatrix} \hat{\ell}_{\frac{1}{2}}(t)\right), \tag{2.52}$$

where $\hat{\ell}_{\frac{1}{2}}(t) = \dfrac{4}{\kappa_n^2}(t - t^n)(t^{n+1} - t)$ is the basis function corresponding to the node $t^{n,1} = \dfrac{t^n + t^{n+1}}{2}$ in the space of functions quadratic in t on the interval I_n.

Proof. The proof comprises evaluation of $\hat{u}(t)$ and $\hat{v}(t)$ at t^n, $t^{n,1}$, and t^{n+1}. It is clear from the definitions of $\hat{u}$ and $\hat{v}$ that $\hat{u}(t^n) = \mathcal{R}u_M^n = \mathcal{R}V(t^n)$ and $\hat{v}(t^n) = \mathcal{R}v_M^n = \mathcal{R}V(t^n)$.

Employ the trapezoidal rule, which is exact for affine functions, to compute $\hat{u}(t^{n,1})$:

$$\begin{aligned}
\hat{u}(t^{n,1}) &= \mathcal{R}\left(u_M^n + \int_{t^n}^{t^{n,1}} F_0(s)\,\mathrm{d}s\right) \\
&= \mathcal{R}\left(u_M^n + \frac{\kappa_n}{4}\left(F_0(t^n) + F_0(t^{n,1})\right)\right) \\
&= \mathcal{R}\left(u_M^n + \frac{\kappa_n}{4}\left(\frac{u_M^{n+1} - u_M^n}{\kappa_n}\left(\ell_{\frac{1}{2}}(t^n) + \ell_{\frac{1}{2}}(t^{n,1})\right) + \frac{u_E^{n+1} - u_M^n}{\kappa_n}\left(\ell_1(t^n) + \ell_1(t^{n,1})\right)\right)\right) \\
&= \mathcal{R}\left(u_M^n + \frac{1}{4}\left(3(u_M^{n+1} - u_M^n) - (u_E^{n+1} - u_M^n)\right)\right) \\
&= \mathcal{R}\left(u_M^n + \frac{3}{4}u_M^{n+1} - \frac{3}{4}u_M^n - \frac{1}{4}u_E^{n+1} + \frac{1}{4}u_M^n\right) \\
&= \mathcal{R}\left(\frac{u_M^n + u_M^{n+1}}{2} + \frac{1}{4}\left(u_M^{n+1} - u_E^{n+1}\right)\right) \\
&= \mathcal{R}\left(u_M^{n,1} + \frac{1}{4}\left(u_M^{n+1} - u_E^{n+1}\right)\right).
\end{aligned} \tag{2.53}$$

An identical argument shows $\hat{v}(t^{n,1}) = \mathcal{R}\left(v_M^{n,1} + \frac{1}{4}\left(v_M^{n+1} - v_E^{n+1}\right)\right)$.

Furthermore, application of the midpoint rule of integration, which is also exact for affine functions, yields the desired result for $\hat{u}(t^{n+1})$:

$$
\begin{aligned}
\hat{u}(t^{n+1}) &= \mathcal{R}\left(u_M^n + \int_{t^n}^{t^{n+1}} F_0(s)\,\mathrm{d}s\right) \\
&= \mathcal{R}\left(u_M^n + \kappa_n F_0(t^{n,1})\right) \\
&= \mathcal{R}\left(u_M^n + \kappa_n\left(\frac{u_M^{n+1} - u_M^n}{\kappa_n}\ell_{\frac{1}{2}}(t^{n,1}) + \frac{u_E^{n+1} - u_M^n}{\kappa_n}\ell_1(t^{n,1})\right)\right) \\
&= \mathcal{R}\left(u_M^n + \kappa_n\left(\frac{u_M^{n+1} - u_M^n}{\kappa_n}\right)\right) \\
&= \mathcal{R}\left(u_M^n + u_M^{n+1} - u_M^n\right) \\
&= \mathcal{R}u_M^{n+1}.
\end{aligned}
\tag{2.54}
$$

By similar means, $\hat{v}(t^{n+1}) = \mathcal{R}v_M^{n+1}$.

As a result, the (piecewise quadratic in time) function $\hat{u}(t)$ (similarly, $\hat{v}(t)$) is given by the sum of the (piecewise linear in time) function $\mathcal{R}U(t)$ (similarly, $\mathcal{R}V(t)$) and the (piecewise quadratic in time) function $\frac{1}{4}(u_M^{n+1} - u_E^{n+1})\hat{\ell}_{\frac{1}{2}}(t)$ (similarly, $\frac{1}{4}(v_M^{n+1} - v_E^{n+1})\hat{\ell}_{\frac{1}{2}}(t)$), yielding the desired result. $\square$

2.5.3 The error estimates

To develop the error estimates, we derive an error equation for $u - \hat{u}$ and $v - \hat{v}$ which features a computable right-hand side.

Lemma 2.11. *The errors $u-\hat{u}$ and $v-\hat{v}$ satisfy the following error equation:*

$$\begin{bmatrix} (u-\hat{u})_t \\ (v-\hat{v})_t \end{bmatrix} + \begin{bmatrix} A & B & C \\ D & E & F \end{bmatrix} \begin{bmatrix} (u^2)_x - (\hat{u}^2)_x \\ (uv)_x - (\hat{u}\hat{v})_x \\ (v^2)_x - (\hat{v}^2)_x \end{bmatrix} + \begin{bmatrix} (u-\hat{u})_{xxx} \\ (v-\hat{v})_{xxx} \end{bmatrix} = \mathcal{E}, \tag{2.55}$$

where $\mathcal{E} = \sum_{i=0}^{2} \mathcal{E}_i$ is a computable quantity with

$$\mathcal{E}_0 := \begin{bmatrix} A & B & C \\ D & E & F \end{bmatrix} \left(\mathcal{R} \begin{bmatrix} \mathcal{N}(u_M^{n,1}, u_M^{n,1}) \\ \mathcal{N}(u_M^{n,1}, v_M^{n,1}) \\ \mathcal{N}(v_M^{n,1}, v_M^{n,1}) \end{bmatrix} \ell_{\frac{1}{2}}(t) + \mathcal{R} \begin{bmatrix} \mathcal{N}(u_E^{n+1}, u_E^{n+1}) \\ \mathcal{N}(u_E^{n+1}, v_E^{n+1}) \\ \mathcal{N}(v_E^{n+1}, v_E^{n+1}) \end{bmatrix} \ell_1(t) - \begin{bmatrix} (\hat{u}^2)_x \\ (\hat{u}\hat{v})_x \\ (\hat{v}^2)_x \end{bmatrix} \right), \tag{2.56}$$

$$\mathcal{E}_1 := \mathcal{R}\mathcal{D} \begin{bmatrix} u_E^{n+1} - u_M^{n+1} \\ v_E^{n+1} - v_M^{n+1} \end{bmatrix} \ell_1(t) + \frac{1}{4}\mathcal{D} \begin{bmatrix} u_E^{n+1} - u_M^{n+1} \\ v_E^{n+1} - v_M^{n+1} \end{bmatrix} \hat{\ell}_{\frac{1}{2}}(t), \text{ and} \tag{2.57}$$

$$\mathcal{E}_2 := (\mathcal{R} - \mathcal{I})\mathcal{D} \begin{bmatrix} U(t) \\ V(t) \end{bmatrix}, \tag{2.58}$$

Proof. To obtain the error equation (2.55), we add the quantity

$$- \begin{bmatrix} \hat{u}_t(t) \\ \hat{v}_t(t) \end{bmatrix} - \begin{bmatrix} A & B & C \\ D & E & F \end{bmatrix} \begin{bmatrix} (\hat{u}^2)_x \\ (\hat{u}\hat{v})_x \\ (\hat{v}^2)_x \end{bmatrix} - \begin{bmatrix} \hat{u}_{xxx} \\ \hat{v}_{xxx} \end{bmatrix} \tag{2.59}$$

to both sides of the system (2.1) and show the resulting right hand side (namely, (2.59)) is equivalent to $\mathcal{E}$. Compute the first term of (2.59) by recalling the definitions of $\hat{u}$ and $\hat{v}$. Indeed, from (2.49)-(2.51), (2.47), and (2.48), it follows that

$$\begin{aligned}
\begin{bmatrix} \hat{u}_t(t) \\ \hat{v}_t(t) \end{bmatrix} &= \mathcal{R} \begin{bmatrix} F_0(t) \\ F_1(t) \end{bmatrix} \\
&= \mathcal{R} \begin{bmatrix} \left(\dfrac{u_M^{n+1} - u_M^n}{\kappa_n}\right) \ell_{\frac{1}{2}}(t) + \left(\dfrac{u_E^{n+1} - u_M^n}{\kappa_n}\right) \ell_1(t) \\ \left(\dfrac{v_M^{n+1} - v_M^n}{\kappa_n}\right) \ell_{\frac{1}{2}}(t) + \left(\dfrac{v_E^{n+1} - v_M^n}{\kappa_n}\right) \ell_1(t) \end{bmatrix} \\
&= -\mathcal{R} \begin{bmatrix} A & B & C \\ D & E & F \end{bmatrix} \left(\begin{bmatrix} \mathcal{N}(u_M^{n,1}, u_M^{n,1}) \\ \mathcal{N}(u_M^{n,1}, v_M^{n,1}) \\ \mathcal{N}(v_M^{n,1}, v_M^{n,1}) \end{bmatrix} \ell_{\frac{1}{2}}(t) + \begin{bmatrix} \mathcal{N}(u_E^{n+1}, u_E^{n+1}) \\ \mathcal{N}(u_E^{n+1}, v_E^{n+1}) \\ \mathcal{N}(v_E^{n+1}, v_E^{n+1}) \end{bmatrix} \ell_1(t) \right) \\
&\quad - \mathcal{R}\mathcal{D} \begin{bmatrix} U(t) \\ V(t) \end{bmatrix} + \begin{bmatrix} u_E^{n+1} - u_M^{n+1} \\ v_E^{n+1} - v_M^{n+1} \end{bmatrix} \ell_1(t),
\end{aligned} \tag{2.60}$$

where in the last step we used the linearity of the operator $\mathcal{D}$. Now, recalling that $(R\phi)_{xxx} = \mathcal{D}\phi$ for ϕ in V_h^q, in view of Lemma 2.10, we obtain the following expression for the last term of (2.59):

$$\begin{bmatrix} \hat{u}_{xxx}(t) \\ \hat{v}_{xxx}(t) \end{bmatrix} = \mathcal{D} \begin{bmatrix} U(t) \\ V(t) \end{bmatrix} + \frac{1}{4}\mathcal{D} \begin{bmatrix} u_M^{n+1} - u_E^{n+1} \\ v_M^{n+1} - v_E^{n+1} \end{bmatrix} \hat{\ell}_{\frac{1}{2}}(t) \tag{2.61}$$

Combining (2.60) and (2.61) and introducing the middle term of (2.59) obtains the desired result.

□

The next result provides an *a posteriori* bound for the error generated by the fully discrete scheme (2.47).

Theorem 2.12. *Let u_M^n, v_M^n denote the solutions of the fully discrete scheme* (2.47) *and let $\hat{u}, \hat{v}$ denote their respective fully discrete reconstructions as defined in* (2.49) *and* (2.50). *The* *following a posteriori estimate holds:*

$$\|u(t^n) - u_M^n\| + \|v(t^n) - v_M^n\| \le \|u_M^n - \hat{u}(t^n)\| + \|u_M^n - \hat{u}(t^n)\| + \|v_M^n - \hat{v}(t^n)\| + \|v_M^n - \hat{v}(t^n)\| + ce^{ct^n}\left(\|u(0) - u_M^0\|^2 + \|v(0) - v_M^0\|^2 + \int_0^{t^n} \|\mathcal{E}(t) \cdot \mathcal{E}(t)\|^2 \, \mathrm{d}t\right)^{\frac{1}{2}} \tag{2.62}$$

Here, the constants depend on the $W^{1,\infty}$ seminorms of $\hat{u}$ and $\hat{v}$. Recall that $\mathcal{E} = \sum_{i=0}^{2} \mathcal{E}_i$ is the computable quantity defined via (2.56), (2.57), and (2.58).

Proof. The proof follows from a similar argument to that of the semidiscrete case in Theorem (2.9). Indeed, left-multiply the error equation (2.55) by an analogous row vector $\tilde{Q} = [2ae^{(u)} + be^{(v)} \quad be^{(u)} + 2ce^{(v)}]$ where, in this case, $e^{(u)} = u - \hat{u}$ and $e^{(v)} = v - \hat{v}$. Integrate over $[0, 1]$ to obtain an equation of the form (2.33). The terms on the left side are handled in an identical fashion to those that occur in the proof of Theorem (2.9), while the terms of the right side are estimated via applications of Cauchy-Schwarz and Young's Inequalities. An application of a differential form of Gronwall's inequality (see, e.g., [27, Appendix B., Inequality j.]) yields a desired bound for $e^{(u)}(t)$ and $e^{(v)}(t)$ in $L^2([0, 1])$. The desired result follows from the triangle inequality. □

Remark. *While the bound given above in terms of $\int_0^{t^n} \mathcal{E}(t) \cdot \mathcal{E}(t) \, \mathrm{d}t$ is reliable, it is also useful to study a coarser bound involving the individual contributions based on each term $\mathcal{E}_i$ of $\mathcal{E}$, i.e., a bound which replaces $\int_0^{t^n} \mathcal{E}(t) \cdot \mathcal{E}(t) \, \mathrm{d}t$ in (2.62) by $\sum_{i=0}^{2} \int_0^{t^n} \mathcal{E}_i(t) \cdot \mathcal{E}_i(t) \, \mathrm{d}t$. This allows the separate consideration of some estimators which are expected to depend on h and others which are expected to depend on the timestep size κ. Indeed, for u_M^n, v_M^n which behave optimally with respect to κ, it is expected that $\mathcal{E}_0$ and $\mathcal{E}_1$ should also behave optimally with respect to κ. Yet, it stands to reason that $\mathcal{E}_2$ should exhibit little, if any, dependence on κ, as $\mathcal{E}_2$ appears to be* *a measure of the spatial reconstruction error. To consider the behavior of the terms $\mathcal{E}_i$ from a spatial perspective, suppose for the moment that u_M^n, v_M^n are known to be $\mathcal{O}(h^\mu)$ approximations to solutions u, v of (2.1). Based on the single spatial derivative present in $\mathcal{E}_0$, one expects the estimator $\mathcal{E}_0$ to suffer by one power of h, behaving as $\mathcal{O}(h^{\mu-1})$. Furthermore, in light of (2.19) and (2.23), one expects the term $\mathcal{E}_2$ to suffer by three powers of h due to the presence of the operator $\mathcal{D}$ in this estimator. The temporal nature of the differences in $\mathcal{E}_1$ suggests only cursory, if any, dependence on h. Each of these intuitions will be studied experimentally below.*

2.6 *A posteriori* error estimates for the dissipative schemes

All techniques utilized above to develop *a posteriori* error estimates for the conservative semidiscrete and fully discrete schemes can be easily adapted to develop estimates for the dissipative analogs discussed in [12]. Indeed, identical versions of Theorems 2.9 and 2.12 hold should the dissipative variant $\tilde{\mathcal{D}}$ (defined in (2.14)) of the dispersive operator be utilized in lieu of the conservative operator $\mathcal{D}$. The only meaningful difference in the analysis is that the spatial reconstruction utilized must reflect the choice of dispersive operator, The dispersive reconstruction $\tilde{\mathcal{R}}$ which is suitable for this analysis was first defined in [31, Section 6] to develop *a posteriori* bounds for the Cheng-Shu Formulation for IBVPs for a single gKdV equation (see [23]). We quote their result [31, Theorem 6.1] here.

Theorem 2.13. *For each $u \in H^3(\mathcal{T}_h)$, there corresponds a unique $\tilde{\sigma} := \tilde{\mathcal{R}}u \in C^2([0,1]) \cap V_h^{q+3,\mathrm{dG}}$ such that for each cell $I = [x_m, x_{m+1}]$, $m = 0, \ldots, M-1$ in $\mathcal{T}_h$ there holds*

$$
\begin{aligned}
(\tilde{\sigma}_{xxx}, \chi)_I &= (\tilde{\mathcal{D}}^{\mathrm{dG}} u, \chi), \quad \textit{for all } \chi \in V_h^{q,\mathrm{dG}}(I), \\
\tilde{\sigma}(x_m^+) &= u(x_m^-) \\
\tilde{\sigma}_x(x_m^+) &= u_x(x_m^+), \\
\tilde{\sigma}_{xx}(x_m^+) &= u_{xx}(x_m^+).
\end{aligned}
\tag{2.63}
$$

Naturally, only two differences of note exist between this definition and that of $\mathcal{R}$ in Theorem 2.6. The first is that the operator $\tilde{\mathcal{D}}^{\mathrm{dG}}$ is used in place of $\mathcal{D}^{\mathrm{dG}}$ in the first condition of (2.63); the second is that $u_x(x_m^+)$ is used in the third condition in place of $\{u_x\}_m$. Thus, as before, we have a dispersive reconstruction $\tilde{\mathcal{R}}u$ corresponding to the dispersive operator $\tilde{\mathcal{D}}$ that is a locally computable, globally smooth function. Therefore, arguments nearly identical to those conducted above, merely replacing $\mathcal{D}$ with $\tilde{\mathcal{D}}$ and $\mathcal{R}$ with $\tilde{\mathcal{R}}$, yield Theorems 2.9 and 2.12 for the dissipative schemes.

2.7 Numerical experiments

We now present numerical experiments designed to gauge the performance of the *a posteriori* error estimates developed above. We highlight a few important issues:

(i) We provide validation of the theoretical results, including a study of the effectiveness of the error indicators $\mathcal{E}_i$, $i = 0, 1, 2$, both individually and in combination as a gauge of the error $\|u(t^n) - u_M^n\| + \|v(t^n) - v_M^n\|$. To do this, we compute several quantities emanating from the bound in Theorem 2.12, namely,

$$\eta_i := \left(\int_0^{t^n} \mathcal{E}_i(t) \cdot \mathcal{E}_i(t)\, \mathrm{d}t \right)^{\frac{1}{2}}, \text{ for } i = 0, 1, 2 \tag{2.64}$$

$$\eta := \left(\int_0^{t^n} \mathcal{E}(t) \cdot \mathcal{E}(t)\, \mathrm{d}t \right)^{\frac{1}{2}}, \text{ and} \tag{2.65}$$

$$\eta_\Sigma := \left(\sum_{i=0}^{2} \eta_i^2 \right)^{\frac{1}{2}}. \tag{2.66}$$

In what follows, effectiveness of the various indicators is quantified via the effectivity index. The effectivity $\mathrm{Eff}(\phi)$ of some indicator ϕ is defined via

$$\mathrm{Eff}(\phi) := \frac{\phi}{\|u(t^n) - u_M^n\| + \|v(t^n) - v_M^n\|}.$$

(ii) We highlight experimentally that the *a posteriori* upper bounds obtained via Theorem 2.12 (see Remark 2.5.3) decrease with the same $\mathcal{O}(\kappa^2)$ rate of the underlying fully discrete method. In this sense, these estimates can be qualified as being of optimal temporal order of accuracy.

(iii) In addition, we confirm experimentally that, in general, the *a posteriori* upper bound obtained in Theorem 2.12 decays suboptimally in terms of the spatial discretization parameter h. Recalling Remark 2.5.3, we study the degree of suboptimality exhibited by the various error indicators $\mathcal{E}_i$, both individually and in combination.

(iv) Finally, we experimentally explore consequences of this spatial suboptimality with regard to effectivity indices. We provide plots illustrating that effectivity indices remain small for reasonable choices of the spatial and temporal discretization parameters. Nevertheless, as we clearly identify a class of cases for which effectivity indices are too large to be practical, we provide heuristic correction factors depending on the polynomial degree of the spatial discretization by which the underlying suboptimality of the indicators can be corrected. We conclude by illustrating experimentally that this correction yields causes effectivity indices to behave as $\mathcal{O}(1)$ for most choices of κ and h.

In what follows, we present experiments utilizing the conservative fully discrete scheme for sake of concision, as the experiments conducted for the dissipative fully discrete scheme are not dissimilar.

As in [12], we adapt the experiments to the interval $[0, 1]$, by multiplying the third derivative terms in (2.1) by a small parameter ϵ, specified below. Consequently, in the experiments below, the indicators featuring the operator $\mathcal{D}$ are also multiplied by such a parameter. The parameters $A, B, \ldots, F$ are taken to be

$$A = \frac{1}{8}, \quad B = \frac{1}{8}, \quad C = \frac{1}{32}, \quad D = \frac{1}{8}, \quad E = 1, \quad F = -\frac{9}{32}. \tag{2.67}$$

These choices result in $a = \frac{118}{17}$, $b = -\frac{28}{17}$, and $c = 1$, which in turn yields the negative discriminant $b^2 - 4ac = -\frac{7240}{289}$.

For the various experiments, two types of solutions of (2.1) were used. These are both proportional traveling waves of the form $(u, v) = (u, 2u)$. The first is adapted from the well known *cnoidal-wave* solution of the KdV equation,

$$u(x,t) = \lambda \operatorname{cn}^2\big(4K(m)(x - \omega t - x_0) : m\big) \tag{2.68}$$

where $\mathrm{cn}(z) = \mathrm{cn}(z : m)$ is the Jacobi elliptic function with modulus $m \in (0, 1)$ (see [1]) and the parameters have the values $m = 0.9$, $\lambda = 192m\epsilon K(m)^2$, $\omega = 64\epsilon(2m-1)K(m)^2$, $\epsilon = \dfrac{1}{5760}$. Since our experiments are conducted on $[0, 1]$, shifting by $x_0 = \dfrac{1}{2}$ centers the initial value in the middle of the interval. Here, the function $K = K(m)$ is the complete elliptic integral of the first kind and the parameters are so organized that u and v have spatial period 1.

The second class of solutions is an approximation of the proportional solitary-wave solutions that were discussed in [12, Section 1.2]. The parameters $A, B, \ldots, F$ are the same as for the cnoidal-wave type solutions, and it is still the case that $(u, v) = (u, 2u)$, but now

$$u(x, t) = \Lambda\,\mathrm{sech}^2\big(K(x - \omega t - x_0)\big), \tag{2.69}$$

with $\Lambda = 1$, $\omega = \Lambda/3$, $\epsilon = \dfrac{1}{5760}$, $K = \dfrac{1}{2}\sqrt{\dfrac{\Lambda}{3\epsilon}}$, again shifting by $x_0 = \dfrac{1}{2}$ to center the initial wave profile. With $v = 2u$, this is an exact solution of the system which is not truly periodic in space. Yet, the initial data can be rendered periodic by simply restricting the above solution at $t = 0$ to the computational domain $[0, 1]$ and imposing periodic boundary conditions across $x = 0$ and $x = 1$. The resulting periodicized initial data yields a periodic solution of the system. Indeed, from previous theory, the resulting solution is approximated to within order ϵ by the restriction of $(u, 2u)$ to the period domain $[0, 1]$ over a time interval of order $\dfrac{1}{\epsilon}$ (c.f. [9] and [22]). The small value of ϵ used in the experiments with proportional solitary waves thus yields a solution, the accuracy of whose numerical approximation can be determined by comparison with the exact solution $(u, 2u)$ with u as in (2.69). Much of the numerical work on the KdV equation has made use of this small trick to check for accuracy and convergence, especially when issues surrounding solitary waves are under consideration.

2.7.1 Temporal rates of decrease

We begin our numerical experiments with a study of the temporal rates of decrease of the indicators η, η_Σ, and η_i for $i = 0, 1, 2$. Recalling Remark 2.5.3, we would like to show that each of η_0, η_1, η, and η_Σ decrease at the rate of $\mathcal{O}(\kappa^2)$ in accord with the predicted rate of decrease for the RK1 temporal discretization. In addition, we would like to show that η_2 is independent of κ, as it appears to be a measure of spatial reconstruction errors. In these experiments, we utilized uniform temporal grids, varying the number of timesteps N. In order to render the spatial errors very small and highlight the temporal errors, we utilized a uniform spatial mesh with $M = 500$ cells and polynomial degree $q = 5$. Each rate presented represents the slope of the line of best fit for the natural logarithm of the respective column, where the independent variable is the natural logarithm of the stepsize $\kappa = 1/N$. Indeed, the results in Tables 2.1 and 2.2 show that each of the indicators exhibit very close to the desired behavior. On a side note, we remark that these experiments feature quite reasonable effectivity indices with values between 3 and 5 for the temporally dependent estimators. Indeed, this is reasonable since the parameters were selected so that temporal error is the major contributor to the errors and the estimators behave optimally with respect to the timestep size κ.

Table 2.1: Computed temporal rates of decrease for *a posteriori* error estimators of the conservative fully-discrete scheme. Proportional cnoidal-wave solution with $T = 1$, $M = 500$, and $q = 5$. Varying number of timesteps N.

N	L^2 error	η_0	η_0 eff.	η_1	η_1 eff.	η_2	η_2 eff.	η	η eff.	η_Σ	η_Σ eff.
16	7.25×10^{-5}	3.09×10^{-4}	4.27	2.40×10^{-4}	3.30	6.92×10^{-7}	0.01	1.85×10^{-4}	2.54	3.91×10^{-4}	5.40
20	4.65×10^{-5}	1.99×10^{-4}	4.29	1.56×10^{-4}	3.36	6.92×10^{-7}	0.01	1.19×10^{-4}	2.57	2.53×10^{-4}	5.45
25	2.98×10^{-5}	1.28×10^{-4}	4.31	1.01×10^{-4}	3.40	6.92×10^{-7}	0.02	7.73×10^{-5}	2.59	1.64×10^{-4}	5.49
32	1.82×10^{-5}	7.87×10^{-5}	4.33	6.26×10^{-5}	3.44	6.90×10^{-7}	0.04	4.76×10^{-5}	2.62	1.01×10^{-4}	5.53
40	1.17×10^{-5}	5.05×10^{-5}	4.34	4.04×10^{-5}	3.47	6.92×10^{-7}	0.06	3.07×10^{-5}	2.64	6.47×10^{-5}	5.56
50	7.46×10^{-6}	3.24×10^{-5}	4.35	2.61×10^{-5}	3.49	6.92×10^{-7}	0.09	1.98×10^{-5}	2.65	4.16×10^{-5}	5.58
64	4.55×10^{-6}	1.98×10^{-5}	4.35	1.60×10^{-5}	3.51	6.91×10^{-7}	0.15	1.22×10^{-5}	2.67	2.55×10^{-5}	5.60
80	2.91×10^{-6}	1.27×10^{-5}	4.36	1.03×10^{-5}	3.53	6.92×10^{-7}	0.24	7.84×10^{-6}	2.69	1.64×10^{-5}	5.61
rate	**2.00**	**1.98**		**1.96**		**0.00**		**1.96**		**1.97**	

Table 2.2: Computed temporal rates of decrease for *a posteriori* error estimators of the conservative fully-discrete scheme. Proportional solitary-wave solution with $T = 1$, $M = 500$, and $q = 5$. Varying number of timesteps N.

N	L^2 error	η_0	η_0 eff.	η_1	η_1 eff.	η_2	η_2 eff.	η	η eff.	η_Σ	η_Σ eff.
16	2.34×10^{-1}	7.57×10^{-1}	3.24	4.60×10^{-1}	1.97	5.19×10^{-5}	0.00	7.33×10^{-1}	3.14	8.86×10^{-1}	3.79
20	1.50×10^{-1}	5.24×10^{-1}	3.49	3.17×10^{-1}	2.11	5.17×10^{-5}	0.00	3.59×10^{-1}	2.39	6.12×10^{-1}	4.08
25	9.78×10^{-2}	3.65×10^{-1}	3.73	2.32×10^{-1}	2.38	5.17×10^{-5}	0.00	2.41×10^{-1}	2.47	4.33×10^{-1}	4.42
32	6.09×10^{-2}	2.40×10^{-1}	3.94	1.59×10^{-1}	2.61	5.17×10^{-5}	0.00	1.62×10^{-1}	2.65	2.88×10^{-1}	4.73
40	3.95×10^{-2}	1.62×10^{-1}	4.10	1.09×10^{-1}	2.76	5.17×10^{-5}	0.00	1.08×10^{-1}	2.75	1.95×10^{-1}	4.94
50	2.55×10^{-2}	1.08×10^{-1}	4.23	7.39×10^{-2}	2.90	5.17×10^{-5}	0.00	7.14×10^{-2}	2.81	1.31×10^{-1}	5.13
64	1.56×10^{-2}	6.81×10^{-2}	4.36	4.74×10^{-2}	3.04	5.17×10^{-5}	0.00	4.45×10^{-2}	2.85	8.30×10^{-2}	5.31
80	1.00×10^{-2}	4.46×10^{-2}	4.44	3.15×10^{-2}	3.14	5.17×10^{-5}	0.01	2.88×10^{-2}	2.87	5.46×10^{-2}	5.44
rate	**1.95**	**1.76**		**1.66**		**0.00**		**1.92**		**1.73**	

2.7.2 Spatial rates of decrease

We continue our numerical experiments with a study of spatial rates of decrease for the various estimators. Recall from [12] that the spatial rates of decrease for the conservative fully discrete schemes are experimentally observed to be $\mathcal{O}(h^{\mu})$ where $\mu = q + 1$ for odd polynomial degree and $\mu = q$ for even polynomial degree. We stress that this is due to experimental observation alone, as the available theory is less generous. Nevertheless, reflecting upon Remark 2.5.3 with this observation in mind, we would like to see the estimator η_0 behave as $\mathcal{O}(h^{\mu-1})$ and η_2 and, consequently, η and η_Σ behave as $\mathcal{O}(h^{\mu-3})$. Furthermore, we expect η_1 to exhibit little to no dependence on h.

In these experiments, we utilize uniform spatial and temporal grids. To allow the spatial errors to dominate by several orders of magnitude (a difficult task due to the high spatial order observed for (2.47), cf. [12], when compared with fixed second order temporal rate), we use an extremely small timestep size $\kappa = 10^{-7}$. We utilize a range of very small numbers of cells M and polynomial degrees $q = 2, 3, 4$. In Tables 2.3, 2.4, and 2.5, we provide results with final time $T = 1/10$ computed with the cnoidal-wave solution. In Tables 2.6, 2.7, and 2.8, we provide results for final time $T = 1/10$ computed with the solitary-wave solution. In Tables 2.9, 2.10, and 2.11, we exhibit similar results for final time $T = 1$ utilizing a cnoidal-wave solution.

Despite the issues plaguing experiments of this kind, Tables 2.3-2.9 exhibit spatial rates of decrease for the estimators which are quite in line with those expected. In several cases, the L^2 errors converge at a higher rate than expected, an issue which seems to be tied to the extremely small number of cells used. Nevertheless, the estimators consistently behave at rates similar to those suggested in Remark 2.5.3 based on the well-observed spatial convergence rates of the fully discrete scheme (2.47) from [12]. Finally, η_1 appears to exhibit the salutary property of being independent of h, so that η_1 and η_2 together seem to provide independent indicators for the temporal and spatial errors.

Nevertheless, in contrast to the temporal experiments of the previous section, the effectivity indices in Tables 2.3-2.9 suffer greatly due to the spatial suboptimality of several indicators. We stress that the parameters chosen for the experiments in Tables 2.3-2.9 were chosen to highlight the spatial suboptimality. Indeed, it is then natural that significant growth in the effectivity indices of the various indicators occurs as the number of cells increases. Due to the computational efficiency with which the fully discrete scheme and *a posteriori* estimators can be computed even for high numbers of cells and high polynomial degree, it is highly unlikely that such a low degree of spatial accuracy as is considered here would ever be used in practice. Instead, spatial errors can be made extremely small with computational ease by selecting a reasonable number of cells and even slightly higher polynomial degree. As hinted at by the previous section, in these cases effectivity indices remain small, as temporal error overshadows spatial error as the primary contributor to the total approximation error.

Finally, though the L^2 errors decay as expected, these errors oscillate as M is increased, causing far more pronounced oscillations in the effectivity indices. These oscillations in the L^2 error is not well-understood, but are well-observed in our experiments and appear most noticeably in cases which feature low numbers of cells. Certain consequences of this behavior are observed for low numbers of cells in the various contour plots of Section 2.7.4.

Table 2.3: Computed spatial rates of decrease for *a posteriori* error estimators of the conservative fully-discrete scheme. Proportional cnoidal-wave solution with $T = \dfrac{1}{10}$, fine temporal resolution with $\kappa = 10^{-7}$. Varying number of cells with $q = 2$.

M	L^2 error	η_0	η_0 eff.	η_1	η_1 eff.	η_2	η_2 eff.	η	η eff.	η_Σ	η_Σ eff.
15	3.13×10^{-3}	5.20×10^{-3}	1.66	0.00	0.00	4.83×10^{-2}	15.44	4.26×10^{-2}	13.62	4.86×10^{-2}	15.52
16	2.97×10^{-3}	4.95×10^{-3}	1.67	0.00	0.00	5.35×10^{-2}	18.02	4.82×10^{-2}	16.26	5.37×10^{-2}	18.10
17	3.80×10^{-3}	4.38×10^{-3}	1.15	0.00	0.00	5.88×10^{-2}	15.48	5.42×10^{-2}	14.26	5.90×10^{-2}	15.52
18	3.39×10^{-3}	4.19×10^{-3}	1.24	0.00	0.00	6.50×10^{-2}	19.17	6.05×10^{-2}	17.84	6.51×10^{-2}	19.21
19	2.62×10^{-3}	3.72×10^{-3}	1.42	0.00	0.00	7.05×10^{-2}	26.97	6.68×10^{-2}	25.56	7.06×10^{-2}	27.00
20	2.12×10^{-3}	3.39×10^{-3}	1.60	0.00	0.00	7.56×10^{-2}	35.66	7.27×10^{-2}	34.30	7.57×10^{-2}	35.70
21	2.16×10^{-3}	3.02×10^{-3}	1.40	0.00	0.00	8.02×10^{-2}	37.19	7.78×10^{-2}	36.08	8.03×10^{-2}	37.21
22	2.50×10^{-3}	2.89×10^{-3}	1.16	0.00	0.00	8.48×10^{-2}	33.89	8.22×10^{-2}	32.87	8.48×10^{-2}	33.91
23	1.56×10^{-3}	2.78×10^{-3}	1.78	0.00	0.00	8.90×10^{-2}	56.99	8.62×10^{-2}	55.21	8.91×10^{-2}	57.02
24	1.71×10^{-3}	2.63×10^{-3}	1.54	0.00	0.00	9.35×10^{-2}	54.77	9.08×10^{-2}	53.20	9.36×10^{-2}	54.80
25	1.62×10^{-3}	2.47×10^{-3}	1.53	0.00	0.00	9.87×10^{-2}	61.07	9.62×10^{-2}	59.49	9.87×10^{-2}	61.08
26	1.69×10^{-3}	2.39×10^{-3}	1.42	0.00	0.00	1.04×10^{-1}	61.73	1.02×10^{-1}	60.16	1.04×10^{-1}	61.75
27	1.17×10^{-3}	2.29×10^{-3}	1.95	0.00	0.00	1.10×10^{-1}	93.83	1.07×10^{-1}	91.53	1.10×10^{-1}	93.85
28	1.30×10^{-3}	2.13×10^{-3}	1.64	0.00	0.00	1.15×10^{-1}	88.73	1.13×10^{-1}	86.86	1.15×10^{-1}	88.75
29	1.35×10^{-3}	1.99×10^{-3}	1.48	0.00	0.00	1.20×10^{-1}	89.25	1.18×10^{-1}	87.65	1.20×10^{-1}	89.27
30	1.00×10^{-3}	1.90×10^{-3}	1.90	0.00	0.00	1.25×10^{-1}	124.56	1.23×10^{-1}	122.43	1.25×10^{-1}	124.57
31	1.03×10^{-3}	1.85×10^{-3}	1.79	0.00	0.00	1.29×10^{-1}	125.16	1.27×10^{-1}	123.09	1.29×10^{-1}	125.18
32	8.52×10^{-4}	1.75×10^{-3}	2.06	0.00	0.00	1.34×10^{-1}	156.81	1.32×10^{-1}	154.43	1.34×10^{-1}	156.82
33	1.11×10^{-3}	1.65×10^{-3}	1.49	0.00	0.00	1.37×10^{-1}	123.63	1.35×10^{-1}	121.91	1.37×10^{-1}	123.64
34	9.76×10^{-4}	1.57×10^{-3}	1.61	0.00	0.00	1.41×10^{-1}	144.32	1.39×10^{-1}	142.50	1.41×10^{-1}	144.33
35	6.97×10^{-4}	1.52×10^{-3}	2.18	0.00	0.00	1.45×10^{-1}	207.46	1.43×10^{-1}	204.91	1.45×10^{-1}	207.47
36	7.83×10^{-4}	1.48×10^{-3}	1.89	0.00	0.00	1.48×10^{-1}	189.34	1.46×10^{-1}	187.09	1.48×10^{-1}	189.35
37	5.09×10^{-4}	1.40×10^{-3}	2.75	0.00	0.00	1.52×10^{-1}	298.49	1.50×10^{-1}	295.26	1.52×10^{-1}	298.50
38	7.34×10^{-4}	1.38×10^{-3}	1.87	0.00	0.00	1.56×10^{-1}	211.91	1.54×10^{-1}	209.62	1.56×10^{-1}	211.92
39	5.57×10^{-4}	1.30×10^{-3}	2.33	0.00	0.00	1.59×10^{-1}	285.57	1.57×10^{-1}	282.81	1.59×10^{-1}	285.58
40	7.38×10^{-4}	1.26×10^{-3}	1.71	0.00	0.00	1.62×10^{-1}	219.56	1.60×10^{-1}	217.51	1.62×10^{-1}	219.57
41	5.06×10^{-4}	1.22×10^{-3}	2.41	0.00	0.00	1.65×10^{-1}	326.20	1.64×10^{-1}	323.30	1.65×10^{-1}	326.21
42	6.72×10^{-4}	1.17×10^{-3}	1.74	0.00	0.00	1.68×10^{-1}	250.41	1.67×10^{-1}	248.31	1.68×10^{-1}	250.42
43	4.13×10^{-4}	1.13×10^{-3}	2.73	0.00	0.00	1.71×10^{-1}	413.78	1.70×10^{-1}	410.48	1.71×10^{-1}	413.79
44	5.48×10^{-4}	1.09×10^{-3}	1.99	0.00	0.00	1.74×10^{-1}	316.67	1.72×10^{-1}	314.27	1.74×10^{-1}	316.67
45	3.56×10^{-4}	1.05×10^{-3}	2.94	0.00	0.00	1.76×10^{-1}	494.31	1.75×10^{-1}	490.75	1.76×10^{-1}	494.32
46	4.35×10^{-4}	1.01×10^{-3}	2.33	0.00	0.00	1.79×10^{-1}	410.97	1.78×10^{-1}	408.16	1.79×10^{-1}	410.98
47	5.05×10^{-4}	9.83×10^{-4}	1.95	0.00	0.00	1.81×10^{-1}	358.43	1.80×10^{-1}	356.05	1.81×10^{-1}	358.43
48	4.62×10^{-4}	9.47×10^{-4}	2.05	0.00	0.00	1.84×10^{-1}	396.94	1.82×10^{-1}	394.47	1.84×10^{-1}	396.94
49	5.20×10^{-4}	9.27×10^{-4}	1.78	0.00	0.00	1.86×10^{-1}	357.72	1.85×10^{-1}	355.53	1.86×10^{-1}	357.72
50	3.20×10^{-4}	8.88×10^{-4}	2.78	0.00	0.00	1.88×10^{-1}	587.93	1.87×10^{-1}	584.57	1.88×10^{-1}	587.93
51	3.64×10^{-4}	8.67×10^{-4}	2.38	0.00	0.00	1.90×10^{-1}	522.16	1.89×10^{-1}	519.25	1.90×10^{-1}	522.17
52	4.74×10^{-4}	8.37×10^{-4}	1.76	0.00	0.00	1.92×10^{-1}	405.03	1.91×10^{-1}	402.88	1.92×10^{-1}	405.03
53	3.49×10^{-4}	8.12×10^{-4}	2.33	0.00	0.00	1.94×10^{-1}	556.48	1.93×10^{-1}	553.65	1.94×10^{-1}	556.49
54	3.11×10^{-4}	7.92×10^{-4}	2.55	0.00	0.00	1.96×10^{-1}	629.67	1.95×10^{-1}	626.54	1.96×10^{-1}	629.67
55	4.18×10^{-4}	7.64×10^{-4}	1.83	0.00	0.00	1.98×10^{-1}	473.40	1.97×10^{-1}	471.17	1.98×10^{-1}	473.40
56	2.92×10^{-4}	7.43×10^{-4}	2.55	0.00	0.00	2.00×10^{-1}	684.31	1.99×10^{-1}	681.20	2.00×10^{-1}	684.31
57	2.87×10^{-4}	7.25×10^{-4}	2.52	0.00	0.00	2.01×10^{-1}	699.99	2.00×10^{-1}	696.89	2.01×10^{-1}	699.99
58	3.96×10^{-4}	7.03×10^{-4}	1.77	0.00	0.00	2.03×10^{-1}	511.81	2.02×10^{-1}	509.64	2.03×10^{-1}	511.82
59	2.53×10^{-4}	6.81×10^{-4}	2.69	0.00	0.00	2.04×10^{-1}	807.49	2.04×10^{-1}	804.21	2.04×10^{-1}	807.50
60	2.91×10^{-4}	6.67×10^{-4}	2.29	0.00	0.00	2.06×10^{-1}	708.12	2.05×10^{-1}	705.31	2.06×10^{-1}	708.12
rate	1.92	1.48		0.00		-1.00		-1.06		-1.00	

Table 2.4: Computed spatial rates of decrease for *a posteriori* error estimators of the conservative fully-discrete scheme. Proportional cnoidal-wave solution with $T = \dfrac{1}{10}$, fine temporal resolution with $\kappa = 10^{-7}$. Varying number of cells with $q = 3$.

M	L^2 error	η_0	η_0 eff.	η_1	η_1 eff.	η_2	η_2 eff.	η	η eff.	η_Σ	η_Σ eff.
15	2.25×10^{-3}	1.52×10^{-3}	0.68	0.00	0.00	5.61×10^{-2}	24.97	5.49×10^{-2}	24.40	5.61×10^{-2}	24.97
16	1.11×10^{-3}	1.11×10^{-3}	1.00	0.00	0.00	2.44×10^{-2}	21.89	2.38×10^{-2}	21.42	2.44×10^{-2}	21.91
17	1.52×10^{-3}	1.08×10^{-3}	0.71	0.00	0.00	4.00×10^{-2}	26.37	3.93×10^{-2}	25.93	4.00×10^{-2}	26.38
18	5.34×10^{-4}	8.03×10^{-4}	1.50	0.00	0.00	2.30×10^{-2}	43.02	2.26×10^{-2}	42.31	2.30×10^{-2}	43.05
19	4.52×10^{-4}	6.21×10^{-4}	1.37	0.00	0.00	2.95×10^{-2}	65.23	2.91×10^{-2}	64.28	2.95×10^{-2}	65.24
20	3.85×10^{-4}	5.12×10^{-4}	1.33	0.00	0.00	1.95×10^{-2}	50.78	1.93×10^{-2}	50.20	1.95×10^{-2}	50.80
21	3.69×10^{-4}	4.84×10^{-4}	1.31	0.00	0.00	2.10×10^{-2}	56.98	2.08×10^{-2}	56.36	2.10×10^{-2}	57.00
22	2.10×10^{-4}	3.92×10^{-4}	1.86	0.00	0.00	1.56×10^{-2}	74.27	1.55×10^{-2}	73.53	1.56×10^{-2}	74.29
23	1.73×10^{-4}	3.18×10^{-4}	1.84	0.00	0.00	1.53×10^{-2}	88.77	1.52×10^{-2}	87.98	1.54×10^{-2}	88.79
24	1.32×10^{-4}	2.78×10^{-4}	2.10	0.00	0.00	1.21×10^{-2}	91.37	1.20×10^{-2}	90.65	1.21×10^{-2}	91.39
25	8.47×10^{-5}	2.53×10^{-4}	2.99	0.00	0.00	1.11×10^{-2}	130.96	1.10×10^{-2}	129.96	1.11×10^{-2}	131.00
26	5.08×10^{-5}	2.22×10^{-4}	4.36	0.00	0.00	9.13×10^{-3}	179.62	9.06×10^{-3}	178.19	9.13×10^{-3}	179.68
27	5.59×10^{-5}	1.93×10^{-4}	3.45	0.00	0.00	7.85×10^{-3}	140.42	7.81×10^{-3}	139.65	7.85×10^{-3}	140.47
28	5.16×10^{-5}	1.74×10^{-4}	3.37	0.00	0.00	6.76×10^{-3}	131.12	6.72×10^{-3}	130.44	6.76×10^{-3}	131.17
29	2.23×10^{-5}	1.58×10^{-4}	7.10	0.00	0.00	5.99×10^{-3}	269.07	5.96×10^{-3}	267.85	5.99×10^{-3}	269.16
30	3.25×10^{-5}	1.44×10^{-4}	4.42	0.00	0.00	5.21×10^{-3}	160.64	5.19×10^{-3}	160.00	5.21×10^{-3}	160.70
31	2.70×10^{-5}	1.31×10^{-4}	4.86	0.00	0.00	4.56×10^{-3}	169.09	4.55×10^{-3}	168.54	4.56×10^{-3}	169.16
32	2.21×10^{-5}	1.21×10^{-4}	5.45	0.00	0.00	4.06×10^{-3}	183.80	4.05×10^{-3}	183.31	4.06×10^{-3}	183.88
33	1.88×10^{-5}	1.11×10^{-4}	5.92	0.00	0.00	3.69×10^{-3}	196.42	3.68×10^{-3}	195.92	3.70×10^{-3}	196.51
34	1.97×10^{-5}	1.03×10^{-4}	5.25	0.00	0.00	3.22×10^{-3}	163.67	3.21×10^{-3}	163.23	3.22×10^{-3}	163.75
35	1.32×10^{-5}	9.60×10^{-5}	7.27	0.00	0.00	2.95×10^{-3}	223.79	2.95×10^{-3}	223.40	2.96×10^{-3}	223.91
36	1.36×10^{-5}	8.96×10^{-5}	6.57	0.00	0.00	2.74×10^{-3}	201.08	2.74×10^{-3}	200.85	2.74×10^{-3}	201.18
37	9.94×10^{-6}	8.38×10^{-5}	8.44	0.00	0.00	2.57×10^{-3}	258.45	2.57×10^{-3}	258.25	2.57×10^{-3}	258.59
38	8.22×10^{-6}	7.86×10^{-5}	9.57	0.00	0.00	2.41×10^{-3}	292.63	2.40×10^{-3}	292.43	2.41×10^{-3}	292.78
39	9.17×10^{-6}	7.39×10^{-5}	8.06	0.00	0.00	2.30×10^{-3}	250.63	2.30×10^{-3}	250.58	2.30×10^{-3}	250.76
40	8.60×10^{-6}	6.97×10^{-5}	8.10	0.00	0.00	2.21×10^{-3}	256.90	2.21×10^{-3}	256.86	2.21×10^{-3}	257.02
41	6.18×10^{-6}	6.58×10^{-5}	10.65	0.00	0.00	2.14×10^{-3}	347.12	2.14×10^{-3}	347.09	2.14×10^{-3}	347.29
42	6.46×10^{-6}	6.22×10^{-5}	9.63	0.00	0.00	2.06×10^{-3}	318.96	2.06×10^{-3}	318.95	2.06×10^{-3}	319.10
43	4.99×10^{-6}	5.90×10^{-5}	11.82	0.00	0.00	2.01×10^{-3}	403.32	2.01×10^{-3}	403.36	2.01×10^{-3}	403.49
44	4.14×10^{-6}	5.60×10^{-5}	13.54	0.00	0.00	1.97×10^{-3}	476.64	1.97×10^{-3}	476.73	1.97×10^{-3}	476.83
45	5.16×10^{-6}	5.32×10^{-5}	10.32	0.00	0.00	1.94×10^{-3}	375.99	1.94×10^{-3}	376.08	1.94×10^{-3}	376.13
46	4.52×10^{-6}	5.07×10^{-5}	11.21	0.00	0.00	1.90×10^{-3}	421.39	1.91×10^{-3}	421.51	1.91×10^{-3}	421.54
47	2.20×10^{-6}	4.83×10^{-5}	21.93	0.00	0.00	1.88×10^{-3}	852.91	1.88×10^{-3}	853.14	1.88×10^{-3}	853.19
48	3.59×10^{-6}	4.61×10^{-5}	12.86	0.00	0.00	1.86×10^{-3}	517.46	1.86×10^{-3}	517.61	1.86×10^{-3}	517.62
49	2.96×10^{-6}	4.41×10^{-5}	14.89	0.00	0.00	1.83×10^{-3}	619.38	1.83×10^{-3}	619.53	1.83×10^{-3}	619.56
50	3.61×10^{-6}	4.21×10^{-5}	11.67	0.00	0.00	1.81×10^{-3}	502.03	1.81×10^{-3}	502.18	1.81×10^{-3}	502.17
51	2.83×10^{-6}	4.04×10^{-5}	14.27	0.00	0.00	1.79×10^{-3}	634.50	1.79×10^{-3}	634.66	1.79×10^{-3}	634.66
52	2.38×10^{-6}	3.87×10^{-5}	16.25	0.00	0.00	1.78×10^{-3}	746.24	1.78×10^{-3}	746.43	1.78×10^{-3}	746.42
53	2.40×10^{-6}	3.71×10^{-5}	15.48	0.00	0.00	1.76×10^{-3}	733.42	1.76×10^{-3}	733.62	1.76×10^{-3}	733.58
54	1.73×10^{-6}	3.57×10^{-5}	20.58	0.00	0.00	1.74×10^{-3}	1,005.48	1.74×10^{-3}	1,005.75	1.74×10^{-3}	1,005.69
55	1.82×10^{-6}	3.43×10^{-5}	18.79	0.00	0.00	1.73×10^{-3}	946.06	1.73×10^{-3}	946.28	1.73×10^{-3}	946.25
56	1.68×10^{-6}	3.30×10^{-5}	19.66	0.00	0.00	1.71×10^{-3}	1,019.86	1.71×10^{-3}	1,020.09	1.71×10^{-3}	1,020.05
57	1.91×10^{-6}	3.18×10^{-5}	16.60	0.00	0.00	1.69×10^{-3}	885.85	1.70×10^{-3}	886.03	1.70×10^{-3}	886.01
58	1.60×10^{-6}	3.06×10^{-5}	19.14	0.00	0.00	1.68×10^{-3}	1,050.61	1.68×10^{-3}	1,050.82	1.68×10^{-3}	1,050.78
59	1.20×10^{-6}	2.95×10^{-5}	24.53	0.00	0.00	1.66×10^{-3}	1,382.95	1.66×10^{-3}	1,383.25	1.66×10^{-3}	1,383.17
60	1.37×10^{-6}	2.85×10^{-5}	20.77	0.00	0.00	1.65×10^{-3}	1,202.40	1.65×10^{-3}	1,202.65	1.65×10^{-3}	1,202.58
rate	5.26	2.77		-		2.55		2.54		2.55	

Table 2.5: Computed spatial rates of decrease for *a posteriori* error estimators of the conservative fully-discrete scheme. Proportional cnoidal-wave solution with $T = \dfrac{1}{10}$, fine temporal resolution with $\kappa = 10^{-7}$. Varying number of cells with $q = 4$.

M	L^2 error	η_0	η_0 eff.	η_1	η_1 eff.	η_2	η_2 eff.	η	η eff.	η_Σ	η_Σ eff.
15	3.83×10^{-5}	2.93×10^{-4}	7.65	0.00	0.00	7.08×10^{-3}	184.65	7.05×10^{-3}	183.96	7.09×10^{-3}	184.81
16	4.17×10^{-5}	2.64×10^{-4}	6.33	0.00	0.00	7.59×10^{-3}	181.79	7.56×10^{-3}	181.16	7.59×10^{-3}	181.90
17	2.70×10^{-5}	1.99×10^{-4}	7.38	0.00	0.00	6.16×10^{-3}	228.13	6.14×10^{-3}	227.37	6.16×10^{-3}	228.25
18	2.21×10^{-5}	1.80×10^{-4}	8.16	0.00	0.00	6.35×10^{-3}	287.59	6.33×10^{-3}	286.64	6.35×10^{-3}	287.71
19	1.95×10^{-5}	1.45×10^{-4}	7.45	0.00	0.00	5.54×10^{-3}	284.57	5.52×10^{-3}	283.79	5.54×10^{-3}	284.67
20	1.59×10^{-5}	1.31×10^{-4}	8.24	0.00	0.00	5.78×10^{-3}	364.41	5.76×10^{-3}	363.04	5.78×10^{-3}	364.51
21	9.45×10^{-6}	1.10×10^{-4}	11.69	0.00	0.00	5.43×10^{-3}	575.22	5.42×10^{-3}	573.38	5.44×10^{-3}	575.34
22	1.24×10^{-5}	9.94×10^{-5}	8.01	0.00	0.00	5.38×10^{-3}	433.38	5.36×10^{-3}	432.03	5.38×10^{-3}	433.45
23	6.97×10^{-6}	8.71×10^{-5}	12.49	0.00	0.00	5.22×10^{-3}	748.64	5.20×10^{-3}	746.43	5.22×10^{-3}	748.74
24	5.60×10^{-6}	7.86×10^{-5}	14.04	0.00	0.00	5.14×10^{-3}	917.82	5.12×10^{-3}	915.26	5.14×10^{-3}	917.93
25	4.41×10^{-6}	7.04×10^{-5}	15.96	0.00	0.00	5.01×10^{-3}	1,136.30	5.00×10^{-3}	1,133.32	5.01×10^{-3}	1,136.41
26	3.89×10^{-6}	6.40×10^{-5}	16.44	0.00	0.00	4.91×10^{-3}	1,263.08	4.90×10^{-3}	1,259.99	4.92×10^{-3}	1,263.19
27	4.58×10^{-6}	5.80×10^{-5}	12.66	0.00	0.00	4.74×10^{-3}	1,034.01	4.73×10^{-3}	1,031.77	4.74×10^{-3}	1,034.09
28	4.09×10^{-6}	5.32×10^{-5}	13.03	0.00	0.00	4.74×10^{-3}	1,159.11	4.73×10^{-3}	1,156.41	4.74×10^{-3}	1,159.18
29	2.55×10^{-6}	4.88×10^{-5}	19.14	0.00	0.00	4.63×10^{-3}	1,813.99	4.62×10^{-3}	1,810.05	4.63×10^{-3}	1,814.09
30	2.64×10^{-6}	4.50×10^{-5}	17.02	0.00	0.00	4.52×10^{-3}	1,709.83	4.51×10^{-3}	1,706.33	4.52×10^{-3}	1,709.91
31	2.59×10^{-6}	4.16×10^{-5}	16.07	0.00	0.00	4.42×10^{-3}	1,707.09	4.41×10^{-3}	1,703.74	4.42×10^{-3}	1,707.17
32	2.50×10^{-6}	3.85×10^{-5}	15.41	0.00	0.00	4.31×10^{-3}	1,723.37	4.30×10^{-3}	1,720.21	4.31×10^{-3}	1,723.44
33	1.79×10^{-6}	3.58×10^{-5}	20.07	0.00	0.00	4.20×10^{-3}	2,354.58	4.20×10^{-3}	2,350.47	4.20×10^{-3}	2,354.66
34	2.04×10^{-6}	3.34×10^{-5}	16.40	0.00	0.00	4.10×10^{-3}	2,011.61	4.09×10^{-3}	2,008.30	4.10×10^{-3}	2,011.68
35	1.30×10^{-6}	3.12×10^{-5}	24.08	0.00	0.00	3.98×10^{-3}	3,068.80	3.97×10^{-3}	3,063.92	3.98×10^{-3}	3,068.90
36	1.58×10^{-6}	2.92×10^{-5}	18.46	0.00	0.00	3.89×10^{-3}	2,460.20	3.89×10^{-3}	2,456.47	3.89×10^{-3}	2,460.27
37	1.32×10^{-6}	2.74×10^{-5}	20.75	0.00	0.00	3.79×10^{-3}	2,869.55	3.79×10^{-3}	2,865.40	3.79×10^{-3}	2,869.62
38	9.53×10^{-7}	2.58×10^{-5}	27.05	0.00	0.00	3.69×10^{-3}	3,874.01	3.69×10^{-3}	3,868.68	3.69×10^{-3}	3,874.11
39	1.15×10^{-6}	2.43×10^{-5}	21.13	0.00	0.00	3.59×10^{-3}	3,127.44	3.59×10^{-3}	3,123.32	3.59×10^{-3}	3,127.51
40	9.83×10^{-7}	2.29×10^{-5}	23.30	0.00	0.00	3.50×10^{-3}	3,558.15	3.49×10^{-3}	3,553.72	3.50×10^{-3}	3,558.24
41	9.27×10^{-7}	2.16×10^{-5}	23.34	0.00	0.00	3.40×10^{-3}	3,670.33	3.40×10^{-3}	3,665.94	3.40×10^{-3}	3,670.40
42	7.86×10^{-7}	2.05×10^{-5}	26.07	0.00	0.00	3.31×10^{-3}	4,213.59	3.31×10^{-3}	4,208.78	3.31×10^{-3}	4,213.68
43	6.58×10^{-7}	1.94×10^{-5}	29.50	0.00	0.00	3.22×10^{-3}	4,892.92	3.22×10^{-3}	4,887.54	3.22×10^{-3}	4,893.01
44	6.99×10^{-7}	1.84×10^{-5}	26.36	0.00	0.00	3.13×10^{-3}	4,481.77	3.13×10^{-3}	4,477.07	3.13×10^{-3}	4,481.86
45	5.78×10^{-7}	1.75×10^{-5}	30.29	0.00	0.00	3.05×10^{-3}	5,271.99	3.05×10^{-3}	5,266.68	3.05×10^{-3}	5,272.08
46	4.39×10^{-7}	1.67×10^{-5}	37.98	0.00	0.00	2.97×10^{-3}	6,757.56	2.96×10^{-3}	6,751.04	2.97×10^{-3}	6,757.67
47	4.60×10^{-7}	1.59×10^{-5}	34.54	0.00	0.00	2.89×10^{-3}	6,275.18	2.88×10^{-3}	6,269.37	2.89×10^{-3}	6,275.28
48	4.68×10^{-7}	1.51×10^{-5}	32.35	0.00	0.00	2.81×10^{-3}	5,998.11	2.81×10^{-3}	5,992.77	2.81×10^{-3}	5,998.20
49	4.16×10^{-7}	1.45×10^{-5}	34.78	1.92×10^{-11}	0.00	2.73×10^{-3}	6,569.90	2.73×10^{-3}	6,564.28	2.73×10^{-3}	6,569.97
50	4.68×10^{-7}	1.38×10^{-5}	29.56	1.87×10^{-10}	0.00	2.66×10^{-3}	5,680.17	2.66×10^{-3}	5,675.49	2.66×10^{-3}	5,680.24
51	3.74×10^{-7}	1.32×10^{-5}	35.35	4.37×10^{-10}	0.00	2.59×10^{-3}	6,907.36	2.58×10^{-3}	6,901.89	2.59×10^{-3}	6,907.44
52	3.29×10^{-7}	1.27×10^{-5}	38.55	7.22×10^{-10}	0.00	2.52×10^{-3}	7,652.80	2.52×10^{-3}	7,646.96	2.52×10^{-3}	7,652.89
53	2.06×10^{-7}	1.22×10^{-5}	58.86	1.05×10^{-9}	0.01	2.45×10^{-3}	11,865.38	2.45×10^{-3}	11,856.66	2.45×10^{-3}	11,865.52
54	3.33×10^{-7}	1.17×10^{-5}	35.05	1.48×10^{-9}	0.00	2.39×10^{-3}	7,168.82	2.38×10^{-3}	7,163.74	2.39×10^{-3}	7,168.91
55	2.24×10^{-7}	1.12×10^{-5}	50.06	1.96×10^{-9}	0.01	2.32×10^{-3}	10,379.46	2.32×10^{-3}	10,372.40	2.32×10^{-3}	10,379.60
56	2.57×10^{-7}	1.08×10^{-5}	41.83	2.52×10^{-9}	0.01	2.26×10^{-3}	8,786.49	2.26×10^{-3}	8,780.70	2.26×10^{-3}	8,786.60
57	2.60×10^{-7}	1.04×10^{-5}	39.88	3.07×10^{-9}	0.01	2.20×10^{-3}	8,482.24	2.20×10^{-3}	8,476.88	2.20×10^{-3}	8,482.35
58	2.52×10^{-7}	9.97×10^{-6}	39.48	3.66×10^{-9}	0.01	2.15×10^{-3}	8,496.83	2.14×10^{-3}	8,491.64	2.15×10^{-3}	8,496.95
59	2.24×10^{-7}	9.60×10^{-6}	42.95	4.26×10^{-9}	0.02	2.09×10^{-3}	9,347.48	2.09×10^{-3}	9,341.98	2.09×10^{-3}	9,347.61
60	2.02×10^{-7}	9.26×10^{-6}	45.81	4.87×10^{-9}	0.02	2.04×10^{-3}	10,078.95	2.04×10^{-3}	10,073.21	2.04×10^{-3}	10,079.05
rate	3.89	2.45		-		0.88		0.88		0.88	

Table 2.6: Computed spatial rates of decrease for *a posteriori* error estimators of the conservative fully-discrete scheme. Proportional solitary-wave solution with $T = \dfrac{1}{10}$, fine temporal resolution with $\kappa = 10^{-7}$. Varying number of cells with $q = 2$.

M	L^2 error	η_0	η_0 eff.	η_1	η_1 eff.	η_2	η_2 eff.	η	η eff.	η_Σ	η_Σ eff.
15	7.47×10^{-2}	3.93×10^{-1}	5.26	0.00	0.00	6.25×10^{-1}	8.36	7.18×10^{-1}	9.61	7.38×10^{-1}	9.88
16	7.73×10^{-2}	4.24×10^{-1}	5.48	0.00	0.00	7.87×10^{-1}	10.18	6.64×10^{-1}	8.60	8.94×10^{-1}	11.56
17	6.29×10^{-2}	3.16×10^{-1}	5.02	0.00	0.00	6.00×10^{-1}	9.54	5.96×10^{-1}	9.48	6.78×10^{-1}	10.78
18	6.49×10^{-2}	3.10×10^{-1}	4.77	0.00	0.00	6.67×10^{-1}	10.28	5.42×10^{-1}	8.35	7.35×10^{-1}	11.33
19	5.46×10^{-2}	2.55×10^{-1}	4.68	0.00	0.00	5.90×10^{-1}	10.82	5.30×10^{-1}	9.71	6.43×10^{-1}	11.79
20	5.40×10^{-2}	2.30×10^{-1}	4.26	0.00	0.00	5.93×10^{-1}	10.97	4.88×10^{-1}	9.04	6.36×10^{-1}	11.77
21	4.79×10^{-2}	2.07×10^{-1}	4.32	0.00	0.00	5.76×10^{-1}	12.01	5.03×10^{-1}	10.49	6.12×10^{-1}	12.76
22	4.56×10^{-2}	1.82×10^{-1}	3.99	0.00	0.00	5.79×10^{-1}	12.70	5.05×10^{-1}	11.07	6.07×10^{-1}	13.31
23	4.27×10^{-2}	1.75×10^{-1}	4.10	0.00	0.00	5.86×10^{-1}	13.73	5.10×10^{-1}	11.96	6.11×10^{-1}	14.33
24	3.95×10^{-2}	1.55×10^{-1}	3.91	0.00	0.00	6.16×10^{-1}	15.58	5.55×10^{-1}	14.04	6.35×10^{-1}	16.07
25	3.74×10^{-2}	1.51×10^{-1}	4.03	0.00	0.00	6.17×10^{-1}	16.52	5.61×10^{-1}	15.01	6.36×10^{-1}	17.00
26	3.49×10^{-2}	1.38×10^{-1}	3.94	0.00	0.00	6.76×10^{-1}	19.34	6.28×10^{-1}	17.97	6.90×10^{-1}	19.74
27	3.31×10^{-2}	1.34×10^{-1}	4.04	0.00	0.00	6.84×10^{-1}	20.70	6.40×10^{-1}	19.37	6.97×10^{-1}	21.10
28	3.09×10^{-2}	1.26×10^{-1}	4.07	0.00	0.00	7.54×10^{-1}	24.42	7.13×10^{-1}	23.09	7.64×10^{-1}	24.75
29	2.96×10^{-2}	1.21×10^{-1}	4.08	0.00	0.00	7.75×10^{-1}	26.21	7.41×10^{-1}	25.06	7.84×10^{-1}	26.52
30	2.71×10^{-2}	1.17×10^{-1}	4.30	0.00	0.00	8.50×10^{-1}	31.33	8.14×10^{-1}	30.01	8.58×10^{-1}	31.62
31	2.65×10^{-2}	1.11×10^{-1}	4.17	0.00	0.00	8.79×10^{-1}	33.12	8.49×10^{-1}	32.01	8.86×10^{-1}	33.38
32	2.46×10^{-2}	1.08×10^{-1}	4.39	0.00	0.00	9.57×10^{-1}	38.85	9.25×10^{-1}	37.56	9.63×10^{-1}	39.09
33	2.41×10^{-2}	1.02×10^{-1}	4.25	0.00	0.00	1.00×10^{0}	41.54	9.74×10^{-1}	40.45	1.01×10^{0}	41.76
34	2.26×10^{-2}	9.98×10^{-2}	4.42	0.00	0.00	1.07×10^{0}	47.35	1.04×10^{0}	46.22	1.07×10^{0}	47.56
35	2.09×10^{-2}	9.61×10^{-2}	4.59	0.00	0.00	1.12×10^{0}	53.57	1.09×10^{0}	52.15	1.13×10^{0}	53.77
36	2.04×10^{-2}	9.26×10^{-2}	4.54	0.00	0.00	1.21×10^{0}	59.19	1.18×10^{0}	57.99	1.21×10^{0}	59.37
37	1.96×10^{-2}	8.87×10^{-2}	4.53	0.00	0.00	1.24×10^{0}	63.29	1.21×10^{0}	61.99	1.24×10^{0}	63.45
38	1.87×10^{-2}	8.61×10^{-2}	4.59	0.00	0.00	1.33×10^{0}	71.05	1.31×10^{0}	69.82	1.33×10^{0}	71.20
39	1.76×10^{-2}	8.30×10^{-2}	4.71	0.00	0.00	1.40×10^{0}	79.14	1.37×10^{0}	77.63	1.40×10^{0}	79.28
40	1.71×10^{-2}	8.00×10^{-2}	4.69	0.00	0.00	1.42×10^{0}	83.14	1.40×10^{0}	81.81	1.42×10^{0}	83.27
41	1.62×10^{-2}	7.72×10^{-2}	4.78	0.00	0.00	1.55×10^{0}	96.24	1.53×10^{0}	94.79	1.56×10^{0}	96.36
42	1.57×10^{-2}	7.41×10^{-2}	4.73	1.01×10^{-10}	0.00	1.55×10^{0}	99.01	1.53×10^{0}	97.72	1.55×10^{0}	99.12
43	1.50×10^{-2}	7.20×10^{-2}	4.79	3.10×10^{-10}	0.00	1.66×10^{0}	110.32	1.64×10^{0}	108.87	1.66×10^{0}	110.43
44	1.43×10^{-2}	7.00×10^{-2}	4.90	5.27×10^{-10}	0.00	1.71×10^{0}	119.56	1.69×10^{0}	117.92	1.71×10^{0}	119.66
45	1.37×10^{-2}	6.67×10^{-2}	4.88	9.57×10^{-10}	0.00	1.77×10^{0}	129.46	1.75×10^{0}	128.07	1.77×10^{0}	129.55
46	1.31×10^{-2}	6.51×10^{-2}	4.97	1.90×10^{-9}	0.00	1.83×10^{0}	140.05	1.81×10^{0}	138.52	1.83×10^{0}	140.14
47	1.25×10^{-2}	6.29×10^{-2}	5.04	3.16×10^{-9}	0.00	1.92×10^{0}	153.74	1.90×10^{0}	152.08	1.92×10^{0}	153.82
48	1.20×10^{-2}	6.08×10^{-2}	5.05	4.45×10^{-9}	0.00	1.93×10^{0}	160.57	1.91×10^{0}	158.96	1.93×10^{0}	160.65
49	1.16×10^{-2}	5.94×10^{-2}	5.11	6.39×10^{-9}	0.00	2.05×10^{0}	176.53	2.03×10^{0}	174.78	2.05×10^{0}	176.60
50	1.13×10^{-2}	5.66×10^{-2}	4.99	8.27×10^{-9}	0.00	2.08×10^{0}	183.73	2.07×10^{0}	182.29	2.08×10^{0}	183.80
51	1.07×10^{-2}	5.56×10^{-2}	5.18	1.05×10^{-8}	0.00	2.13×10^{0}	198.84	2.12×10^{0}	197.07	2.14×10^{0}	198.91
52	1.05×10^{-2}	5.45×10^{-2}	5.19	1.34×10^{-8}	0.00	2.23×10^{0}	212.16	2.21×10^{0}	210.24	2.23×10^{0}	212.23
53	1.01×10^{-2}	5.20×10^{-2}	5.13	1.59×10^{-8}	0.00	2.24×10^{0}	220.91	2.22×10^{0}	219.28	2.24×10^{0}	220.98
54	9.52×10^{-3}	5.10×10^{-2}	5.36	1.93×10^{-8}	0.00	2.32×10^{0}	244.09	2.30×10^{0}	242.20	2.32×10^{0}	244.15
55	9.21×10^{-3}	4.92×10^{-2}	5.34	2.28×10^{-8}	0.00	2.39×10^{0}	259.82	2.38×10^{0}	257.99	2.39×10^{0}	259.87
56	9.15×10^{-3}	4.77×10^{-2}	5.21	2.62×10^{-8}	0.00	2.41×10^{0}	263.45	2.40×10^{0}	261.70	2.41×10^{0}	263.51
57	8.65×10^{-3}	4.68×10^{-2}	5.41	3.07×10^{-8}	0.00	2.51×10^{0}	290.17	2.49×10^{0}	288.21	2.51×10^{0}	290.22
58	8.48×10^{-3}	4.52×10^{-2}	5.33	3.49×10^{-8}	0.00	2.55×10^{0}	301.11	2.54×10^{0}	299.28	2.56×10^{0}	301.16
59	8.15×10^{-3}	4.43×10^{-2}	5.43	3.95×10^{-8}	0.00	2.60×10^{0}	319.39	2.59×10^{0}	317.42	2.60×10^{0}	319.44
60	8.05×10^{-3}	4.33×10^{-2}	5.38	4.52×10^{-8}	0.00	2.70×10^{0}	335.02	2.68×10^{0}	333.01	2.70×10^{0}	335.07
rate	1.68	1.55		-		-1.29		-1.37		-1.20	

Table 2.7: Computed spatial rates of decrease for *a posteriori* error estimators of the conservative fully-discrete scheme. Proportional solitary-wave solution with $T = \dfrac{1}{10}$, fine temporal resolution with $\kappa = 10^{-7}$. Varying number of cells with $q = 3$.

M	L^2 error	η_0	η_0 eff.	η_1	η_1 eff.	η_2	η_2 eff.	η	η eff.	η_Σ	η_Σ eff.
15	9.81×10^{-2}	2.32×10^{-1}	2.37	0.00	0.00	2.94×10^{0}	29.99	2.83×10^{0}	28.89	2.95×10^{0}	30.08
16	1.43×10^{-1}	2.39×10^{-1}	1.67	0.00	0.00	1.19×10^{0}	8.33	1.16×10^{0}	8.12	1.22×10^{0}	8.49
17	7.58×10^{-2}	2.16×10^{-1}	2.84	0.00	0.00	3.10×10^{0}	40.89	3.01×10^{0}	39.71	3.11×10^{0}	40.98
18	1.07×10^{-1}	1.63×10^{-1}	1.52	0.00	0.00	9.51×10^{-1}	8.85	9.30×10^{-1}	8.66	9.65×10^{-1}	8.98
19	7.28×10^{-2}	2.11×10^{-1}	2.90	0.00	0.00	3.18×10^{0}	43.71	3.11×10^{0}	42.74	3.19×10^{0}	43.80
20	8.79×10^{-2}	1.21×10^{-1}	1.37	0.00	0.00	6.88×10^{-1}	7.83	6.71×10^{-1}	7.63	6.99×10^{-1}	7.95
21	4.82×10^{-2}	1.54×10^{-1}	3.20	0.00	0.00	3.11×10^{0}	64.49	3.06×10^{0}	63.45	3.11×10^{0}	64.57
22	8.05×10^{-2}	1.01×10^{-1}	1.26	0.00	0.00	4.28×10^{-1}	5.32	4.21×10^{-1}	5.23	4.40×10^{-1}	5.47
23	3.60×10^{-2}	1.16×10^{-1}	3.23	0.00	0.00	2.95×10^{0}	81.83	2.91×10^{0}	80.81	2.95×10^{0}	81.90
24	7.30×10^{-2}	9.34×10^{-2}	1.28	0.00	0.00	2.63×10^{-1}	3.61	2.66×10^{-1}	3.65	2.79×10^{-1}	3.83
25	4.01×10^{-2}	9.41×10^{-2}	2.35	6.84×10^{-11}	0.00	2.73×10^{0}	67.93	2.70×10^{0}	67.19	2.73×10^{0}	67.97
26	6.28×10^{-2}	8.62×10^{-2}	1.37	0.00	0.00	2.55×10^{-1}	4.06	2.61×10^{-1}	4.16	2.69×10^{-1}	4.29
27	3.34×10^{-2}	7.35×10^{-2}	2.21	1.02×10^{-9}	0.00	2.47×10^{0}	74.09	2.45×10^{0}	73.44	2.47×10^{0}	74.13
28	5.30×10^{-2}	8.10×10^{-2}	1.53	0.00	0.00	3.57×10^{-1}	6.75	3.63×10^{-1}	6.86	3.66×10^{-1}	6.92
29	2.53×10^{-2}	5.62×10^{-2}	2.22	3.15×10^{-9}	0.00	2.19×10^{0}	86.28	2.17×10^{0}	85.65	2.19×10^{0}	86.31
30	4.28×10^{-2}	7.47×10^{-2}	1.74	0.00	0.00	4.53×10^{-1}	10.57	4.57×10^{-1}	10.68	4.59×10^{-1}	10.71
31	1.78×10^{-2}	4.37×10^{-2}	2.45	6.32×10^{-9}	0.00	1.91×10^{0}	107.42	1.90×10^{0}	106.72	1.91×10^{0}	107.45
32	3.35×10^{-2}	6.66×10^{-2}	1.99	1.07×10^{-9}	0.00	5.20×10^{-1}	15.54	5.23×10^{-1}	15.63	5.24×10^{-1}	15.67
33	1.02×10^{-2}	3.44×10^{-2}	3.36	1.04×10^{-8}	0.00	1.66×10^{0}	162.12	1.65×10^{0}	161.21	1.66×10^{0}	162.16
34	2.53×10^{-2}	5.79×10^{-2}	2.29	4.54×10^{-9}	0.00	5.56×10^{-1}	22.00	5.58×10^{-1}	22.06	5.59×10^{-1}	22.11
35	6.59×10^{-3}	2.74×10^{-2}	4.15	1.54×10^{-8}	0.00	1.42×10^{0}	214.98	1.41×10^{0}	213.91	1.42×10^{0}	215.02
36	1.85×10^{-2}	4.92×10^{-2}	2.66	9.71×10^{-9}	0.00	5.66×10^{-1}	30.69	5.67×10^{-1}	30.73	5.69×10^{-1}	30.80
37	5.63×10^{-3}	2.24×10^{-2}	3.97	2.11×10^{-8}	0.00	1.20×10^{0}	213.33	1.19×10^{0}	212.38	1.20×10^{0}	213.36
38	1.30×10^{-2}	4.08×10^{-2}	3.13	1.62×10^{-8}	0.00	5.50×10^{-1}	42.29	5.51×10^{-1}	42.32	5.52×10^{-1}	42.40
39	3.89×10^{-3}	1.85×10^{-2}	4.75	2.74×10^{-8}	0.00	1.02×10^{0}	261.62	1.01×10^{0}	260.56	1.02×10^{0}	261.66
40	8.87×10^{-3}	3.31×10^{-2}	3.74	2.36×10^{-8}	0.00	5.24×10^{-1}	59.01	5.24×10^{-1}	59.01	5.25×10^{-1}	59.13
41	1.94×10^{-3}	1.53×10^{-2}	7.88	3.45×10^{-8}	0.00	8.57×10^{-1}	441.82	8.54×10^{-1}	440.20	8.57×10^{-1}	441.89
42	5.82×10^{-3}	2.66×10^{-2}	4.56	3.19×10^{-8}	0.00	4.92×10^{-1}	84.48	4.92×10^{-1}	84.42	4.93×10^{-1}	84.60
43	1.37×10^{-3}	1.30×10^{-2}	9.46	4.22×10^{-8}	0.00	7.20×10^{-1}	523.89	7.18×10^{-1}	522.14	7.20×10^{-1}	523.98
44	3.67×10^{-3}	2.11×10^{-2}	5.75	4.08×10^{-8}	0.00	4.54×10^{-1}	123.51	4.53×10^{-1}	123.38	4.54×10^{-1}	123.64
45	1.01×10^{-3}	1.13×10^{-2}	11.12	5.06×10^{-8}	0.00	6.05×10^{-1}	597.58	6.03×10^{-1}	595.74	6.05×10^{-1}	597.68
46	2.20×10^{-3}	1.67×10^{-2}	7.60	5.03×10^{-8}	0.00	4.10×10^{-1}	185.93	4.09×10^{-1}	185.71	4.10×10^{-1}	186.09
47	7.62×10^{-4}	9.66×10^{-3}	12.68	5.98×10^{-8}	0.00	5.09×10^{-1}	667.89	5.07×10^{-1}	666.01	5.09×10^{-1}	668.01
48	1.28×10^{-3}	1.33×10^{-2}	10.38	6.06×10^{-8}	0.00	3.65×10^{-1}	284.38	3.64×10^{-1}	283.99	3.65×10^{-1}	284.57
49	6.19×10^{-4}	8.39×10^{-3}	13.56	6.96×10^{-8}	0.00	4.27×10^{-1}	689.60	4.26×10^{-1}	687.87	4.27×10^{-1}	689.73
50	7.34×10^{-4}	1.07×10^{-2}	14.59	7.14×10^{-8}	0.00	3.28×10^{-1}	446.44	3.27×10^{-1}	445.78	3.28×10^{-1}	446.67
51	3.41×10^{-4}	7.39×10^{-3}	21.69	8.00×10^{-8}	0.00	3.60×10^{-1}	1,055.86	3.59×10^{-1}	1,053.46	3.60×10^{-1}	1,056.08
52	4.07×10^{-4}	8.75×10^{-3}	21.51	8.27×10^{-8}	0.00	2.90×10^{-1}	713.69	2.90×10^{-1}	712.62	2.90×10^{-1}	714.02
53	3.74×10^{-4}	6.52×10^{-3}	17.46	9.09×10^{-8}	0.00	3.07×10^{-1}	822.54	3.07×10^{-1}	820.86	3.07×10^{-1}	822.72
54	2.47×10^{-4}	7.29×10^{-3}	29.53	9.44×10^{-8}	0.00	2.55×10^{-1}	1,034.48	2.55×10^{-1}	1,032.94	2.55×10^{-1}	1,034.90
55	2.56×10^{-4}	5.81×10^{-3}	22.72	1.02×10^{-7}	0.00	2.61×10^{-1}	1,021.16	2.61×10^{-1}	1,019.40	2.61×10^{-1}	1,021.41
56	1.78×10^{-4}	6.20×10^{-3}	34.72	1.06×10^{-7}	0.00	2.24×10^{-1}	1,254.68	2.24×10^{-1}	1,252.90	2.24×10^{-1}	1,255.16
57	1.72×10^{-4}	5.22×10^{-3}	30.29	1.14×10^{-7}	0.00	2.23×10^{-1}	1,293.99	2.23×10^{-1}	1,292.09	2.23×10^{-1}	1,294.35
58	1.35×10^{-4}	5.37×10^{-3}	39.73	1.19×10^{-7}	0.00	1.97×10^{-1}	1,458.33	1.97×10^{-1}	1,456.41	1.97×10^{-1}	1,458.87
59	1.79×10^{-4}	4.71×10^{-3}	26.29	1.26×10^{-7}	0.00	1.90×10^{-1}	1,061.83	1.90×10^{-1}	1,060.54	1.90×10^{-1}	1,062.16
60	1.06×10^{-4}	4.74×10^{-3}	44.75	1.31×10^{-7}	0.00	1.73×10^{-1}	1,632.35	1.73×10^{-1}	1,630.37	1.73×10^{-1}	1,632.96
rate	5.38	3.03		-		1.59		1.57		1.60	

Table 2.8: Computed spatial rates of decrease for *a posteriori* error estimators of the conservative fully-discrete scheme. Proportional solitary-wave solution with $T = \dfrac{1}{10}$, fine temporal resolution with $\kappa = 10^{-7}$. Varying number of cells with $q = 4$.

M	L^2 error	η_0	η_0 eff.	η_1	η_1 eff.	η_2	η_2 eff.	η	η eff.	η_Σ	η_Σ eff.
15	4.22×10^{-2}	1.39×10^{-1}	3.29	0.00	0.00	5.43×10^{-1}	12.86	4.91×10^{-1}	11.65	5.60×10^{-1}	13.28
16	3.32×10^{-2}	1.31×10^{-1}	3.96	0.00	0.00	4.09×10^{-1}	12.34	3.58×10^{-1}	10.80	4.30×10^{-1}	12.96
17	2.51×10^{-2}	1.04×10^{-1}	4.16	0.00	0.00	3.81×10^{-1}	15.17	3.46×10^{-1}	13.79	3.95×10^{-1}	15.73
18	1.85×10^{-2}	9.15×10^{-2}	4.95	0.00	0.00	3.72×10^{-1}	20.11	3.49×10^{-1}	18.88	3.83×10^{-1}	20.71
19	1.30×10^{-2}	7.21×10^{-2}	5.54	0.00	0.00	2.94×10^{-1}	22.64	2.77×10^{-1}	21.31	3.03×10^{-1}	23.30
20	8.91×10^{-3}	5.94×10^{-2}	6.67	0.00	0.00	3.72×10^{-1}	41.71	3.63×10^{-1}	40.78	3.76×10^{-1}	42.24
21	5.87×10^{-3}	4.72×10^{-2}	8.03	2.44×10^{-11}	0.00	2.52×10^{-1}	42.89	2.44×10^{-1}	41.58	2.56×10^{-1}	43.63
22	3.73×10^{-3}	3.75×10^{-2}	10.05	1.12×10^{-9}	0.00	3.44×10^{-1}	92.22	3.41×10^{-1}	91.42	3.46×10^{-1}	92.76
23	2.24×10^{-3}	3.07×10^{-2}	13.70	1.15×10^{-9}	0.00	2.07×10^{-1}	92.61	2.04×10^{-1}	91.15	2.10×10^{-1}	93.62
24	1.37×10^{-3}	2.43×10^{-2}	17.74	4.38×10^{-9}	0.00	3.21×10^{-1}	233.95	3.19×10^{-1}	233.00	3.21×10^{-1}	234.62
25	7.20×10^{-4}	2.06×10^{-2}	28.66	3.71×10^{-9}	0.00	1.73×10^{-1}	240.49	1.72×10^{-1}	238.44	1.74×10^{-1}	242.19
26	4.74×10^{-4}	1.68×10^{-2}	35.48	9.45×10^{-9}	0.00	2.90×10^{-1}	611.46	2.89×10^{-1}	610.09	2.90×10^{-1}	612.49
27	2.07×10^{-4}	1.47×10^{-2}	70.74	7.63×10^{-9}	0.00	1.47×10^{-1}	709.94	1.47×10^{-1}	706.92	1.48×10^{-1}	713.45
28	3.01×10^{-4}	1.24×10^{-2}	41.32	1.62×10^{-8}	0.00	2.58×10^{-1}	857.13	2.58×10^{-1}	855.95	2.59×10^{-1}	858.12
29	1.05×10^{-4}	1.10×10^{-2}	105.02	1.34×10^{-8}	0.00	1.34×10^{-1}	1,276.97	1.33×10^{-1}	1,274.54	1.34×10^{-1}	1,281.28
30	1.84×10^{-4}	9.72×10^{-3}	52.97	2.47×10^{-8}	0.00	2.30×10^{-1}	1,253.48	2.30×10^{-1}	1,252.24	2.30×10^{-1}	1,254.61
31	8.76×10^{-5}	8.59×10^{-3}	98.01	2.18×10^{-8}	0.00	1.26×10^{-1}	1,443.12	1.26×10^{-1}	1,442.43	1.27×10^{-1}	1,446.45
32	1.29×10^{-4}	7.85×10^{-3}	60.98	3.55×10^{-8}	0.00	2.06×10^{-1}	1,597.69	2.06×10^{-1}	1,596.58	2.06×10^{-1}	1,598.86
33	7.65×10^{-5}	6.94×10^{-3}	90.74	3.32×10^{-8}	0.00	1.25×10^{-1}	1,633.80	1.25×10^{-1}	1,633.45	1.25×10^{-1}	1,636.33
34	1.07×10^{-4}	6.49×10^{-3}	60.45	4.92×10^{-8}	0.00	1.85×10^{-1}	1,722.21	1.85×10^{-1}	1,721.34	1.85×10^{-1}	1,723.28
35	7.42×10^{-5}	5.76×10^{-3}	77.71	4.86×10^{-8}	0.00	1.25×10^{-1}	1,685.30	1.25×10^{-1}	1,685.19	1.25×10^{-1}	1,687.09
36	7.78×10^{-5}	5.44×10^{-3}	69.96	6.66×10^{-8}	0.00	1.69×10^{-1}	2,171.34	1.69×10^{-1}	2,170.50	1.69×10^{-1}	2,172.47
37	6.06×10^{-5}	4.89×10^{-3}	80.73	6.88×10^{-8}	0.00	1.26×10^{-1}	2,076.71	1.26×10^{-1}	2,076.15	1.26×10^{-1}	2,078.27
38	6.04×10^{-5}	4.63×10^{-3}	76.71	8.94×10^{-8}	0.00	1.55×10^{-1}	2,568.04	1.55×10^{-1}	2,567.31	1.55×10^{-1}	2,569.19
39	3.89×10^{-5}	4.22×10^{-3}	108.42	9.53×10^{-8}	0.00	1.26×10^{-1}	3,245.47	1.26×10^{-1}	3,244.44	1.26×10^{-1}	3,247.30
40	4.83×10^{-5}	3.98×10^{-3}	82.49	1.18×10^{-7}	0.00	1.46×10^{-1}	3,024.08	1.46×10^{-1}	3,023.10	1.46×10^{-1}	3,025.19
41	4.19×10^{-5}	3.67×10^{-3}	87.71	1.29×10^{-7}	0.00	1.26×10^{-1}	3,016.59	1.26×10^{-1}	3,015.35	1.26×10^{-1}	3,017.86
42	3.69×10^{-5}	3.46×10^{-3}	93.96	1.56×10^{-7}	0.00	1.38×10^{-1}	3,732.68	1.38×10^{-1}	3,731.59	1.38×10^{-1}	3,733.87
43	3.62×10^{-5}	3.23×10^{-3}	89.37	1.71×10^{-7}	0.00	1.26×10^{-1}	3,484.62	1.26×10^{-1}	3,482.90	1.26×10^{-1}	3,485.78
44	2.85×10^{-5}	3.04×10^{-3}	106.85	2.02×10^{-7}	0.01	1.33×10^{-1}	4,677.31	1.33×10^{-1}	4,675.73	1.33×10^{-1}	4,678.54
45	3.01×10^{-5}	2.86×10^{-3}	94.98	2.23×10^{-7}	0.01	1.25×10^{-1}	4,154.38	1.25×10^{-1}	4,152.35	1.25×10^{-1}	4,155.47
46	2.31×10^{-5}	2.70×10^{-3}	116.61	2.59×10^{-7}	0.01	1.28×10^{-1}	5,525.38	1.28×10^{-1}	5,523.48	1.28×10^{-1}	5,526.59
47	2.43×10^{-5}	2.55×10^{-3}	104.87	2.87×10^{-7}	0.01	1.24×10^{-1}	5,075.68	1.24×10^{-1}	5,073.17	1.24×10^{-1}	5,076.79
48	1.97×10^{-5}	2.41×10^{-3}	122.58	3.27×10^{-7}	0.02	1.26×10^{-1}	6,397.55	1.26×10^{-1}	6,395.01	1.26×10^{-1}	6,398.72
49	2.17×10^{-5}	2.29×10^{-3}	105.75	3.62×10^{-7}	0.02	1.23×10^{-1}	5,664.97	1.23×10^{-1}	5,662.11	1.23×10^{-1}	5,665.98
50	1.72×10^{-5}	2.17×10^{-3}	125.99	4.10×10^{-7}	0.02	1.22×10^{-1}	7,066.21	1.22×10^{-1}	7,063.54	1.22×10^{-1}	7,067.32
51	1.78×10^{-5}	2.06×10^{-3}	115.95	4.52×10^{-7}	0.03	1.21×10^{-1}	6,785.06	1.21×10^{-1}	6,781.74	1.21×10^{-1}	6,786.01
52	1.84×10^{-5}	1.96×10^{-3}	106.46	5.05×10^{-7}	0.03	1.21×10^{-1}	6,553.01	1.21×10^{-1}	6,550.24	1.21×10^{-1}	6,553.88
53	1.57×10^{-5}	1.87×10^{-3}	119.22	5.56×10^{-7}	0.04	1.19×10^{-1}	7,603.34	1.19×10^{-1}	7,599.65	1.19×10^{-1}	7,604.30
54	1.54×10^{-5}	1.78×10^{-3}	115.65	6.18×10^{-7}	0.04	1.18×10^{-1}	7,623.13	1.17×10^{-1}	7,619.82	1.18×10^{-1}	7,624.04
55	1.39×10^{-5}	1.70×10^{-3}	122.64	6.76×10^{-7}	0.05	1.17×10^{-1}	8,445.46	1.17×10^{-1}	8,441.50	1.17×10^{-1}	8,446.40
56	1.22×10^{-5}	1.63×10^{-3}	133.65	7.45×10^{-7}	0.06	1.16×10^{-1}	9,550.57	1.16×10^{-1}	9,546.39	1.16×10^{-1}	9,551.47
57	1.10×10^{-5}	1.56×10^{-3}	142.29	8.14×10^{-7}	0.07	1.16×10^{-1}	10,545.66	1.15×10^{-1}	10,540.82	1.16×10^{-1}	10,546.66
58	1.08×10^{-5}	1.49×10^{-3}	138.80	8.92×10^{-7}	0.08	1.14×10^{-1}	10,622.89	1.14×10^{-1}	10,618.15	1.14×10^{-1}	10,623.82
59	9.49×10^{-6}	1.43×10^{-3}	150.82	9.70×10^{-7}	0.10	1.13×10^{-1}	11,944.23	1.13×10^{-1}	11,938.85	1.13×10^{-1}	11,945.17
60	9.11×10^{-6}	1.37×10^{-3}	150.78	1.06×10^{-6}	0.12	1.12×10^{-1}	12,290.85	1.12×10^{-1}	12,285.69	1.12×10^{-1}	12,291.73
rate	6.17	3.45		-		1.01		0.96		1.04	

Table 2.9: Computed spatial rates of decrease for *a posteriori* error estimators of the conservative fully-discrete scheme. Proportional cnoidal-wave solution with $T = 1$, fine temporal resolution with $\kappa = 10^{-7}$. Varying number of cells with $q = 2$.

M	L^2 error	η_0	η_0 eff.	η_1	η_1 eff.	η_2	η_2 eff.	η	η eff.	η_Σ	η_Σ eff.
15	1.13×10^{-2}	1.50×10^{-2}	1.33	0.00	0.00	1.29×10^{-1}	11.44	1.15×10^{-1}	10.13	1.30×10^{-1}	11.52
16	1.06×10^{-2}	1.42×10^{-2}	1.34	0.00	0.00	1.87×10^{-1}	17.70	1.72×10^{-1}	16.28	1.88×10^{-1}	17.75
17	9.52×10^{-3}	1.27×10^{-2}	1.33	0.00	0.00	2.04×10^{-1}	21.48	1.93×10^{-1}	20.28	2.05×10^{-1}	21.52
18	8.55×10^{-3}	1.15×10^{-2}	1.35	0.00	0.00	2.09×10^{-1}	24.40	1.99×10^{-1}	23.25	2.09×10^{-1}	24.43
19	7.41×10^{-3}	1.05×10^{-2}	1.42	0.00	0.00	2.03×10^{-1}	27.39	1.95×10^{-1}	26.27	2.03×10^{-1}	27.43
20	6.97×10^{-3}	1.03×10^{-2}	1.47	0.00	0.00	2.49×10^{-1}	35.72	2.39×10^{-1}	34.34	2.49×10^{-1}	35.75
21	6.37×10^{-3}	9.39×10^{-3}	1.47	0.00	0.00	2.56×10^{-1}	40.12	2.47×10^{-1}	38.79	2.56×10^{-1}	40.15
22	5.91×10^{-3}	8.77×10^{-3}	1.48	0.00	0.00	2.66×10^{-1}	45.07	2.58×10^{-1}	43.73	2.67×10^{-1}	45.10
23	5.38×10^{-3}	8.16×10^{-3}	1.52	0.00	0.00	2.76×10^{-1}	51.27	2.69×10^{-1}	49.89	2.76×10^{-1}	51.29
24	5.00×10^{-3}	7.68×10^{-3}	1.53	0.00	0.00	2.87×10^{-1}	57.39	2.80×10^{-1}	55.97	2.87×10^{-1}	57.41
25	4.56×10^{-3}	7.28×10^{-3}	1.60	0.00	0.00	2.91×10^{-1}	63.86	2.84×10^{-1}	62.34	2.91×10^{-1}	63.88
26	4.29×10^{-3}	7.35×10^{-3}	1.71	0.00	0.00	3.12×10^{-1}	72.63	3.04×10^{-1}	70.69	3.12×10^{-1}	72.65
27	4.11×10^{-3}	7.07×10^{-3}	1.72	0.00	0.00	3.49×10^{-1}	84.90	3.41×10^{-1}	82.89	3.49×10^{-1}	84.92
28	3.60×10^{-3}	6.59×10^{-3}	1.83	0.00	0.00	3.67×10^{-1}	101.84	3.59×10^{-1}	99.75	3.67×10^{-1}	101.86
29	3.56×10^{-3}	6.19×10^{-3}	1.74	0.00	0.00	3.79×10^{-1}	106.43	3.72×10^{-1}	104.46	3.79×10^{-1}	106.44
30	3.29×10^{-3}	5.73×10^{-3}	1.74	0.00	0.00	3.78×10^{-1}	114.70	3.72×10^{-1}	112.81	3.78×10^{-1}	114.71
31	2.97×10^{-3}	5.76×10^{-3}	1.94	0.00	0.00	4.09×10^{-1}	137.58	4.02×10^{-1}	135.32	4.09×10^{-1}	137.59
32	2.90×10^{-3}	5.43×10^{-3}	1.87	0.00	0.00	4.23×10^{-1}	145.83	4.16×10^{-1}	143.66	4.23×10^{-1}	145.84
33	2.70×10^{-3}	5.18×10^{-3}	1.91	0.00	0.00	4.34×10^{-1}	160.61	4.28×10^{-1}	158.38	4.34×10^{-1}	160.62
34	2.61×10^{-3}	4.93×10^{-3}	1.89	0.00	0.00	4.45×10^{-1}	170.55	4.39×10^{-1}	168.35	4.45×10^{-1}	170.57
35	2.48×10^{-3}	4.75×10^{-3}	1.91	0.00	0.00	4.56×10^{-1}	183.79	4.50×10^{-1}	181.55	4.56×10^{-1}	183.80
36	2.30×10^{-3}	4.58×10^{-3}	1.99	0.00	0.00	4.65×10^{-1}	202.08	4.60×10^{-1}	199.73	4.65×10^{-1}	202.09
37	2.23×10^{-3}	4.44×10^{-3}	1.99	0.00	0.00	4.79×10^{-1}	215.27	4.74×10^{-1}	212.86	4.79×10^{-1}	215.28
38	2.09×10^{-3}	4.27×10^{-3}	2.04	0.00	0.00	4.92×10^{-1}	235.13	4.87×10^{-1}	232.67	4.92×10^{-1}	235.14
39	1.92×10^{-3}	4.09×10^{-3}	2.13	0.00	0.00	5.03×10^{-1}	261.45	4.98×10^{-1}	258.88	5.03×10^{-1}	261.46
40	1.88×10^{-3}	3.93×10^{-3}	2.09	0.00	0.00	5.12×10^{-1}	272.32	5.07×10^{-1}	269.81	5.12×10^{-1}	272.33
41	1.80×10^{-3}	3.76×10^{-3}	2.09	0.00	0.00	5.09×10^{-1}	283.43	5.05×10^{-1}	280.93	5.09×10^{-1}	283.43
42	1.71×10^{-3}	3.67×10^{-3}	2.14	0.00	0.00	5.32×10^{-1}	310.39	5.27×10^{-1}	307.79	5.32×10^{-1}	310.40
43	1.64×10^{-3}	3.54×10^{-3}	2.16	0.00	0.00	5.41×10^{-1}	330.06	5.36×10^{-1}	327.44	5.41×10^{-1}	330.07
44	1.52×10^{-3}	3.42×10^{-3}	2.25	0.00	0.00	5.49×10^{-1}	361.97	5.45×10^{-1}	359.23	5.49×10^{-1}	361.97
45	1.50×10^{-3}	3.30×10^{-3}	2.20	0.00	0.00	5.57×10^{-1}	371.70	5.53×10^{-1}	369.02	5.57×10^{-1}	371.70
46	1.39×10^{-3}	3.19×10^{-3}	2.30	0.00	0.00	5.65×10^{-1}	407.51	5.61×10^{-1}	404.70	5.65×10^{-1}	407.51
47	1.37×10^{-3}	3.09×10^{-3}	2.26	0.00	0.00	5.73×10^{-1}	418.28	5.69×10^{-1}	415.52	5.73×10^{-1}	418.29
48	1.30×10^{-3}	2.99×10^{-3}	2.30	0.00	0.00	5.80×10^{-1}	445.34	5.77×10^{-1}	442.53	5.80×10^{-1}	445.34
49	1.26×10^{-3}	2.90×10^{-3}	2.31	0.00	0.00	5.88×10^{-1}	467.36	5.84×10^{-1}	464.54	5.88×10^{-1}	467.37
50	1.22×10^{-3}	2.81×10^{-3}	2.30	0.00	0.00	5.95×10^{-1}	487.35	5.91×10^{-1}	484.53	5.95×10^{-1}	487.35
51	1.17×10^{-3}	2.72×10^{-3}	2.32	0.00	0.00	6.01×10^{-1}	513.39	5.98×10^{-1}	510.55	6.01×10^{-1}	513.40
52	1.10×10^{-3}	2.64×10^{-3}	2.41	0.00	0.00	6.07×10^{-1}	554.37	6.04×10^{-1}	551.42	6.08×10^{-1}	554.38
53	1.08×10^{-3}	2.56×10^{-3}	2.37	0.00	0.00	6.14×10^{-1}	566.79	6.11×10^{-1}	563.89	6.14×10^{-1}	566.80
54	1.02×10^{-3}	2.49×10^{-3}	2.44	0.00	0.00	6.20×10^{-1}	607.50	6.17×10^{-1}	604.51	6.20×10^{-1}	607.50
55	9.89×10^{-4}	2.42×10^{-3}	2.44	0.00	0.00	6.25×10^{-1}	632.25	6.22×10^{-1}	629.26	6.25×10^{-1}	632.26
56	9.75×10^{-4}	2.34×10^{-3}	2.40	0.00	0.00	6.31×10^{-1}	646.78	6.28×10^{-1}	643.84	6.31×10^{-1}	646.79
57	9.38×10^{-4}	2.28×10^{-3}	2.43	0.00	0.00	6.36×10^{-1}	678.54	6.33×10^{-1}	675.56	6.36×10^{-1}	678.55
58	8.76×10^{-4}	2.22×10^{-3}	2.53	0.00	0.00	6.41×10^{-1}	732.47	6.39×10^{-1}	729.36	6.41×10^{-1}	732.47
59	9.05×10^{-4}	2.15×10^{-3}	2.38	0.00	0.00	6.46×10^{-1}	713.90	6.44×10^{-1}	710.98	6.46×10^{-1}	713.91
60	8.41×10^{-4}	2.10×10^{-3}	2.49	0.00	0.00	6.51×10^{-1}	774.67	6.49×10^{-1}	771.61	6.51×10^{-1}	774.68
rate	1.91	1.41		-		-1.01		-1.06		-1.01	

Table 2.10: Computed spatial rates of decrease for *a posteriori* error estimators of the conservative fully-discrete scheme. Proportional cnoidal-wave solution with $T = 1$, fine temporal resolution with $\kappa = 10^{-7}$. Varying number of cells with $q = 3$.

M	L^2 error	η_0	η_0 eff.	η_1	η_1 eff.	η_2	η_2 eff.	η	η eff.	η_Σ	η_Σ eff.
15	2.20×10^{-3}	4.79×10^{-3}	2.18	0.00	0.00	1.77×10^{-1}	80.62	1.73×10^{-1}	78.81	1.77×10^{-1}	80.65
16	2.10×10^{-2}	1.81×10^{-2}	0.86	0.00	0.00	7.14×10^{-2}	3.40	7.47×10^{-2}	3.56	7.37×10^{-2}	3.51
17	1.45×10^{-3}	3.67×10^{-3}	2.53	0.00	0.00	1.26×10^{-1}	87.07	1.24×10^{-1}	85.59	1.26×10^{-1}	87.11
18	5.50×10^{-4}	2.29×10^{-3}	4.16	0.00	0.00	7.27×10^{-2}	132.19	7.15×10^{-2}	130.04	7.27×10^{-2}	132.26
19	6.40×10^{-4}	1.93×10^{-3}	3.02	0.00	0.00	9.10×10^{-2}	142.17	8.97×10^{-2}	140.26	9.10×10^{-2}	142.20
20	6.14×10^{-3}	8.92×10^{-3}	1.45	0.00	0.00	6.27×10^{-2}	10.21	6.37×10^{-2}	10.36	6.34×10^{-2}	10.32
21	3.33×10^{-4}	1.54×10^{-3}	4.61	0.00	0.00	6.64×10^{-2}	199.22	6.57×10^{-2}	197.08	6.64×10^{-2}	199.27
22	1.98×10^{-4}	1.18×10^{-3}	5.99	0.00	0.00	4.94×10^{-2}	250.01	4.89×10^{-2}	247.55	4.94×10^{-2}	250.08
23	1.76×10^{-4}	1.01×10^{-3}	5.72	0.00	0.00	4.85×10^{-2}	275.38	4.80×10^{-2}	272.86	4.85×10^{-2}	275.44
24	1.09×10^{-3}	3.00×10^{-3}	2.74	0.00	0.00	3.83×10^{-2}	35.02	3.83×10^{-2}	35.04	3.84×10^{-2}	35.13
25	1.16×10^{-4}	7.96×10^{-4}	6.85	0.00	0.00	3.51×10^{-2}	301.85	3.48×10^{-2}	299.58	3.51×10^{-2}	301.93
26	6.40×10^{-5}	6.91×10^{-4}	10.80	0.00	0.00	2.90×10^{-2}	454.15	2.88×10^{-2}	450.62	2.91×10^{-2}	454.28
27	6.22×10^{-5}	6.10×10^{-4}	9.80	0.00	0.00	2.49×10^{-2}	400.03	2.48×10^{-2}	397.75	2.49×10^{-2}	400.15
28	1.15×10^{-4}	9.16×10^{-4}	7.95	0.00	0.00	2.14×10^{-2}	185.47	2.13×10^{-2}	184.89	2.14×10^{-2}	185.64
29	4.42×10^{-5}	5.00×10^{-4}	11.30	0.00	0.00	1.89×10^{-2}	428.03	1.88×10^{-2}	426.07	1.89×10^{-2}	428.18
30	2.68×10^{-5}	4.53×10^{-4}	16.89	0.00	0.00	1.65×10^{-2}	613.62	1.64×10^{-2}	611.13	1.65×10^{-2}	613.86
31	2.94×10^{-5}	4.15×10^{-4}	14.11	0.00	0.00	1.44×10^{-2}	491.00	1.44×10^{-2}	489.32	1.44×10^{-2}	491.20
32	2.17×10^{-5}	4.16×10^{-4}	19.21	0.00	0.00	1.28×10^{-2}	592.48	1.28×10^{-2}	590.89	1.28×10^{-2}	592.79
33	2.16×10^{-5}	3.52×10^{-4}	16.31	0.00	0.00	1.16×10^{-2}	539.04	1.16×10^{-2}	537.57	1.17×10^{-2}	539.28
34	1.71×10^{-5}	3.27×10^{-4}	19.13	0.00	0.00	1.01×10^{-2}	593.97	1.01×10^{-2}	592.39	1.02×10^{-2}	594.28
35	1.58×10^{-5}	3.04×10^{-4}	19.26	0.00	0.00	9.33×10^{-3}	591.76	9.31×10^{-3}	590.84	9.33×10^{-3}	592.07
36	9.20×10^{-6}	2.86×10^{-4}	31.03	0.00	0.00	8.67×10^{-3}	941.87	8.66×10^{-3}	940.80	8.67×10^{-3}	942.38
37	1.25×10^{-5}	2.65×10^{-4}	21.19	0.00	0.00	8.12×10^{-3}	648.95	8.11×10^{-3}	648.41	8.12×10^{-3}	649.30
38	1.12×10^{-5}	2.49×10^{-4}	22.10	0.00	0.00	7.56×10^{-3}	671.94	7.55×10^{-3}	671.60	7.56×10^{-3}	672.31
39	7.50×10^{-6}	2.34×10^{-4}	31.19	0.00	0.00	7.27×10^{-3}	969.53	7.26×10^{-3}	969.19	7.27×10^{-3}	970.03
40	7.67×10^{-6}	2.20×10^{-4}	28.75	0.00	0.00	6.98×10^{-3}	911.18	6.98×10^{-3}	911.03	6.99×10^{-3}	911.64
41	7.09×10^{-6}	2.08×10^{-4}	29.35	0.00	0.00	6.78×10^{-3}	956.15	6.78×10^{-3}	955.97	6.78×10^{-3}	956.60
42	5.35×10^{-6}	1.97×10^{-4}	36.81	0.00	0.00	6.52×10^{-3}	1,219.11	6.52×10^{-3}	1,219.16	6.52×10^{-3}	1,219.67
43	4.81×10^{-6}	1.86×10^{-4}	38.78	0.00	0.00	6.36×10^{-3}	1,322.99	6.36×10^{-3}	1,323.15	6.36×10^{-3}	1,323.56
44	4.76×10^{-6}	1.77×10^{-4}	37.17	0.00	0.00	6.23×10^{-3}	1,308.77	6.23×10^{-3}	1,309.01	6.24×10^{-3}	1,309.30
45	5.24×10^{-6}	1.68×10^{-4}	32.11	0.00	0.00	6.13×10^{-3}	1,169.29	6.13×10^{-3}	1,169.55	6.13×10^{-3}	1,169.73
46	5.04×10^{-6}	1.60×10^{-4}	31.79	0.00	0.00	6.02×10^{-3}	1,195.11	6.03×10^{-3}	1,195.41	6.03×10^{-3}	1,195.53
47	2.88×10^{-6}	1.53×10^{-4}	53.05	0.00	0.00	5.94×10^{-3}	2,063.57	5.94×10^{-3}	2,064.10	5.94×10^{-3}	2,064.25
48	3.81×10^{-6}	1.46×10^{-4}	38.29	0.00	0.00	5.87×10^{-3}	1,541.09	5.87×10^{-3}	1,541.50	5.87×10^{-3}	1,541.57
49	3.05×10^{-6}	1.39×10^{-4}	45.67	0.00	0.00	5.80×10^{-3}	1,900.32	5.80×10^{-3}	1,900.81	5.80×10^{-3}	1,900.87
50	3.07×10^{-6}	1.33×10^{-4}	43.35	0.00	0.00	5.73×10^{-3}	1,864.73	5.73×10^{-3}	1,865.22	5.73×10^{-3}	1,865.23
51	2.86×10^{-6}	1.28×10^{-4}	44.57	0.00	0.00	5.67×10^{-3}	1,981.33	5.68×10^{-3}	1,981.85	5.68×10^{-3}	1,981.83
52	2.66×10^{-6}	1.22×10^{-4}	45.98	0.00	0.00	5.62×10^{-3}	2,110.65	5.62×10^{-3}	2,111.20	5.62×10^{-3}	2,111.15
53	1.38×10^{-6}	1.17×10^{-4}	85.25	0.00	0.00	5.56×10^{-3}	4,038.63	5.56×10^{-3}	4,039.66	5.56×10^{-3}	4,039.53
54	2.01×10^{-6}	1.13×10^{-4}	56.03	0.00	0.00	5.51×10^{-3}	2,737.59	5.51×10^{-3}	2,738.27	5.51×10^{-3}	2,738.17
55	2.00×10^{-6}	1.08×10^{-4}	54.18	0.00	0.00	5.46×10^{-3}	2,728.26	5.46×10^{-3}	2,728.93	5.46×10^{-3}	2,728.80
56	1.53×10^{-6}	1.04×10^{-4}	68.17	0.00	0.00	5.41×10^{-3}	3,535.48	5.41×10^{-3}	3,536.30	5.41×10^{-3}	3,536.13
57	1.58×10^{-6}	1.00×10^{-4}	63.55	0.00	0.00	5.36×10^{-3}	3,391.17	5.36×10^{-3}	3,391.93	5.36×10^{-3}	3,391.76
58	1.15×10^{-6}	9.68×10^{-5}	84.25	0.00	0.00	5.31×10^{-3}	4,623.07	5.31×10^{-3}	4,624.09	5.31×10^{-3}	4,623.84
59	1.65×10^{-6}	9.33×10^{-5}	56.61	0.00	0.00	5.26×10^{-3}	3,191.93	5.26×10^{-3}	3,192.62	5.26×10^{-3}	3,192.43
60	1.24×10^{-6}	9.01×10^{-5}	72.90	0.00	0.00	5.21×10^{-3}	4,221.33	5.22×10^{-3}	4,222.20	5.22×10^{-3}	4,221.96
rate	6.03	3.16		-		2.54		2.54		2.55	

Table 2.11: Computed spatial rates of decrease for *a posteriori* error estimators of the conservative fully-discrete scheme. Proportional cnoidal-wave solution with $T = 1$, fine temporal resolution with $\kappa = 10^{-7}$. Varying number of cells with $q = 4$.

M	L^2 error	η_0	η_0 eff.	η_1	η_1 eff.	η_2	η_2 eff.	η	η eff.	η_Σ	η_Σ eff.
15	4.78×10^{-5}	9.20×10^{-4}	19.26	0.00	0.00	2.24×10^{-2}	468.86	2.23×10^{-2}	467.13	2.24×10^{-2}	469.25
16	4.10×10^{-5}	7.76×10^{-4}	18.95	0.00	0.00	2.40×10^{-2}	585.48	2.39×10^{-2}	583.54	2.40×10^{-2}	585.78
17	2.81×10^{-5}	6.30×10^{-4}	22.42	0.00	0.00	1.95×10^{-2}	693.65	1.94×10^{-2}	691.35	1.95×10^{-2}	694.01
18	2.76×10^{-5}	5.38×10^{-4}	19.46	0.00	0.00	2.01×10^{-2}	726.79	2.00×10^{-2}	724.53	2.01×10^{-2}	727.05
19	1.09×10^{-5}	4.58×10^{-4}	42.10	0.00	0.00	1.75×10^{-2}	1,613.33	1.75×10^{-2}	1,608.79	1.76×10^{-2}	1,613.88
20	1.19×10^{-5}	4.01×10^{-4}	33.78	0.00	0.00	1.83×10^{-2}	1,540.24	1.82×10^{-2}	1,534.71	1.83×10^{-2}	1,540.61
21	1.28×10^{-5}	3.50×10^{-4}	27.24	0.00	0.00	1.72×10^{-2}	1,339.26	1.71×10^{-2}	1,334.87	1.72×10^{-2}	1,339.54
22	6.28×10^{-6}	3.10×10^{-4}	49.33	0.00	0.00	1.70×10^{-2}	2,710.22	1.70×10^{-2}	2,702.00	1.70×10^{-2}	2,710.66
23	8.51×10^{-6}	2.75×10^{-4}	32.34	0.00	0.00	1.66×10^{-2}	1,949.79	1.66×10^{-2}	1,944.01	1.66×10^{-2}	1,950.06
24	7.82×10^{-6}	2.47×10^{-4}	31.57	0.00	0.00	1.62×10^{-2}	2,076.55	1.62×10^{-2}	2,070.83	1.62×10^{-2}	2,076.79
25	7.12×10^{-6}	2.23×10^{-4}	31.27	0.00	0.00	1.59×10^{-2}	2,227.78	1.58×10^{-2}	2,221.97	1.59×10^{-2}	2,228.00
26	5.37×10^{-6}	2.02×10^{-4}	37.55	0.00	0.00	1.55×10^{-2}	2,893.64	1.55×10^{-2}	2,886.59	1.55×10^{-2}	2,893.89
27	4.26×10^{-6}	1.84×10^{-4}	43.11	0.00	0.00	1.50×10^{-2}	3,526.47	1.50×10^{-2}	3,518.65	1.50×10^{-2}	3,526.76
28	4.12×10^{-6}	1.68×10^{-4}	40.79	0.00	0.00	1.50×10^{-2}	3,632.04	1.49×10^{-2}	3,623.53	1.50×10^{-2}	3,632.28
29	3.64×10^{-6}	1.54×10^{-4}	42.42	0.00	0.00	1.46×10^{-2}	4,019.61	1.46×10^{-2}	4,010.87	1.46×10^{-2}	4,019.83
30	2.95×10^{-6}	1.42×10^{-4}	48.26	0.00	0.00	1.43×10^{-2}	4,849.67	1.43×10^{-2}	4,839.76	1.43×10^{-2}	4,849.91
31	2.46×10^{-6}	1.31×10^{-4}	53.40	0.00	0.00	1.40×10^{-2}	5,672.30	1.39×10^{-2}	5,661.21	1.40×10^{-2}	5,672.54
32	1.99×10^{-6}	1.22×10^{-4}	61.25	0.00	0.00	1.36×10^{-2}	6,849.49	1.36×10^{-2}	6,836.87	1.36×10^{-2}	6,849.74
33	1.96×10^{-6}	1.13×10^{-4}	57.85	0.00	0.00	1.33×10^{-2}	6,786.92	1.33×10^{-2}	6,775.12	1.33×10^{-2}	6,787.17
34	2.01×10^{-6}	1.06×10^{-4}	52.48	0.00	0.00	1.29×10^{-2}	6,433.45	1.29×10^{-2}	6,422.86	1.29×10^{-2}	6,433.65
35	1.43×10^{-6}	9.87×10^{-5}	69.20	0.00	0.00	1.26×10^{-2}	8,825.03	1.26×10^{-2}	8,811.00	1.26×10^{-2}	8,825.31
36	1.30×10^{-6}	9.24×10^{-5}	70.88	0.00	0.00	1.23×10^{-2}	9,446.60	1.23×10^{-2}	9,432.25	1.23×10^{-2}	9,446.91
37	1.40×10^{-6}	8.67×10^{-5}	61.79	0.00	0.00	1.20×10^{-2}	8,546.25	1.20×10^{-2}	8,533.91	1.20×10^{-2}	8,546.46
38	1.29×10^{-6}	8.15×10^{-5}	63.25	0.00	0.00	1.17×10^{-2}	9,059.44	1.17×10^{-2}	9,047.02	1.17×10^{-2}	9,059.67
39	9.12×10^{-7}	7.67×10^{-5}	84.16	0.00	0.00	1.14×10^{-2}	12,459.51	1.13×10^{-2}	12,443.17	1.14×10^{-2}	12,459.84
40	1.14×10^{-6}	7.24×10^{-5}	63.54	0.00	0.00	1.11×10^{-2}	9,702.99	1.10×10^{-2}	9,690.88	1.11×10^{-2}	9,703.17
41	6.44×10^{-7}	6.84×10^{-5}	106.26	0.00	0.00	1.08×10^{-2}	16,707.20	1.07×10^{-2}	16,687.32	1.08×10^{-2}	16,707.66
42	7.91×10^{-7}	6.48×10^{-5}	81.92	0.00	0.00	1.05×10^{-2}	13,238.80	1.05×10^{-2}	13,223.62	1.05×10^{-2}	13,239.05
43	5.86×10^{-7}	6.14×10^{-5}	104.74	0.00	0.00	1.02×10^{-2}	17,371.68	1.02×10^{-2}	17,352.58	1.02×10^{-2}	17,372.03
44	7.32×10^{-7}	5.83×10^{-5}	79.62	0.00	0.00	9.91×10^{-3}	13,539.45	9.90×10^{-3}	13,525.22	9.91×10^{-3}	13,539.68
45	5.81×10^{-7}	5.54×10^{-5}	95.30	0.00	0.00	9.64×10^{-3}	16,587.35	9.63×10^{-3}	16,570.65	9.64×10^{-3}	16,587.62
46	5.67×10^{-7}	5.27×10^{-5}	92.94	0.00	0.00	9.38×10^{-3}	16,538.10	9.37×10^{-3}	16,522.14	9.38×10^{-3}	16,538.36
47	4.63×10^{-7}	5.02×10^{-5}	108.51	0.00	0.00	9.13×10^{-3}	19,716.59	9.12×10^{-3}	19,698.33	9.13×10^{-3}	19,716.89
48	5.13×10^{-7}	4.79×10^{-5}	93.38	0.00	0.00	8.88×10^{-3}	17,311.04	8.87×10^{-3}	17,295.64	8.88×10^{-3}	17,311.29
49	3.48×10^{-7}	4.58×10^{-5}	131.51	6.86×10^{-11}	0.00	8.64×10^{-3}	24,847.82	8.64×10^{-3}	24,826.55	8.65×10^{-3}	24,848.17
50	4.53×10^{-7}	4.37×10^{-5}	96.62	5.99×10^{-10}	0.00	8.40×10^{-3}	18,564.00	8.40×10^{-3}	18,548.74	8.40×10^{-3}	18,564.27
51	3.04×10^{-7}	4.19×10^{-5}	137.50	1.37×10^{-9}	0.00	8.18×10^{-3}	26,868.15	8.17×10^{-3}	26,846.86	8.18×10^{-3}	26,868.48
52	3.01×10^{-7}	4.01×10^{-5}	133.11	2.28×10^{-9}	0.01	7.96×10^{-3}	26,428.30	7.95×10^{-3}	26,408.18	7.96×10^{-3}	26,428.63
53	2.73×10^{-7}	3.84×10^{-5}	140.61	3.35×10^{-9}	0.01	7.75×10^{-3}	28,343.73	7.74×10^{-3}	28,322.95	7.75×10^{-3}	28,344.10
54	3.34×10^{-7}	3.69×10^{-5}	110.37	4.66×10^{-9}	0.01	7.54×10^{-3}	22,573.25	7.54×10^{-3}	22,557.27	7.54×10^{-3}	22,573.52
55	2.50×10^{-7}	3.54×10^{-5}	141.44	6.24×10^{-9}	0.02	7.34×10^{-3}	29,327.91	7.34×10^{-3}	29,307.90	7.34×10^{-3}	29,328.23
56	2.29×10^{-7}	3.40×10^{-5}	148.64	7.95×10^{-9}	0.03	7.15×10^{-3}	31,225.88	7.15×10^{-3}	31,205.36	7.15×10^{-3}	31,226.23
57	2.39×10^{-7}	3.27×10^{-5}	136.75	9.72×10^{-9}	0.04	6.96×10^{-3}	29,085.64	6.96×10^{-3}	29,067.18	6.96×10^{-3}	29,085.97
58	2.27×10^{-7}	3.15×10^{-5}	138.69	1.16×10^{-8}	0.05	6.78×10^{-3}	29,849.97	6.78×10^{-3}	29,831.71	6.78×10^{-3}	29,850.32
59	1.93×10^{-7}	3.04×10^{-5}	156.96	1.34×10^{-8}	0.07	6.61×10^{-3}	34,162.17	6.61×10^{-3}	34,141.96	6.61×10^{-3}	34,162.53
60	1.73×10^{-7}	2.93×10^{-5}	168.75	1.54×10^{-8}	0.09	6.44×10^{-3}	37,123.52	6.44×10^{-3}	37,102.31	6.44×10^{-3}	37,123.92
rate	3.96	2.43		-		0.88		0.88		0.88	

2.7.3 Effectivity of the various indicators

In this section, examine the dependence on t of the estimators η, η_Σ, and η_i for $i = 0, 1, 2$. Each plot records how the values of the L^2 errors and the various estimators vary with time when the solutions to (2.1) are approximated up to a final time T via (2.47). We have not recorded the values of the terms $\|u_M^n - \hat{u}(t^n)\| + \|v_M^n - \hat{v}(t^n)\|$ that appear in Theorem 2.12 as they are negligible when compared with those we have recorded.

Figure 2.1 records the behavior of the L^2 error and the estimators with the uniform timestep $\kappa = 1/16$ chosen to effect a low temporal accuracy. Figures 2.1a-2.1d treat increasing levels of spatial accuracy given a fixed uniform mesh of $M = 200$ cells. Indeed, these subplots report the error and estimator values for polynomial degree $q = 2, 3, 4, 5$, respectively. Figure 2.2 records similar behavior, yet with the uniform timestep $\kappa = 1/100$ chosen to effect a higher degree of temporal accuracy. Finally, two longer time experiments with high spatial accuracy ($q = 6, M = 200$) are shown in Figures 2.3 (final time $T = 5$, $\kappa = 1/100$, solitary wave) and 2.4 (final time $T = 10$, $\kappa = 1/16$, cnoidal wave). We remark that the values considered here for the discretization parameters are more than reasonable for use in application, especially those which afforded higher temporal accuracy.

In each of the experiments, we consistently see reasonable ($\mathcal{O}(1)$) effectivity indices for the various indicators. We highlight several important observations:

1. Recall that, in the previous sections, η_2 was observed to be solely dependent on h, albeit with a rate of decrease which was suboptimal by three powers of h. This, of course, results in an extremely coarse bound for the spatial errors. Nevertheless, this (suboptimal) dependence on h comes into view again in Figures 2.1 and 2.2. As spatial accuracy

increases with the choice of polynomial degree, η_2 becomes much smaller than the error by several orders of magnitude. In addition, we note that the plots of η_2 and the L^2 error for $q = 3$ and $q = 4$ are essentially the same, while the plots for $q = 5$ and $q = 6$ are essentially the same, which is reasonable since the convergence rates for (2.47) are observed to be $\mathcal{O}(h^4)$ for both $q = 3$ and $q = 4$ and $\mathcal{O}(h^6)$ for $q = 5$ and $q = 6$.

2. Even in the cases of lower spatial accuracy, η_2, which may be viewed as an estimator of the spatial error that is suboptimal by several orders of magnitude, is around the same order of magnitude as the error. This suggests that the primary contributor to the error in each of these experiments is the temporal error. Recall that η_1 was observed to be solely dependent on time, with optimal rate of decrease. In light of the behavior of η_2, we expect η_1 to be a good estimator of the error. In each figure presented here, this is indeed the case, with the curve for η_1 closely mimicing that of the error itself.

3. Indeed, the curves for each the estimators $\eta_0, \eta_1, \eta,$ and η_Σ closely mimic that of the L^2 error. Indeed, though the L^2 error appears to increase at a rate linear in t^n and the various estimators appear to increase at a rate proportional to $\sqrt{t^n}$, for the majority of each plot, the curves are near parallel to each other. Note that this $\sqrt{t^n}$ rate is reasonable for the various indicators as we did not plot the exponential factor entering from the estimate in Theorem 2.12.

4. We observe that the estimator η_Σ consistently bounds the error. Naturally, η provides a sharper bound, however.

5. Finally, recall that the estimator η_0 was expected and observed to behave optimally with respect to κ and suboptimally with respect to h. Yet, η_0 was only suboptimal by a factor of h, as opposed to the suboptimality by a factor of h^3 which plagues η_2, η, and η_Σ. Combining this fact with the observation that in each of the figures the graph of η_0 closely mimics the error, we suggest that it might be useful to develop a heuristic of using only η_0 in practice.

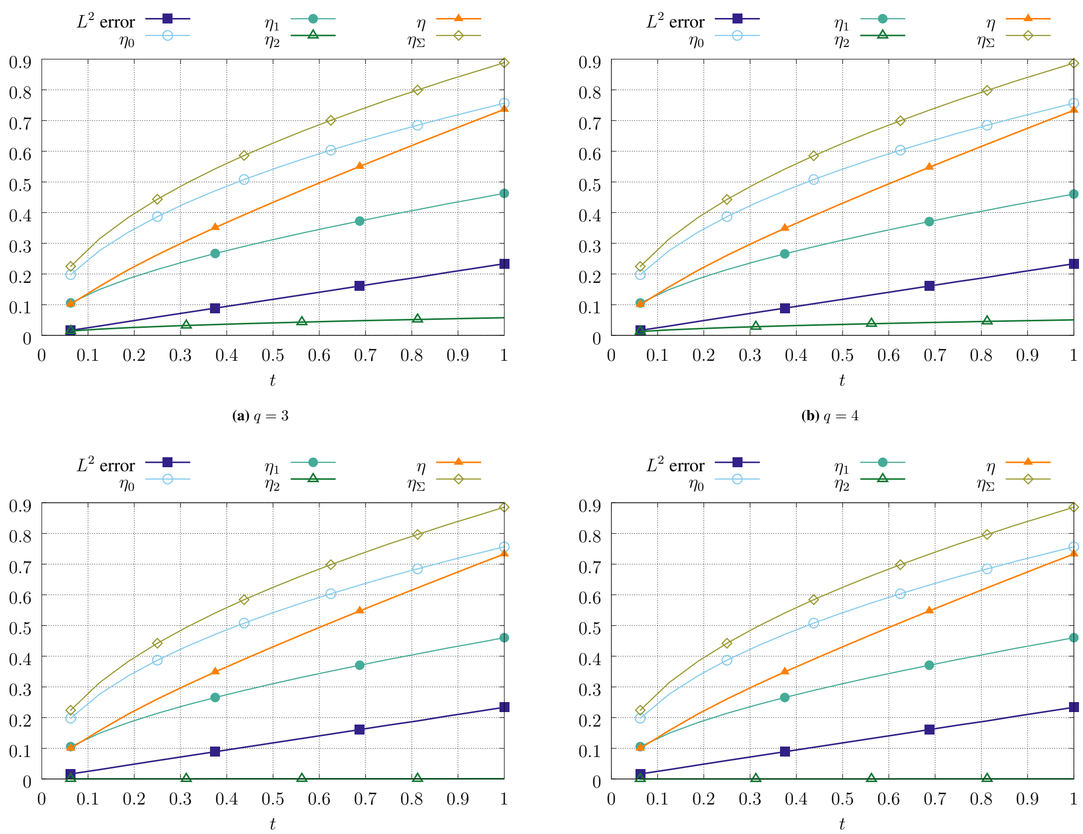

(a) $q = 3$ **(b)** $q = 4$

(c) $q = 5$ **(d)** $q = 6$

Figure 2.1: The L^2 error and *a posteriori* estimators vs. time: $\kappa = \dfrac{1}{16}$, $T = 1$, $M = 200$, solitary wave solution

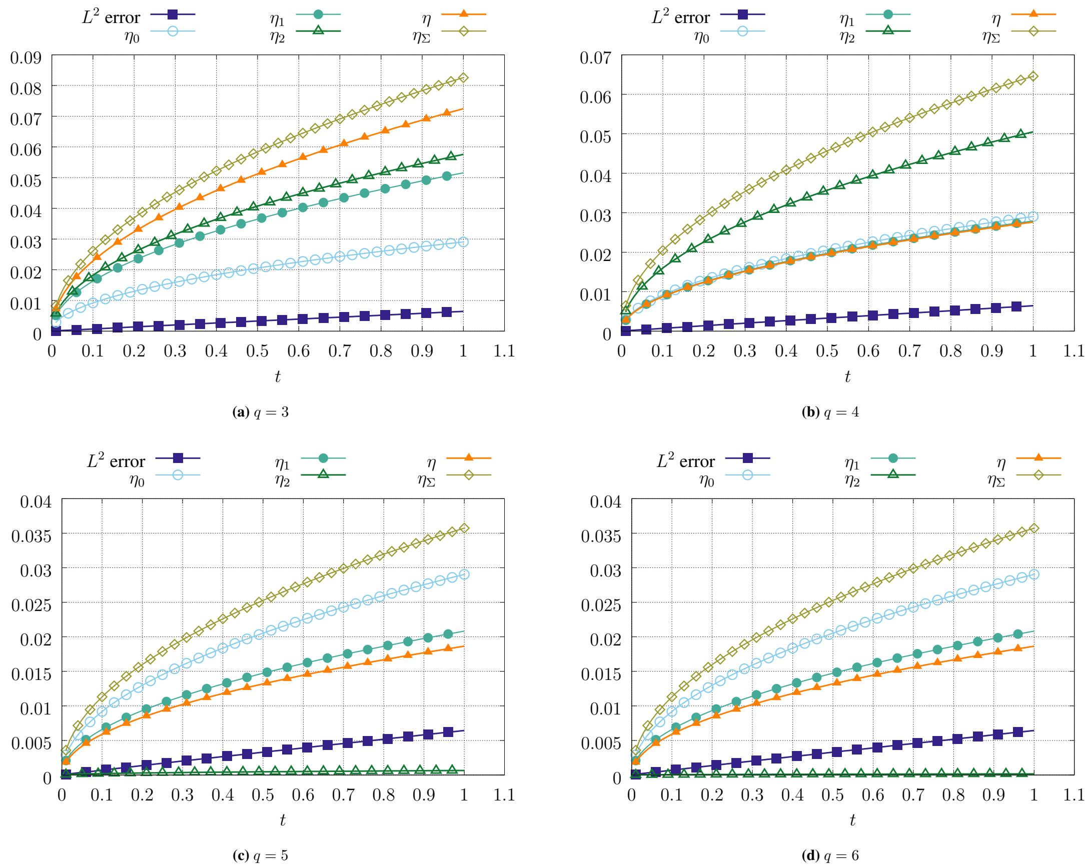

(a) $q = 3$ (b) $q = 4$ (c) $q = 5$ (d) $q = 6$

Figure 2.2: The L^2 error and *a posteriori* estimators vs. time: $\kappa = \dfrac{1}{100}, T = 1, M = 200$, solitary wave solution

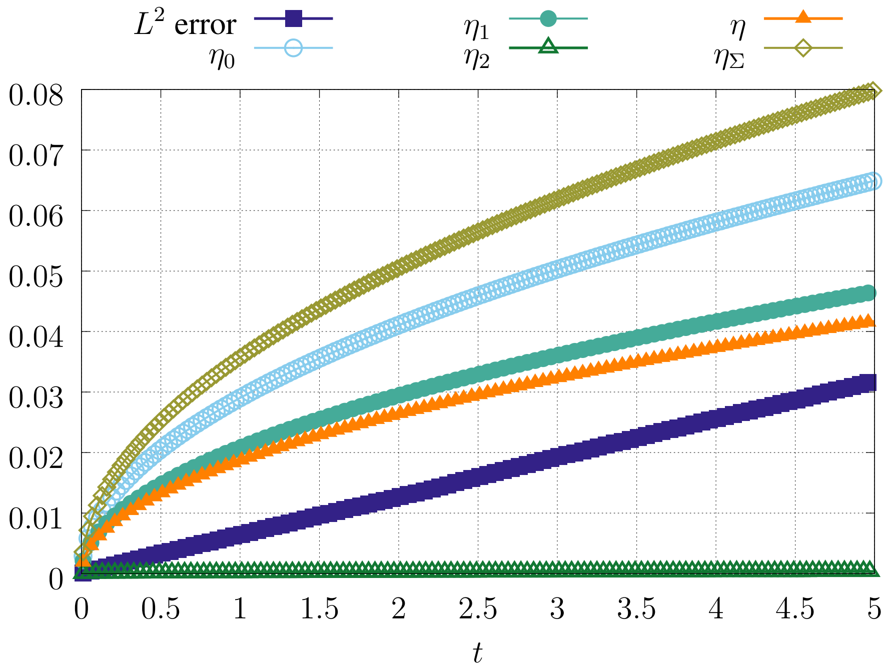

Figure 2.3: The L^2 error and *a posteriori* estimators vs. time: $\kappa = \dfrac{1}{100}$, $T = 5$, $M = 200$, $q = 6$ solitary wave solution

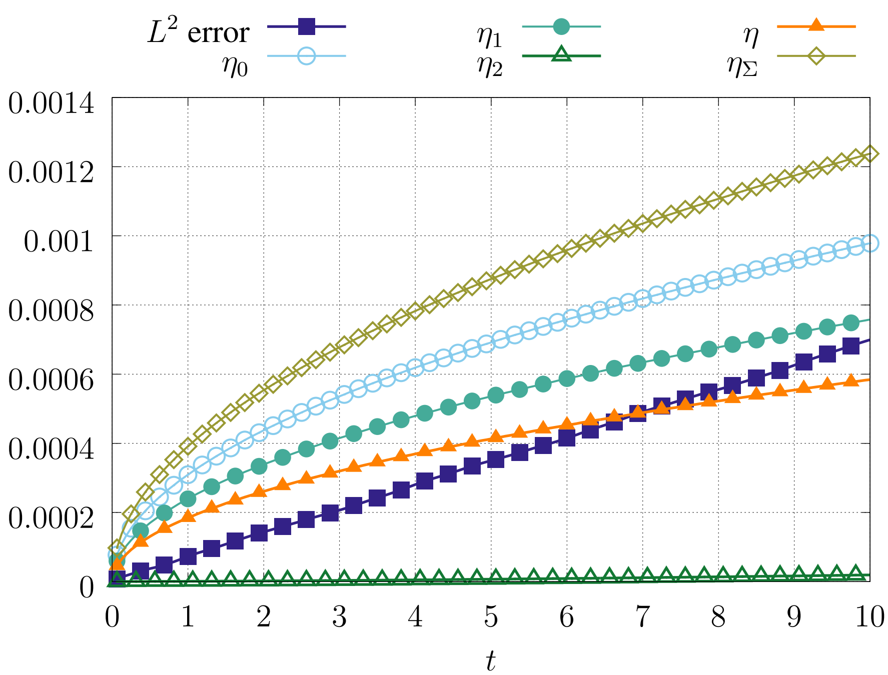

Figure 2.4: The L^2 error and *a posteriori* estimators vs. time: $\kappa = \dfrac{1}{16}$, $T = 10$, $M = 200$, $q = 6$ cnoidal wave solution

2.7.4 Suboptimality and heuristic correction

Finally, we conduct experiments to gain a deeper understanding of how the observed spatial suboptimality affects the effectiveness of these estimators. We remind the reader, that, in most practical cases, effectivity indices of the various indicators remain small. This is possible due to the computational ease with which the fully discrete scheme (2.47) can be computed. Indeed, high spatial accuracy can be effected with ease by using a higher number of cells M or larger polynomial degree q, causing the temporal error to be the main contributor to the total error. In these cases, the temporal optimality of the indicators keeps the effectivity indices small, as the spatial errors can be made several orders of magnitude smaller than the temporal errors and, consequently, do not affect the size of the effectivity indices.

Nevertheless, it is still important to understand, on a practical level, how the suboptimality affects the effectivity indices. Varying the number of cells M and the number of timesteps N, we compute the cnoidal wave solution till final time $T = 1$, employing polynomial degree $q = 5$. In Figures 2.5-2.9, we provide plots of the base-10 logarithms of the effectivity indices of the various indicators.

Recalling that η_0 behaved spatially suboptimally by one power of h coincides with the observation that most of Figure 2.5 is green, i.e., for most values of M and N, the effectivity index of η_0 is $\mathcal{O}(1)$. This is in contrast to the less desirable behavior of the estimators $\eta_2, \eta,$ and η_Σ (each of which were seen to behave suboptimally by three powers of h) depicted in Figures 2.7-2.9. This lends additional support to the heuristic of using η_0 alone as an estimator, as discussed in the previous section. In addition, the black portion of Figure 2.7 illustrates how η_2 can be used as an indicator of the spatial errors. Indeed, if the number of cells M is chosen so that $M > 100$, the contour plots in 2.8 and 2.9 show that effectivity indices consistently remain less than $10^{1.5} \approx 31.6$ with most values remaining less than 10. Indeed, these ranges for M and N are sufficient for practical computation.

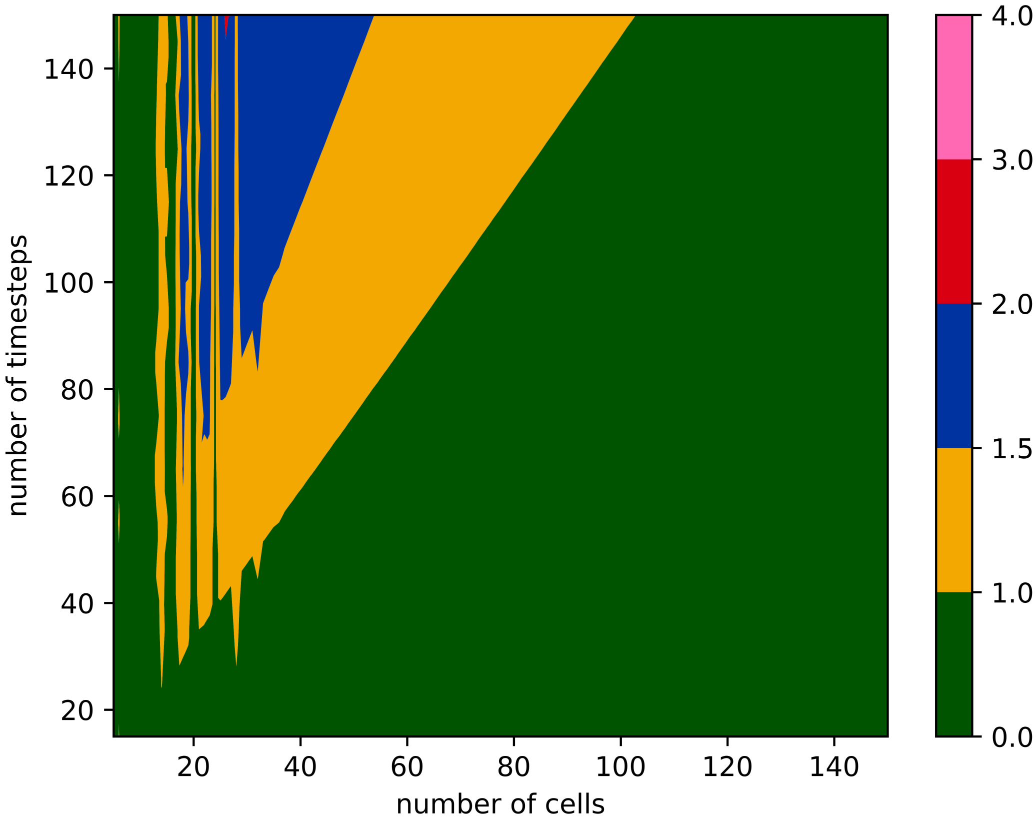

Figure 2.5: Contour plot of $\log_{10}(\mathrm{Eff}(\eta_0))$ for $T = 1$, $q = 5$

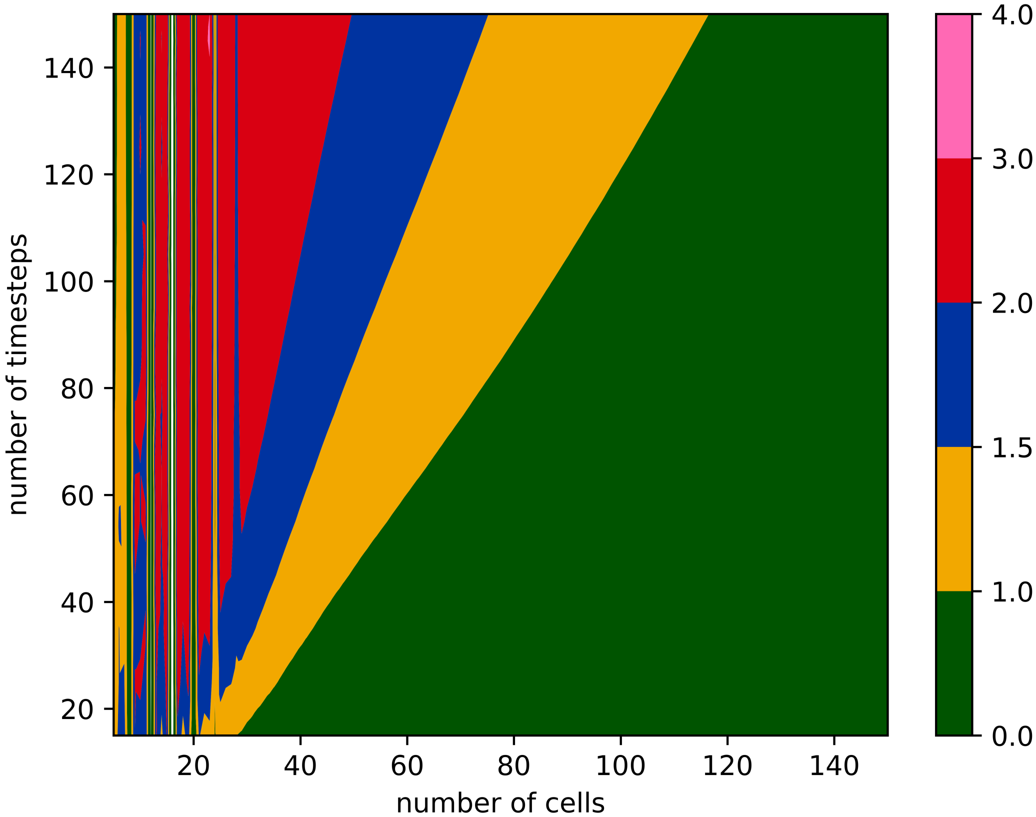

Figure 2.6: Contour plot of $\log_{10}(\mathrm{Eff}(\eta_1))$ for $T = 1$, $q = 5$

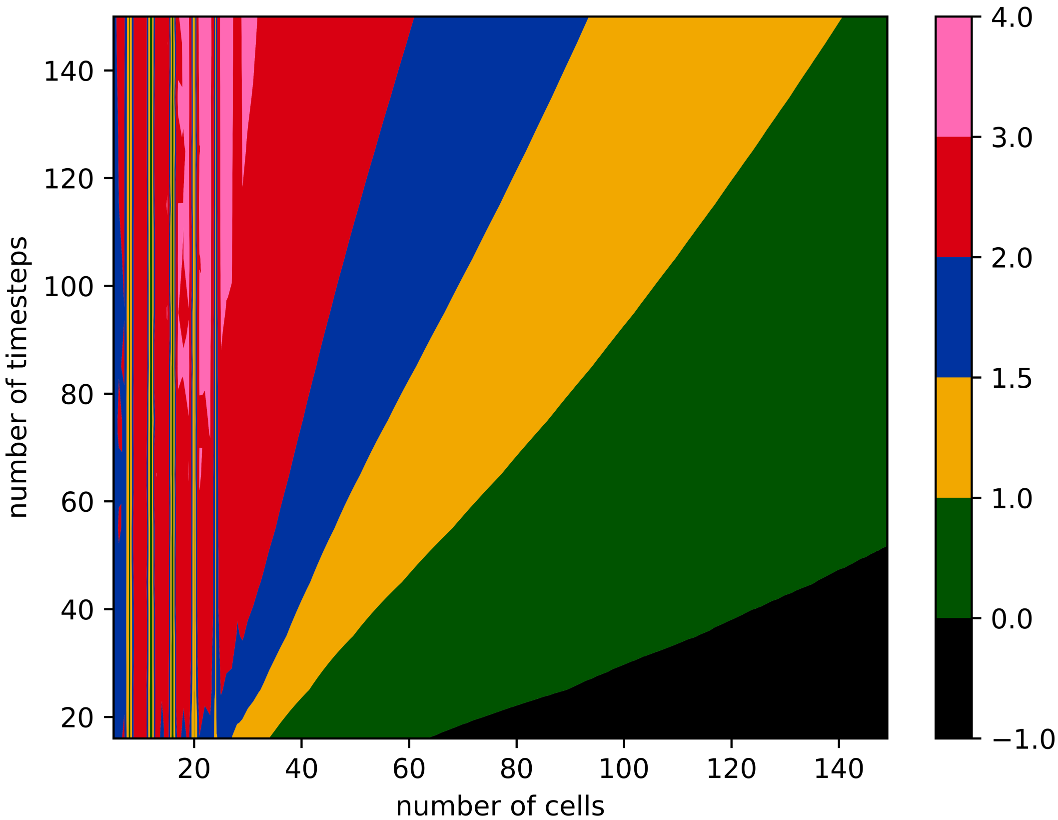

Figure 2.7: Contour plot of $\log_{10}(\mathrm{Eff}(\eta_2))$ for $T = 1$, $q = 5$

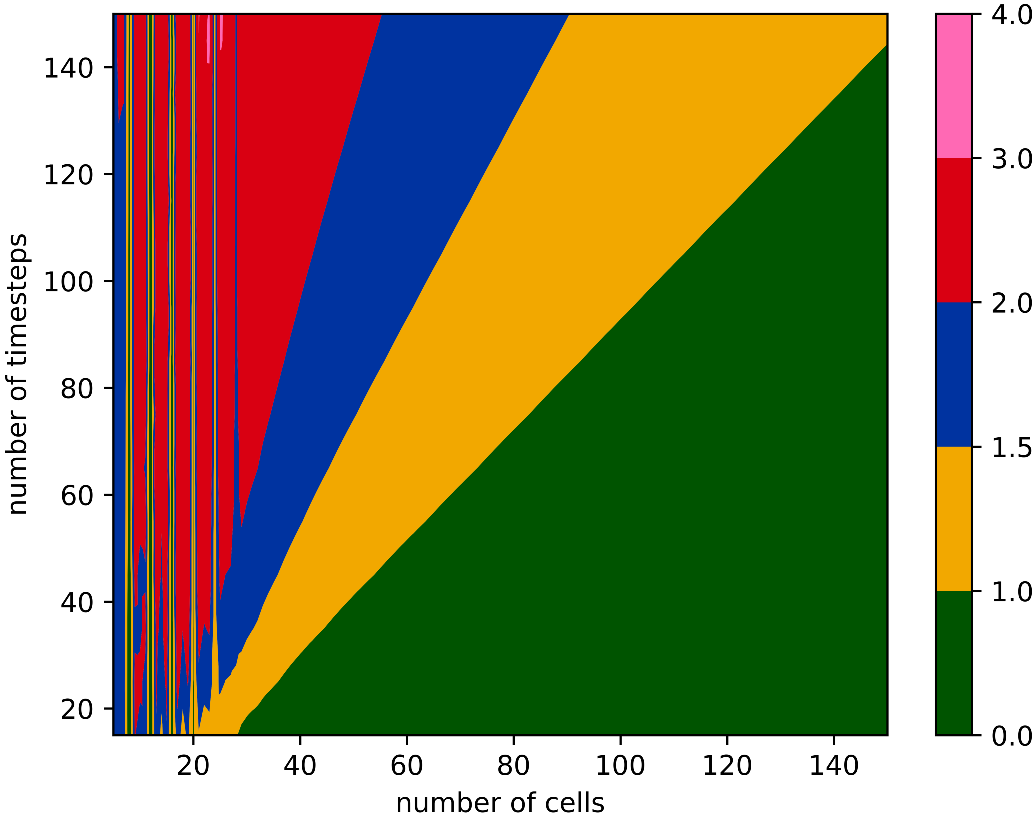

Figure 2.8: Contour plot of $\log_{10}(\mathrm{Eff}(\eta))$ for $T = 1$, $q = 5$

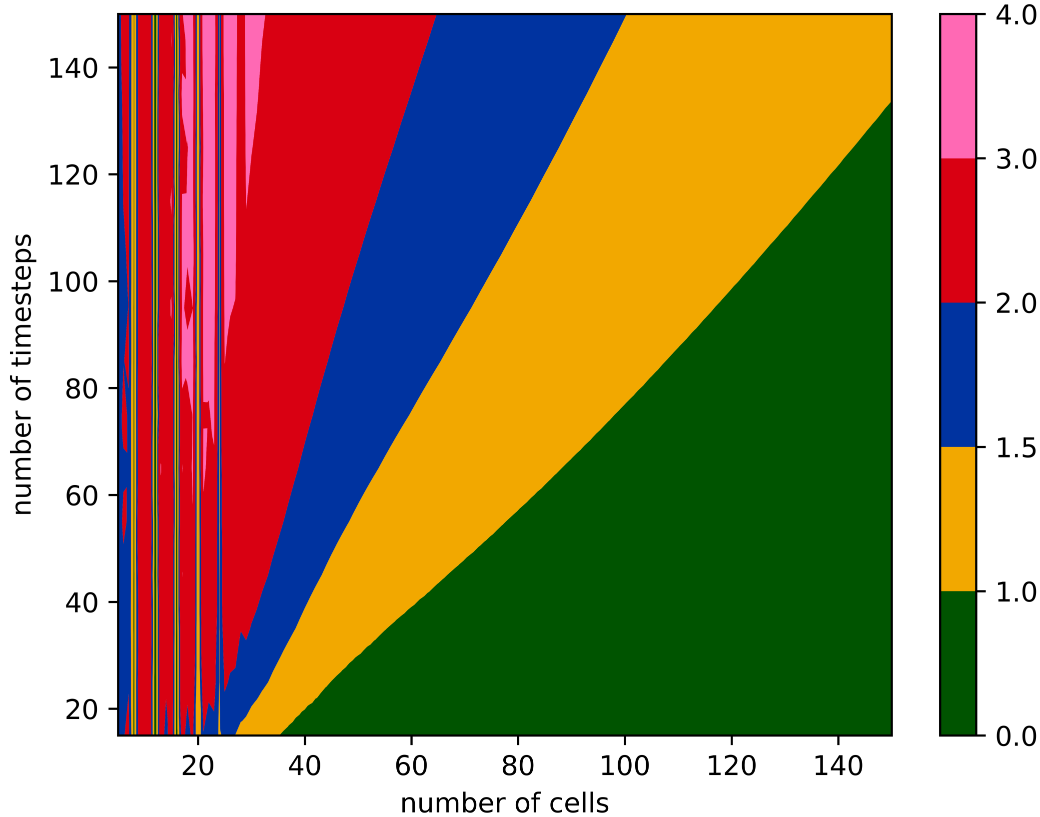

Figure 2.9: Contour plot of $\log_{10}(\mathrm{Eff}(\eta_\Sigma))$ for $T = 1$, $q = 5$

Nevertheless, it is desirable that effectivity indices remain $\mathcal{O}(1)$ regardless of the choice of discretization parameters. As a result, we seek a heuristic correction factor by which we can multiply the spatially suboptimal indicators to correct their behavior. In Figure 2.10, we depict the base-10 logarithm of η as in Figure 2.8 except we consider a significantly larger range for the number of timesteps, to further highlight the issues caused by the spatial suboptimality we seek to correct. In light of the data collected, the appropriate heuristic correction factor was $C_\star := (M/N)^p = (\kappa/h)^p$, where experiments suggest that the power p depends on the polynomial degree q used in the spatial discretization. For $q = 5$, $p = 2$ seems reasonable. Indeed, correction by the resulting $C_\star$ results in a much more effective estimator $\eta_\star := C_\star \eta$. Figure 2.11 depicts the base-10 logarithm of the heuristic estimator $\eta_\star$ for the same choices of M and N taken in Figure 2.10. It is of note that the suitable correction factor $C_\star$ depends on the polynomial degree. Indeed, similar results can be obtained even for low polynomial degree: for $q = 2$, a useful estimator is obtained by taking $p = 3$.

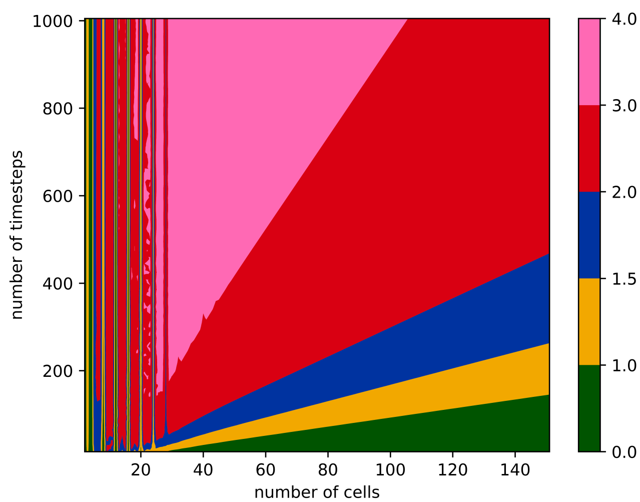

Figure 2.10: Base-10 logarithm of the effectivity index of the estimator η

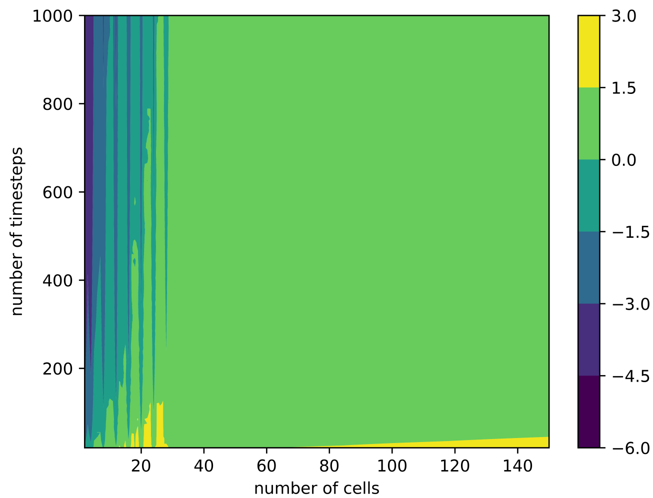

Figure 2.11: Base-10 logarithm of the effectivity indices of the corrected estimator $\eta_\star$

2.8 Summary and future work

We have constructed *a posteriori* error estimates for semidiscrete and fully discrete finite element methods for a paradigm class of coupled systems of nonlinear, dispersive equations. To the best of our knowledge, these were the first results of their kind extant for numerical methods for this class of PDEs. Our estimate for the fully discrete methods provide several useful indicators of the error in $L^2([0,1])$. One of these indicators, η_1, was experimentally verified to be an indicator of the temporal error. Another, η_2, was experimentally verified to be an indicator of the spatial error. Indeed, each of the temporally dependent indicators were seen to exhibit optimal temporal rates of decrease when compared to the underlying timestepping method of the fully discrete scheme.

Noting the spatial suboptimality of the behavior of several of the error indicators, we provided several observations regarding their practical use. First, we noted that computational efficiency of these methods allow the spatial error to be made so small that the temporal error is the primary contributor to the total approximation error by several orders of magnitude. Under this condition, effectivity indices remain within a practical range. A second heuristic was to use the estimator η_0 alone, which was only suboptimal by one power of h due to the nonlinear terms, as opposed to the suboptimality by three powers of h affecting η_2, η, and η_Σ. A final heuristic suggestion was to multiply the suboptimal indicators by a correction factor, resulting in another error indicator with effectivity indices that were generally observed to remain $\mathcal{O}(1)$, independent of the choice of discretization parameters.

Many avenues exist for future exploration. From a computational perspective, a natural next step is to utilize the estimates developed herein to develop adaptive methods. From a theoretical perspective, while suboptimality of η_0 is somewhat expected, it would be useful to obtain estimators which do not incur the suboptimality that plagues η_2, η, and η_Σ and stems from the dispersive terms. Removal or at least amelioration of this suboptimality would greatly benefit the effectiveness of the resulting indicators. Finally, extending the results obtained for fully discrete schemes to the remaining members of the family of implicit Runge-Kutta methods of Gauss-Legendre type is of interest.

Bibliography

[1] Abramowitz, M. and Stegun, I. (1965). *Handbook of Mathematical Functions with Formulas, Graphs and Mathematical Tables*, volume 55 of *Applied Mathematics Series*. National Bureau of Standards. 43, 92

[2] Adams, R. (1975). *Sobolev Spaces*. Academic Press, New York. 11

[3] Akrivis, G., Makridakis, C., and Nochetto, R. (2011). Galerkin and Runge–Kutta methods: unified formulation, a posteriori error estimates and nodal superconvergence. *Numerische Mathematik*, 118(3):429–456. xii, 61, 81

[4] Ash, J., Cohen, J., and Wang, G. (1996). On strongly interacting internal solitary waves. *Journal of Fourier Analysis and Applications*, 2:507–517. 3

[5] Baker, G. A., Dougalis, V. A., and Karakashian, O. A. (1983a). Convergence of Galerkin approximations for the Korteweg-de Vries equation. *Mathematics of Computation*, 40:419–433. 6

[6] Baker, G. A., Dougalis, V. A., and Karakashian, O. A. (1983b). Convergence of galerkin approximations for the korteweg-de vries equation. *Mathematics of Computation*, 40(162):419–433. 81

[7] Bänsch, E., Karakatsani, F., and Makridakis, C. (2012). A posteriori error control for fully discrete crank–nicolson schemes. *SIAM Journal on Numerical Analysis*, 50(6):2845–2872. 81

[8] Biello, J. (2009). Nonlinearly coupled KdV equations describing the interaction of equatorial and midlatitude Rossby waves. *Chinese Annals of Mathematics, Series B*, 30(5):483–504. ix

[9] Bona, J. L. (1981). Convergence of periodic wavetrains in the limit of large wavelength. *Applied Scientific Research*, 37(1):21–30. 44, 92

[Bona et al.] Bona, J. L., Chen, H., and Karakashian, O. A. Instability of solitary-wave solutions of systems of coupled KdV equations: Theory and numerical results. Preprint. x, 6

[11] Bona, J. L., Chen, H., and Karakashian, O. A. (2017). Stability of solitary-wave solutions of systems of dispersive equations. *Applied Mathematics & Optimization*, 75:27–53. x, 4, 5, 6, 53, 59

[12] Bona, J. L., Chen, H., Karakashian, O. A., and Wise, M. M. (2018). Finite element methods for a system of dispersive equations. *Journal of Scientific Computing*, 77(3):1371–1401. iv, xi, 1, 58, 60, 61, 63, 64, 65, 68, 70, 71, 88, 91, 92, 96, 97

[13] Bona, J. L., Chen, H., Karakashian, O. A., and Xing, Y. (2013). Conservative, discontinuous Galerkin–methods for the generalized Korteweg–de Vries equation. *Mathematics of Computation*, 82(283):1401–1432. 7, 8, 14, 15, 17, 26, 63, 64, 66, 67

[14] Bona, J. L., Chen, H., and Saut, J.-C. (2002). Boussinesq equations and other systems for small-amplitude long waves in nonlinear dispersive media. I: Derivation and linear theory. *Journal of Nonlinear Science*, 12(4):283–318. x, 2

[15] Bona, J. L., Chen, H., and Saut, J.-C. (2004). Boussinesq equations and other systems for small-amplitude long waves in nonlinear dispersive media. II: The nonlinear theory. *Nonlinearity*, 17(3):925–952. x, 2

[16] Bona, J. L., Cohen, J., and Wang, G. (2014). Global well-posedness for a system of KdV-type equations with coupled quadratic nonlinearities. *Nagoya Mathematical Journal*, 215(1):67–149. x, 3

[17] Bona, J. L., Dougalis, V. A., and Mitsotakis, D. E. (2007). Numerical solution of KdV–KdV systems of Boussinesq equations. I: The numerical scheme and generalized solitary waves. 74(2-3):214–228. 2

[18] Bona, J. L., Dougalis, V. A., and Mitsotakis, D. E. (2008). Numerical solution of Boussinesq systems of KdV-KdV type. II: Evolution of radiating solitary waves. *Nonlinearity*, 21(12):2825–2848. 2

[19] Bona, J. L. and Smith, R. (1975). The initial-value problem for the Korteweg-de Vries equation. *Philosophical Transactions of the Royal Society of London. Series A, Mathematical and Physical Sciences (1934-1990)*, 278(1287):555–601. 5, 59

[20] Bona, J. L. and Soyeur, A. (1994). On the stability of solitary-wave solutions of model equations for long waves. *Journal of Nonlinear Science*, 4(1):449–470. 54

[21] Brenner, S. C. and Scott, L. R. (2008). *The Mathematical Theory of Finite Element Methods*, volume 15 of *Texts in Applied Mathematics*. Springer New York, New York, NY. 12, 19

[22] Chen, H. (2006). Long-period limit of nonlinear dispersive waves. *Differential and Integral Equations*, 19:463–480. 44, 92

[23] Cheng, Y. and Shu, C. W. (2008). A discontinuous Galerkin finite element method for time dependent partial differential equations with higher order derivatives. *Mathematics of Computation*, 77(262):699–730. 6, 7, 8, 88

[Ciarlet] Ciarlet, P. G. *The finite element method for elliptic problems*. Classics in applied mathematics ; 40. Society for Industrial and Applied Mathematics SIAM, 3600 Market Street, Floor 6, Philadelphia, PA 19104, Philadelphia, Pa. 19

[25] Colliander, J., Keel, M., Staffilani, G., Takaoka, H., and Tao, T. (2003). Sharp global well-posedness for KdV and modified KdV on $\mathbb{R}$ and $\mathbb{T}$. *Journal of the American Mathematical Society*, 16(3):705–749. 3, 4, 59

[Dekker and Verwer] Dekker, K. and Verwer, J. Stability of Runge-Kutta methods for stiff nonlinear differential equations. 9

[27] Evans, L. C. (2010). *Partial Differential Equations*, volume 19 of *Graduate Studies in Mathematics*. American Mathematical Society, 2 edition. 78, 87

[28] Gear, J. A. and Grimshaw, R. (1984). Weak and strong interactions between internal solitary waves. *Studies in Applied Mathematics*, 65:235–258. 2

[29] Hakkaev, S. (2003). Stability and instability of solitary wave solutiosn of a nonlinear dispersive system of Benjamin-Bona-Mahony type. *Serdica Mathematics Journal*, 29:337–354. x, 3

[30] Kappeler, T. and Topalov, P. (2006). Global well-posedness of KdV in $H^{-1}(\mathbb{T}, \mathbb{R})$. *Duke Mathematics Journal*, 135:327–360. 4

[31] Karakashian, O. and Makridakis, C. (2015). A posteriori error estimates for discontinuous Galerkin methods for the generalized Korteweg-de Vries equation. *Mathematics of Computation*, 84(293):1145–1167. xii, 7, 60, 61, 63, 64, 66, 67, 68, 69, 79, 80, 81, 88

[32] Karakashian, O. and Xing, Y. (2016). A posteriori error estimates for conservative local discontinuous Galerkin methods for the generalized Korteweg-de Vries equation. *Communications in Computational Physics*, 20(1):250–278. 7, 8

[33] Liu, H. and Yi, N. (2016). A Hamiltonian preserving discontinuous Galerkin method for the generalized Korteweg–de Vries equation. *Journal of Computational Physics*, 321:776–796. 7, 8

[34] Majda, A. and Biello, J. (2003). The nonlinear interaction of barotropic and equatorial baroclinic Rossby waves. *Journal of the Atmospheric Sciences*, 60(15):1809. ix, 2

[35] Majda, A. and Biello, J. (2004). Boundary layer dissipation and the nonlinear interaction of equatorial baroclinic and barotropic rossby waves. *Geophysical and Astrophysical Fluid Dynamics*, 98(2):85–127. ix

[36] Miura, R. M. (1976). The Korteweg-de Vries equation: A survey of results. *SIAM Review*, 18(3):412–459. 1

[37] Pego, R. and Weinstein, M. (1994). Asymptotic stability of solitary waves. *Communications in Mathematical Physics*, 164(2). 54

[38] Wahlbin, L. B. (1974). Dissipative Galerkin method for the numerical solution of first order hyperbolic equations. In de Boor, C., editor, *Mathematical Aspects of Finite Elements in Partial Differential Equations, Proceedings of a Symposium at the Mathematics Research Center, the University of Wisconsin Madison*, pages 147–169. Academic Press. 6

[39] Winther, R. (1980). A conservative finite element method for the Korteweg-de Vries equation. *Mathematics of Computation*, 34(149):23–43. 6

[40] Xu, Y. and Shu, C.-W. (2007). Error estimates of the semi-discrete local discontinuous Galerkin method for nonlinear convection–diffusion and KdV equations. *Computer Methods in Applied Mechanics and Engineering*, 196(37):3805–3822. 6

[41] Yan, J. and Shu, C.-W. (2002). A local discontinuous Galerkin method for KdV type equations. *SIAM Journal on Numerical Analysis*, 40(2):769–791. 6

Vita

Michael Morgan Wise was born to Rodney Jay Wise and Misty Karen Wise (née Williams) in Merriam, Kansas on 25 November 1994. He received his primary and secondary education privately at home. His parents instilled in him a deep love of learning and education, particularly emphasizing the value of science, technology, engineering, and mathematics and the critical importance of their use for the benefit of mankind.

Upon completing his pre-collegiate education in 2010 at the age of fifteen, he attended Copiah-Lincoln Community College in Wesson, Mississippi, completing an Associate in Arts degree with highest honors. In addition to receiving the college's awards for excellence in mathematics and computer science, Michael was a 2012 inductee of the Copiah-Lincoln Community College Hall of Fame, the highest honor awarded to a student at this institution. He attended Mississippi College, graduating *summa cum laude* with a Bachelor of Science degree in Mathematics in 2014, minoring in Computer Science. At Mississippi College, Michael served as President of Pi Mu Epsilon and a Vice President of the Phi Theta Kappa Alumni Chapter. He was awarded the Senior Mathematics Award, was named to the President's List each semester, and was inducted into Alpha Chi.

At age nineteen, Michael enrolled in the University of Tennessee as a doctoral student in Mathematics, funded by a Chancellor's Fellowship. Under his doctoral advisor Ohannes Karakashian, he became an active researcher in discontinuous Galerkin methods, finite element methods, nonlinear dispersive equations, and domain decomposition. He applied his knowledge of computer science to learn high performance computing from Jack Dongarra and his researchers at the Innovative Computing Laboratory. Through collaborations with Ibrahim Aslan, Mahir Demir, and Suzanne Lenhart he also developed interest in mathematical biology, specifically mathematical modelling of infectious diseases. His active curiosity toward artificial intelligence and machine learning which began under Glenn Wiggins at Mississippi College was stimulated via his independent work and collaboration with Joseph Daws at the University of Tennessee. For his final year of doctoral study, he was awarded the generous Spike Tickle STEM Fellowship from the Department of Mathematics "for outstanding academic performance and desire to use [his] talents and education in science, technology, engineering or mathematics."

After his graduation in May 2020 at the age of twenty-five, Michael Morgan Wise became a Scientist at Dynetics, Inc., an applied science and information technology company serving the United States Department of Defense, United States Intelligence Community, National Aeronautics and Space Administration (NASA) and more. In addition to his work for Dynetics, he continues to actively research and publish in his many areas of interest, always seeking to use his knowledge of mathematics to engage others and to fuel the development of a better world.